

DEVELOPMENT OF A COMPREHENSIVE AND MODULAR
MODELLING, ANALYSIS AND SIMULATION TOOL FOR HELICOPTERS

A THESIS SUBMITTED TO
THE GRADUATE SCHOOL OF NATURAL AND APPLIED SCIENCES
OF
MIDDLE EAST TECHNICAL UNIVERSITY

BY

ARDA YÜCEKAYALI

IN PARTIAL FULFILLMENT OF THE REQUIREMENTS
FOR
THE DEGREE OF MASTER OF SCIENCE
IN
AEROSPACE ENGINEERING

SEPTEMBER 2011

Approval of the thesis:

**DEVELOPMENT OF A COMPREHENSIVE AND MODULAR MODELLING,
ANALYSIS AND SIMULATION TOOL FOR HELICOPTERS**

submitted by **ARDA YÜCEKAYALI** in partial fulfillment of the requirements for the degree of **Master of Science in Aerospace Engineering Department, Middle East Technical University** by,

Prof. Dr. Canan Özgen
Dean, Graduate School of **Natural and Applied Science** _____

Prof. Dr. Ozan Tekinalp
Head of Department, **Aerospace Engineering** _____

Asst. Prof. Dr. Ali Türker Kutay
Supervisor, **Aerospace Engineering Dept., METU** _____

Examining Committee Members:

Prof. Dr. Ozan Tekinalp
Aerospace Engineering Dept., METU _____

Asst. Prof. Dr. Ali Türker Kutay
Aerospace Engineering Dept., METU _____

Prof. Dr. Yusuf Özyörük
Aerospace Engineering Dept., METU _____

Assoc. Prof. Dr. D. Funda Kurtuluş
Aerospace Engineering Dept., METU _____

Chief Eng., MSc. Yüksel Ortakaya
Aeromechanics Group, TAI _____

Date: 09.09.2011

I hereby declare that all information in this document has been obtained and presented in accordance with academic rules and ethical conduct. I also declare that, as required by these rules and conduct, I have fully cited and referenced all material and results that are not original to this work.

Name, Last Name: Arda Yücekayalı

Signature:

ABSTRACT

DEVELOPMENT OF A COMPREHENSIVE AND MODULAR MODELLING, ANALYSIS AND SIMULATION TOOL FOR HELICOPTERS

Yücekayalı, Arda

M.S, Department of Aerospace Engineering

Supervisor: Asst. Prof. Dr. Ali Türker Kutay

September 2011, 196 pages

Helicopter flight dynamic, rotor aerodynamic and dynamic analyses activities have been a great dispute since the first helicopters, at both design and test stages. Predicting rotor aerodynamic and dynamic characteristics, helicopter dynamic behavior and trimmed flight conditions is a huge challenge to engineers as it involves the tradeoff between accuracy, fidelity, complexity and computational cost.

Flight dynamic activities such as; predicting trim conditions, helicopter dynamic behavior and simulation of a flight condition or maneuver mostly require analysis tools with low computational cost and complexity. However this decreases accuracy and fidelity of the model. On the other hand, analyses at design stages, such as; blade geometric and structural design mostly requires accurate and higher fidelity aerodynamic load predictions over the rotor disk. Contrarily this brings high computational cost and complexity. Therefore separate analysis tools for each objective or one complete tool that can be used for all purposes are essential.

Throughout this study a helicopter mathematical including trim model with a selective and modular structure is developed as a generic analysis tool. The selective structure enables the mathematical model to be used in both flight dynamic and comprehensive analysis while the modular structure plays a role as an infrastructure for further developments. The mathematical model developed is validated with flight test data of several helicopters. Besides, commercial helicopter comprehensive analysis tools are used to validate the mathematical model analyses. Results showed good agreement with the compared data.

Keywords: Helicopter modeling, rotor aerodynamics, rotor dynamics

ÖZ

HELİKOPTERLER İÇİN MODÜLER VE KAPSAMLI MODELLEME, ANALİZ VE SİMÜLASYON ARACI GELİŞTİRİLMESİ

Yücekayalı, Arda

Yüksel Lisans, Havacılık ve Uzay Mühendisliği Bölümü

Tez Yöneticisi: Asst. Prof. Dr. Ali Türker Kutay

Eylül, 2011, 196 sayfa

Helikopter tasarım ve test aşamalarında uçuş dinamiği, rotor aerodinamik ve dinamik analiz çalışmaları ilk helikopterlerden bu yana büyük bir önem taşımıştır. Rotor aerodinamik ve dinamik karakterinin, helikopter tepki ve denge koşullarının tahminleri doğruluk, hassasiyet, karmaşıklık ve hesaba dayalı efor arasında bir alışveriş içerdiğinden mühendisler için zorlu bir iş olmuştur.

Helikopterin denge koşullarının, dinamik tepkisinin ve bir uçuş koşulunun veya manevranın simülasyonu gibi uçuş dinamiği çalışmaları genellikle düşük hesap eforu ve karmaşıklığa sahip metot ve araçlar gerektirmektedir. Fakat bu doğruluk ve hassasiyetin azalmasına sebep olmaktadır. Buna karşılık, pala geometrik veya yapısal tasarımı gibi tasarım faaliyetleri genellikle doğruluğu ve hassasiyeti yüksek araçlar ile yapılmaktadır. Benzer bir şekilde bu da yüksek hesap eforu ve karmaşıklık getirmektedir. Dolayısıyla, ya her amaç için farklı bir analiz aracına ya da her alanda kullanılacak bütün bir analiz aracına ihtiyaç duyulmaktadır.

Bu tez çalışmasında bu ihtiyacı karşılamaya yönelik hem seçmeli hem de modüler bir yapıda, denge modelini de içeren bir helikopter matematik modeli geliştirilmiştir. Seçmeli yapı, geliştirilen matematik modelin hem uçuş dinamiği hem de detaylı analiz faaliyetlerinde kullanılmasını, modüler yapı ise geliştirmeler ve iyileştirmeler için bir altyapı görevi görmesini sağlamaktadır. Geliştirilen matematik model, literatürde bulunan helikopter uçuş test verileri ve ticari helikopter analiz ve simulasyon araçları ile doğrulanmış ve sonuçların tutarlı ve uyumlu olduğu görülmüştür.

Anahtar Kelimeler: helikopter modelleme, rotor aerodinamiği, rotor dinamiği

I would like to dedicate this study to my mother, Esin and to my father, Ferhat.

ACKNOWLEDGEMENTS

First of all I would like to declare my gratitude to Prof. Dr. Cahit ıray, for introducing me to the very subject of this study; helicopters, and for making me love them.

I would like to thank to the members of dissertation committee for their valuable feedback; Prof. Dr. Ozan Tekinalp, Prof. Dr. Yusuf zyrk, Assoc. Prof. Dr. D. Funda Kurtuluş, Asst. Prof. Dr. Ali Trker Kutay, Chief Eng. Yksel Ortakaya.

I especially would like to thank to Asst. Prof. Dr. Ali Trker Kutay, my dissertation director, for his guidance and supporting throughout this dissertation.

I would also like to thank to Asst. Prof. Dr. İlkey Yavrucuk for his feedback and valuable opinions, while I was writing this dissertation.

I would like to thank to my company Turkish Aerospace Industry (TAI) for supporting and encouraging me to write this dissertation.

I especially would like to thank to my Chief Engineer Yksel Ortakaya for his support, effort and valuable guidance in both my academic and professional life.

I would like to thank to my friend and colleague Ahmet Alper Ezertaş for his endeavor and feedback especially in the format of this dissertation.

I would like to thank to my colleagues and friends for their friendship and making both work and academic life enjoyable.

I would like to thank to Bařak Dilber for her endeavor and help on writing this dissertation, bringing joy to my life, her support, trust and love, or simply I am grateful for her existence in my life.

Finally, I would like to thank to my mother, Esin, who was always compassionate to me even during my fake stomachaches; and to my father, Ferhat, who was always a promoter even when I capsized the sailboat. Besides I would like to thank them for their endless love, effort and support throughout my life.

TABLE OF CONTENTS

ABSTRACT	iv
ÖZ	vi
ACKNOWLEDGEMENTS	ix
TABLE OF CONTENTS	x
LIST OF FIGURES	xiii
LIST OF TABLES	xvii
LIST OF SYMBOLS	xviii
CHAPTERS	
1.INTRODUCTION	1
1.1 Initial Mathematical Model.....	4
1.2 Refined Main and Tail Rotor Aerodynamic Models.....	6
1.3 Trim Model	8
1.4 Validation	9
1.5 Goals & Outputs.....	9
2.LITERATURE REVIEW	11
2.1 Mathematical Flight Dynamics Model	11
2.2 Refined Main and Tail Rotor Aerodynamic Models.....	14
2.3 Tip Path Plane Dynamics.....	20
3.MATHEMATICAL MODEL	22
3.1 Introduction	22
3.2 Flow Chart.....	25
3.3 Reference Coordinate Systems	28
3.3.1 Inertial Reference Frame	28

3.3.2	Vehicle Carried Reference Frame	29
3.3.3	Body Axis Reference Frame	29
3.3.4	Wind Axis Reference Frame	30
3.3.5	Hub Axis Reference Frame.....	30
3.3.6	Blade Reference Frame	32
3.3.7	Blade Element Reference Frame.....	32
3.3.8	Tail Rotor Reference Frame	34
3.3.9	Horizontal Tail Reference Frame	35
3.3.10	Vertical Tail Reference Frame	35
3.4	Main Rotor Model.....	35
3.4.1	Main Rotor Blade Model	36
3.4.2	Initial Inflow Model	38
3.4.3	Aerodynamic Load Model	40
3.4.4	Blade Dynamics & Hub Model	50
3.5	Re-Fined Main Rotor Model	54
3.5.1	Hover Inflow Model	54
3.5.2	Hover Wake Model	56
3.5.3	Hover Wake Induced Velocity Model.....	60
3.5.4	Forward Flight Inflow Models	62
3.5.5	Forward Flight Wake Models	69
3.5.6	Forward Flight Wake Induced Velocity Model.....	75
3.6	Tail Rotor Model.....	76
3.6.1	Tail Rotor Hub & Blade Model	76
3.6.2	Inflow Model.....	77
3.6.3	Aerodynamic Model	79
3.7	Fuselage Model	83

3.8	Horizontal Tail Model	89
3.9	Vertical Tail Model.....	95
3.10	6-DOF Solver	100
3.11	Environmental Model	102
4.	MATHEMATICAL MODEL VALIDATION.....	105
4.1	WESSEX VALIDATION WITH EXPERIMENTAL DATA.....	105
4.2	OH-58 VALIDATION WITH FLIGHT TEST DATA	109
4.3	SA-349 / GAZALLE VALIDATION WITH CAMRAD	115
4.4	UH-60 VALIDATION WITH FLIGHTLAB.....	127
5.	TRIM MODEL.....	138
6.	TRIM MODEL VALIDATION.....	144
6.1	VALIDATION WITH FLIGHTLAB	144
7.	SIMULATION RESULTS	152
8.	SUMMARY AND CONCLUSIONS.....	160
8.1	Summary.....	160
8.2	Conclusion	169
9.	FUTURE WORKS	173
	REFERENCES	175
	APPENDICES	
A.	TRANSFORMATIONS BETWEEN DIFFERENT REFERENCE FRAMES .	183
B.	ALTERNATIVE METHOD FOR BLADE FLAPPING MODEL.....	188
C.	MAIN ROTOR AERODYNAMIC ANALYSIS FOR WESSEX.....	190

LIST OF FIGURES

FIGURES

Figure 1-1 Azimuth angle definition	5
Figure 3-1 Matlab & Simulink model of the developed mathematical model.....	26
Figure 3-2 Hub reference frame coordinate system.....	31
Figure 3-3 Blade and Blade Reference Frame systems.....	33
Figure 3-4 Blade and Blade Reference Frame systems.....	34
Figure 3-5 Example blade segmentation of the developed mathematical model.....	37
Figure 3-6 Blade element force and angle definitions	41
Figure 3-7 Dynamic inflow development	43
Figure 3-8 Force components acting on each blade element	47
Figure 3-9 Landgrebe's Prescribed Wake Model (with/without rolling-up tip vortex)	59
Figure 3-10 Comparison of prescribed and free wake methods with experimental measurement. [19]	60
Figure 3-11 Biot-Savart's Law for curved and straight vortex filament segments [19]	61
Figure 3-12 Drees and M&S inflow distribution comparison with experimental results [28]	68
Figure 3-13 Drees and M&S inflow distribution comparison with experimental results [28]	68
Figure 3-14 Undistorted Prescribed Wake Model.....	71
Figure 3-15 Undistorted Prescribed Wake Model.....	71
Figure 3-16 Beddoes' Prescribed Wake Model.....	74
Figure 3-17 Blade element force and angle definitions	80
Figure 3-18 Horizontal tail reference system and angle definitions.....	90
Figure 3-19 Vertical tail reference system and angle definitions	96
Figure 4-1 Westland Wessex [69]	105
Figure 4-2 Wessex Helicopter Ct&Cq validation with experimental data	107
Figure 4-3 Effect of blade element number on accuracy of the results	108
Figure 4-4 OH-58 / Kiowa [72].....	109

Figure 4-5 Validation with OH-58 Ct&Cp experimental data	111
Figure 4-6 Validation with OH-58 radial thrust distribution experimental data.....	112
Figure 4-7 Validation with OH-58 main rotor power & thrust coefficient with experimental data.....	113
Figure 4-8 SA-349 / Gazalle [73].....	115
Figure 4-9 Gazalle's main rotor blade geometry [67]	116
Figure 4-10 Ct vs Advance Ratio validation with CAMRAD	119
Figure 4-11 Cq vs Advance Ratio validation with CAMRAD	119
Figure 4-12 Ct vs Cq validation with CAMRAD	120
Figure 4-13 Aoa vs Azimuth angle at r/R = 0.28 (105 kts)	121
Figure 4-14 Aoa vs Azimuth angle at r/R = 0.59 (105 kts)	122
Figure 4-15 Aoa vs Azimuth angle at r/R = 0.79 (105 kts)	122
Figure 4-16 Aoa vs Azimuth angle at r/R = 0.87 (105 kts)	123
Figure 4-17 Aoa vs Azimuth angle at r/R = 0.28 (125 kts)	123
Figure 4-18 Aoa vs Azimuth angle at r/R = 0.59 (125 kts)	124
Figure 4-19 Aoa vs Azimuth angle at r/R = 0.79 (125 kts)	124
Figure 4-20 Aoa vs Azimuth angle at r/R = 0.87 (125 kts)	125
Figure 4-21 Blade Flapping Harmonics vs Advance Ratio validation with CAMRAD	126
Figure 4-22 UH-60 / Blackhawk [71].....	127
Figure 4-23 Cq vs Forward Flight validation with FLIGHTLAB.....	130
Figure 4-24 Cl vs Azimuth Angle distribution validation with FLIGHTLAB at r/R = 0.50, 20 kts.....	131
Figure 4-25 Cl vs Azimuth Angle distribution validation with FLIGHTLAB at r/R = 0.75, 20 kts.....	132
Figure 4-26 Cl vs Azimuth Angle distribution validation with FLIGHTLAB at r/R = 0.90, 20 kts.....	132
Figure 4-27 Cl vs Azimuth Angle distribution validation with FLIGHTLAB at r/R = 0.50, 40 kts.....	133
Figure 4-28 Cl vs Azimuth Angle distribution validation with FLIGHTLAB at r/R = 0.75, 40 kts.....	134
Figure 4-29 Cl vs Azimuth Angle distribution validation with FLIGHTLAB at r/R = 0.90, 40 kts.....	134

Figure 4-30 Cl vs Azimuth Angle distribution validation with FLIGHTLAB at $r/R = 0.50$, 80 kts	135
Figure 4-31 Cl vs Azimuth Angle distribution validation with FLIGHTLAB at $r/R = 0.75$, 80 kts	136
Figure 4-32 Cl vs Azimuth Angle distribution validation with FLIGHTLAB at $r/R = 0.90$, 80 kts	136
Figure 5-1 Trim analysis variations.....	139
Figure 5-2 Flow chart of the developed trim model	141
Figure 6-1 Mosquito XE [74].....	145
Figure 6-2 Collective vs Forward Flight trim validation with FLIGHTLAB.....	148
Figure 6-3 Longitudinal Cyclic vs Forward Flight trim validation with FLIGHTLAB	149
Figure 6-4 Lateral Cyclic vs Forward Flight trim validation with FLIGHTLAB.....	150
Figure 6-5 Helicopter Pitch Angle vs Forward Flight trim validation with FLIGHTLAB	150
Figure 6-6 Helicopter Roll Angle vs Forward Flight trim validation with FLIGHTLAB	151
Figure 7-1 Bo 105 Masserschmidt [70].....	153
Figure 7-2 Helicopter Roll, Pitch and Yaw Angle vs Simulation Time	155
Figure 7-3 Helicopter Earth x,y and z position vs simulation time	156
Figure 7-4 Helicopter p,q and r rates vs simulation time	157
Figure 7-5 Collective control vs simulation time	158
Figure 7-6 Helicopter x,y and z velocities vs simulation time (in earth reference frame).....	158
Figure 7-7 Helicopter Earth x,y and z positions vs simulation time	159
Figure 8-1 Basic flowchart of the mathematical model developed	161
Figure 8-2 Basic trim model flowchart including the mathematical model.....	162
Figure A-1 Coordinate systems used in the developed mathematical model.....	183
Figure A-2 Transformation between inertial and body reference frame systems ...	185
Figure B-1 Blade element force equilibrium	188
Figure C-1 Load distribution over the rotor disk [28] (Drees, Mangler & Squire and Vortex Wake).....	192
Figure C-2 Load distribution over the rotor disk [28] (Drees, Mangler & Squire and Vortex Wake).....	193

Figure C-3 Hover flight and 9 degrees of collective load distribution	194
Figure C-4 μ : 0.15, Coll.: 6°, Long. cyclic: -5° load distribution	195
Figure C-5 μ : 0.15, Coll.: 6°, Long. cyclic: -5°, Lat. cyclic:-5° load distribution.....	195
Figure C-6 μ : 0.40, Coll.: 9°, Long. cyclic: -8° load distribution	195
Figure C-7 μ : 0.40, Coll.: 9°, Long. cyclic: -7°, Lat. cyclic:-7.5° load distribution...	196
Figure C-8 Blade root total shear force azimuthal distribution.....	196

LIST OF TABLES

TABLES

Table 1 Estimated values of first harmonic inflow gradient coefficient formulas [19]65	
Table 2 Sutherland's Law Coefficients	104
Table 3 Wessex Helicopter main rotor parameters [37]	106
Table 4 OH-58 Main Rotor Parameters [66].....	110
Table 5 Gazalle/SA349 Main rotor parameters [67]	117
Table 6 UH-60 Main Rotor Parameters [31]	128
Table 7 UH-60 Main Rotor twist distribution [13].....	129
Table 8 Mosquito Helicopter parameters.....	146
Table 9 BO105 Helicopter Parameters [31].....	154
Table 10 Westland Wessex helicopter main rotor parameters.....	191

LIST OF SYMBOLS

LATIN SYMBOLS

C_T	: Rotor thrust coefficient
C_D	: Drag coefficient
C_L	: Lift coefficient
$C_{l\alpha}$: Lift curve slope
C_M	: Aerodynamic moment coefficient
C_P	: Rotor power coefficient
C_Q	: Rotor torque coefficient
D	: Drag force
F	: Prandtl tip loss correction
$F_{x,y,z}$: x,y,z axis force component
I_{xx}	: Fuselage roll moment of inertia
I_{yy}	: Fuselage pitch moment of inertia
I_{zz}	: Fuselage yaw moment of inertia
I_β	: Blade flapping inertia
K_1, K_2	: Landgrebe's prescribed wake model coefficients
K_β	: Flapping hinge spring stiffness
L	: Lift force
M	: Total platform mass
M	: Mach number, Aerodynamic moment
N	: Rotor blade number
P	: Air pressure
R	: Rotor radius, air (ideal gas) constant
S_{ref}	: Reference area
T	: Rotor thrust
V	: Total local velocity

W	: Total platform weight
a	: Speed of sound
$a_{x,y,z}$: Translational accelerations
$c_{0,1\dots n}$: Mangler & Squier Inflow model coefficients
e	: non-dimensional flapping hinge position
f	: Prandtl tip loss function coefficient
g	: Gravitational acceleration
k_1, k_2	: Landgrebe's prescribed wake model coefficients
k_x, k_y	: Glauert inflow coefficients
m	: Blade element mass
p, q, r	: Helicopter Euler angle rates
q	: Dynamic pressure
r	: non-dimensional radial location
r_c	: Vortex core radius
u, v, w	: x,y,z axis velocity components
u_{dyn}	: Dynamic velocity component
u_p	: Blade element perpendicular velocity component
u_t	: Blade element tangential velocity component
x	: Helicopter states
x, y, z	: Wake element coordinates

GREEK SYMBOLS

α	: Blade element angle of attack
α_{eff}	: Effective angle of attack
α_{fus}	: Fuselage angle of attack
α_{ht}	: Horizontal tail angle of attack
α_{TPP}	: Rotor tip path plane angle
α_{vt}	: Vertical tail angle of attack

β	: Blade flap angle, blade precone angle
β_0	: Blade coning angle
β_{1c}	: Rotor longitudinal flapping angle
β_{1s}	: Rotor lateral flapping angle
β_{fus}	: Fuselage side slip angle
β_{ht}	: Horizontal tail side slip angle
β_{vt}	: Vertical tail side slip angle
θ	: Helicopter pitch angle, blade element incidence
θ_0	: Main rotor collective angle
$\theta_{1,2}$: Biot-Savart coefficients
θ_{1c}	: Main rotor lateral cyclic angle
θ_{1s}	: Main rotor longitudinal cyclic angle
θ_{shaft}	: Mast tilt angle
θ_t	: Main rotor blade twist angle
θ_{tr}	: Tail rotor collective angle
λ	: Induced velocity ratio
λ_0	: Mean inflow ratio
λ_c	: Climb velocity ratio
λ_i	: Local induced velocity ratio
μ	: Advance ratio, air viscosity
π	: Pi number
ρ	: Air density
σ	: Rotor solidity
σ_{ij}	: Influence coefficient matrix
φ	: Helicopter roll angle, blade element inflow angle
χ	: Wake skew angle
ψ	: Helicopter yaw angle, azimuth angle
ψ_w	: Wake age (wake element position)
Ω	: Rotor rotational speed
Γ	: Circulation strength

SUBSCRIPTS

- i : inertial reference frame
- b : body axis reference frame
- h : main rotor hub reference frame
- bl : main rotor blade reference frame
- tr : tail rotor hub reference frame
- ht : horizontal tail reference frame
- vt : vertical tail reference frame

CHAPTER 1

INTRODUCTION

Within the last few decades, the interest in more accurate and reliable helicopter flight dynamics mathematical models has been increased. There are several factors behind this. One reason for that is the increase in interest for more reliable and maneuverable helicopter came with the necessity of more accurate flight dynamics mathematical models. With the advances in construction, design and controllability technologies, the common interest has been concentrated to lighter and more maneuverable helicopters. As a consequence the interest on such helicopters brought more complex helicopter configurations for which more accurate and reliable mathematical models are essential. Today's high fidelity flight control systems require more accurate mathematical models that can define the dynamic response of the helicopter under both steady and unsteady transient flight conditions accurately, which may be considered as another reason. Also in order to understand the physical mechanism associated with helicopter specific problems such as rotor dynamics and aerodynamics in any flight conditions, mathematical models that define both rotor and helicopter dynamic behaviors accurately are required. A third reason for the increase of interest in helicopter mathematical models appears at preliminary design stages. In preliminary design stages of helicopters or helicopter autopilots, computationally affordable and simple, yet, accurate enough mathematical models are valuable in order to estimate approximate performance specifications. In addition, the initial designs of new components or sub-systems that are planned to be implemented on a platform such as helicopter, may be modeled by empirical or analytical models and integrated to a flight dynamics mathematical model in order to analyze the individual performance as well as the effect to whole helicopter performance.

When helicopter flight dynamics is considered, the force and moments generated by main and tail rotors are the main contributors to helicopter dynamic response under any flight condition. For an accurate and reliable helicopter mathematical model, it is essential to calculate the load contributions from main and tail rotor to the total helicopter force and moments, accurately. Besides, the success of a mathematical model lies beneath the ability of modeling the main and tail rotors accurately enough, which are the main sources of aerodynamic loads associated with flight conditions and maneuvers, so that rotor dynamic behavior and loads transferred to the fuselage, are determined correctly. On the other hand, mathematical models used in real time piloted simulators or flight control systems have to be fast enough to enable user to simulate trimmed or untrimmed maneuvers and give perturbations to obtain the desired behavior of the helicopter. Therefore, accurate, computationally efficient and fast flow prediction over a rotor is essential for helicopter flight dynamics mathematical models and has been a continuous problem for engineers over a half century.

There still is a powerful analytical method, blade element method [2, 19], which can calculate aerodynamic force and moments generated by rotor accurately if the inflow distribution is known. The accuracy of the blade element method depends on the inflow distribution data resolution and to the parameters that are required for modeling and defined by the user. Therefore, for an accurate aerodynamic, inflow distribution over the rotor disc should be calculated accurately. In addition to the flight conditions and wake induced velocity, one of the main inflow contributors to rotor is blade dynamic behavior. Relative velocities on a flapping could change the whole dynamic behavior of the rotor. In addition with the existence of hubs which enable blades to flap freely or damped, result in tilt in tip path plane, which would also tilt the thrust vector of the rotor. Tilt in thrust vector results in change in the force and moments that are transferred to the hub and to the fuselage. Therefore a good flapping model is essential for an accurate and reliable mathematical model, in order to capture blade dynamic behavior including the tip path plane dynamics.

Since the first helicopters, low forward speed and limited range have been the biggest two weaknesses for helicopters when compared with fixed wing aircraft.

In 1950's and 1960's the interest was concentrated on compound helicopters which eliminates the weaknesses while maintaining the advantages of helicopters over fixed wings. With the advances in construction and design methods, nowadays the trends is again headed to compound helicopter configurations which combines rotary and fixed wing aircrafts principles in order to reach high forward speeds as well as have hover capability. This brings interest on modular structured mathematical models. Modular structure enables user to exclude or attach component models such as aerodynamic surfaces, landing gears, auxiliary bodies, stores or rotors so that any configuration is modelled without requiring a new mathematical model. Therefore, in order to model the complex configurations of compound helicopters, mathematical models have to be built with a flexible, modular and selective structure, so that it can easily be modified and can capture the dynamic behavior of the platforms. Otherwise a new mathematical model would be necessary for each new configuration.

Keeping in mind all these aspects, an accurate, reliable and widely used mathematical model should comprised of a good aerodynamic and dynamic model of the main and tail rotors, should have a modular and selective structure and should be computationally cheap.

In this study, a mathematical model is developed according to all the aspects mentioned. Several analytical and empirical models for aerodynamic force and moment calculations are implemented and selection option is left to the user. According to the aim of the analysis, the accuracy and computational cost can be chosen. For example if a trim analysis and critical load investigation is to be studied, then higher fidelity model can be activated, whereas if a dynamic response of a helicopter under pilot inputs is to be investigated then lower accuracy but faster models can be used. In addition modular structure enables user to expand and improve the desired modules or gives him/her the option to replace them with higher or lower fidelity models. With the ability of excluding or attaching new modules and components the mathematical model can easily be modified to analyze various systems such as wind turbines, compound helicopters, intermeshing, tandem or classical helicopter configurations.

The mathematical model developed behaves like a system consisting of sub systems that they define the helicopter and its components. The non-linear mathematical model developed is suitable for simulators, trim analyses, aerodynamic force and moment studies, critical loads and case investigations and maneuver modeling. Each helicopter component is approximated as a point mass, generating a force and moment on its center of gravity. The forces and moments for all the components are transferred to the center of gravity of the whole helicopter in order to obtain total force and moments that would define the helicopter dynamic behavior. Then the dynamic behavior of the helicopter can be calculated by integrating the linear and angular accelerations in time domain.

1.1 Initial Mathematical Model

To start with an initial mathematical model which defines the basic helicopter dynamic behavior is developed and validated. Afterwards, modules such as main and tail rotor aerodynamic and main rotor tip path plane dynamics models are replaced with higher fidelity modules that described the force and moments generated more accurately. The initial mathematical model, similar to minimum complexity mathematical model [6], is built from simplified force and moment equations. Main rotor aerodynamic force and moments are calculated with blade element momentum theory [19] which combines classical strip element method with momentum theory. The induced velocity distribution over the rotor disc for both hover and forward flight conditions are calculated from momentum theory. Blade's dynamic responses under blade geometric and structural properties, and pilot controls, are calculated by the method of Chen [41] where blades are assumed rigid. Rigid and uniform structure assumptions are also applied to inertial and centrifugal force and moment calculations. The force and moment distributions are then integrated along the blade and azimuth angle [Figure 1-1]. Combined with inertial and centrifugal forces, hub force and moments are also calculated and transferred to the fuselage.

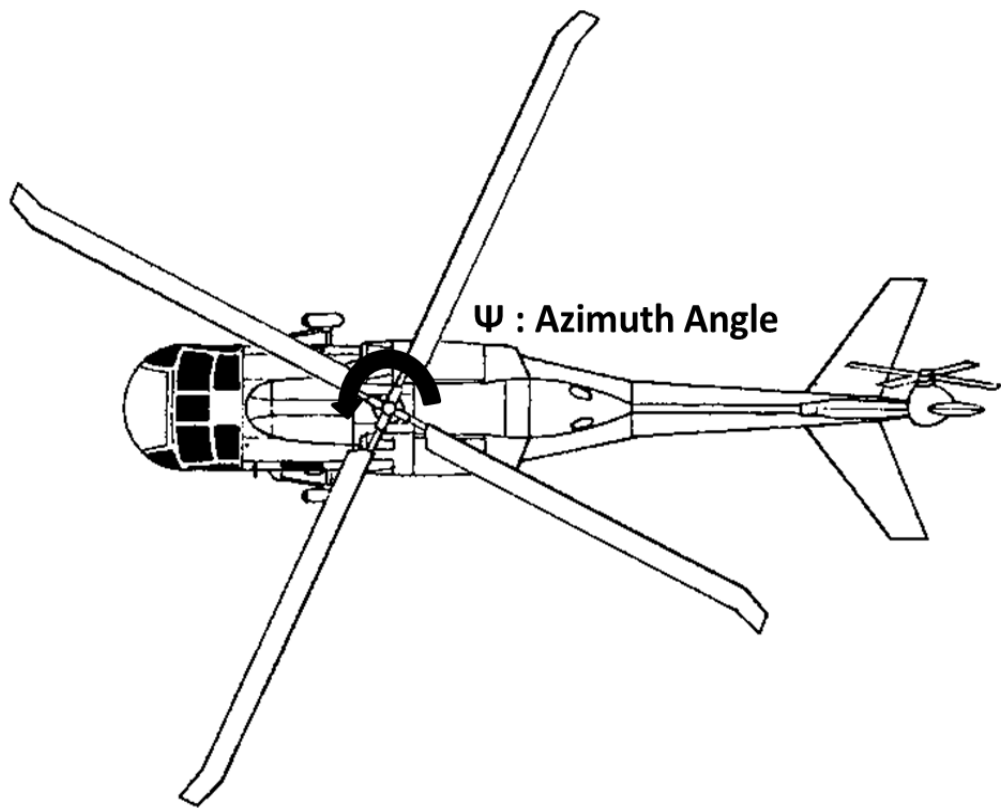


Figure 1-1 Azimuth angle definition

Tail rotor aerodynamic force and moment are calculated in a similar way with the main rotor. The induced velocity distribution over the disk is calculated from momentum theory and aerodynamic loads are obtained with blade element method. Unlike to the main rotor, tip path plane dynamics of the blades are ignored, resulting in a hingeless like hub type. Force and moments transferred to the fuselage are calculated from spanwise and azimuthwise integrations of aerodynamic forces. The absence of flapping dynamics, simplifies the loads generated by tail rotor while eliminating centrifugal and inertial force and moments.

Fuselage, horizontal and vertical tail models, which are replaced with higher fidelity models in final mathematical model, are initially modeled with simplified

equations of force and moments neglecting stall, non-linearity in aerodynamic forces and force components that are in second order importance.

1.2 Refined Main and Tail Rotor Aerodynamic Models

The success of a mathematical model depends on the accuracy and fidelity of the main and tail rotor aerodynamic models since they are the main force and moment contributors. Therefore the basic aerodynamic modules implemented in the initial mathematical model are refined for higher accuracy and fidelity. For main and tail rotor aerodynamic models, in the initial mathematical model, blade element momentum method was implemented. Aerodynamic force and moments were calculated by classical strip element method while induced velocity was derived from uniform inflow model [19, 28]. The aerodynamic module built from simplified equations for main and tail rotor is replaced with a higher fidelity aerodynamic module which consists of several inflow prediction methods and an iterative tip path plane dynamics model.

Blade element methods, which are widely used, are still very powerful methods in calculation aerodynamic force and moment distributions radially and azimuthally. The strength of this method comes from its simplicity. Blade is divided into strips. Each strip defines a blade element. If the velocity components that each blade element encounter is known, than using airfoil aerodynamic coefficients which may be obtained by table look-up methods or lift curve slope and linearity assumption, aerodynamic force and moments generated by each blade element can be calculated with simple lift, drag and moment equations. Therefore the main aspect that determines the accuracy of blade element methods is the prediction method of induced velocity.

The aerodynamic model that is replaced with blade element momentum method that is implemented initially is built up with several methods at various levels of fidelity. Method for hover and forward flight conditions are developed separately. For hover flight cases, momentum theory combined with Prandtl's tip loss function is implemented for initial induced velocity distribution. Blade element method is used in order to calculate initial load, circulation distribution on rotor disc and initial thrust

value of the rotor. The higher fidelity method implemented for hover flight cases is vortex theory, which takes rotor wake and wake induced velocity into account. Rotor wake geometry is predicted by Landgrebe's prescribed wake model [53]. Wake geometry and initial circulation distributions are used to predict the whole vortex sheet strengths, tip and roll-up vortex strengths. Wake induced velocity distribution on the rotor disc is calculated by the help of Biot-Savart rule [36]. As a result taking the wake induced velocity into account, tip and root losses are modeled and aerodynamic loads are predicted. The option of induced velocity model is left to user according to the aim of the analyses.

On the other hand for forward flight cases, a modified uniform inflow model is used in order to determine the required initial values for non-uniform induced velocity model. Uniform inflow distribution calculated from momentum theory is modified by Drees [18] so that induced velocity distribution depends on both radial and azimuthal location. Calculated initial thrust is used in Mangler & Squire's non-uniform induced velocity model [19].

Mangler & Squire inflow is a linear combination of two types of inflow distributions [19]. With the combination of two types of inflow distributions and the initial values obtained from uniform inflow distribution, circulation and inflow distribution values are calculated and supplied to vortex theory as initial values.

Vortex theory as the highest fidelity induced velocity model for forward flight along the models implemented requires wake geometry and vortex strength predictions. Unlike hover, in forward flight vortices from adjacent blades in rotor wake interacts with each other causing wake geometry to be distorted. Similar to vortex theory for hover flight, wake geometry is predicted with prescribed wake models. Two wake geometry prediction models, undistorted wake model and Beddoes' distorted wake model [57], are implemented for forward flight conditions. For forward flight, unlike hover, circulation distribution is not symmetrical over the rotor disk. Therefore vortex strengths of the trailing vortices are not constant and are changing with azimuth angle. Vortex theory for forward flight calculates the wake induced velocity with Biot-Savart rule [36] while taking the non-uniform and non-symmetric circulation distribution over the rotor disk into account.

Blade dynamic behavior is determined with an iterative process between tip path plane dynamics module and aerodynamic module. Starting with the initial values supplied to the mathematical model, aerodynamic moment generated at the blade root and flapping angles are exchanged between tip path plane dynamics module and aerodynamic module until convergence is obtained. The developed tip path plane dynamics module takes centrifugal forces, inertial forces, if exists flapping spring, and Coriolis accelerations into account while calculating flapping angle which is also a function of azimuth angle.

As the mathematical model developed is built with a selective structure, each inflow model could be used individually. Therefore, the accuracy, fidelity and computational cost for the mathematical model could be decided by the user.

1.3 Trim Model

Unlike fixed wing aircraft, for rotary wing aircraft it is not suggested to decouple longitudinal and lateral trim solutions [2]. It is not possible to completely separate longitudinal and lateral dynamic from each other. Therefore longitudinal and lateral trim controls have to be solved simultaneously in order to obtain an accurate trim solution.

In this study, an optimization method is used as a trim model. The optimization method iterates six variables; main rotor collective, main rotor longitudinal and lateral cyclic, tail rotor collective and helicopter Euler phi and theta angles, in order to minimize the objective function, which is defined by square roots of squared linear accelerations and angular velocities.

Initial values are used in order to find the trim solution as a local minimum of a mathematical function with six variables. The better the initial values, the faster the trim iteration is. Therefore, for complex maneuvers, initial values may be set from trim conditions of simple maneuvers.

Again the selective structure enables user to add and subtract variables from objective function so that the maneuver is desired could be modeled. For example if a pull up maneuver desired to be modeled, then z component of the linear

accelerations and pitch attitude of the helicopter are left out of the objective function and assigned constant values that represent the desired maneuver. Then, the optimization process determines the pilot controls and helicopter attitude that result in zero acceleration for the maneuver given in the objective function.

1.4 Validation

The mathematical model developed in this study is validated with both test data that is available in literature and FLIGHTLAB, a tool widely used in helicopter mathematical modeling, analyses and simulation [13]. Same helicopter is modeled with FLIGHTLAB at same fidelity with each aerodynamic module developed. Main rotor collective and cyclic, tail rotor collective, main rotor flapping angles, main rotor hub forces, main and tail rotor power required values and helicopter accelerations are analyzed and compared for both trimmed and untrimmed flight conditions. For example, at first step velocity sweep analysis is done at sea level for leveled forward flight cases with FLIGHTLAB and pilot controls for trimmed conditions are extracted from analyses. These pilot controls are used as inputs for the mathematical model and helicopter linear and angular accelerations, flapping angles and hub forces generated by main rotor are compared and validated. At second step, in order to validate the trim model, at several flight conditions analyses are conducted and pilot controls for trimmed cases are compared.

On the other hand, each aerodynamic module is validated with test data available in the literature. Force and moments generated by main rotor, trim values of pilot controls under several flight conditions and helicopter attitudes are compared and validated with flight test data of several helicopters.

1.5 Goals & Outputs

The main goal of this study is to develop a mathematical model with a modular structure with refined rotor aerodynamics models so that dynamic behavior of the helicopter is captured accurately. The model developed is useful for flight dynamics analyses, simulators and preliminary designs. For flight dynamic analyses and simulators, helicopter behavior can be modeled under any pilot input. Trim

conditions and helicopter attitudes for trimmed flight conditions can be calculated with the mathematical model running under the trim model developed. Flight performances for trimmed flights or maneuvers can be analyzed. Besides, time based integration enables user to simulate a maneuver or a mission profile and flight performances and requirements can be calculated. For example with simple modifications, fuel consumption and fuel weight for a single flight or a complex mission can be calculated.

The mathematical model developed can also be used in preliminary design phase of helicopter configurations. Main rotor distributed and integrated loads are calculated and critical loads, location of critical loads and under what conditions critical loads occur can be obtained. This would give an initial idea to engineers at preliminary design stage of main rotor and helicopter and would enable engineers to estimate preliminary performance values of the configuration.

The study done throughout this thesis is supported by the Rotor design and infrastructure development Project (ROTA) which is prosecuted in Turkish Aerospace Industries (TAI) with the support of Scientific and Technological Research Council of Turkey (TUBITAK). Besides the main rotor aerodynamic module developed in this study is used and improved by the ROTA Project as it has evolved. Therefore ROTA Project has directly contributed to the main rotor aerodynamic module and as a consequence to the mathematical model developed. The main rotor aerodynamic module developed in this study will called as xBEM from this point. x represents the helicopter group in TAI and the remaining represents Blade Element Method. On the other hand, the mathematical model developed throughout this study will be called as HELCOMAS from this point. HELCOMAS is an acronym for Helicopter Comprehensive and Modular Modeling, Analysis and Simulation tool.

CHAPTER 2

LITERATURE REVIEW

2.1 Mathematical Flight Dynamics Model

One of the biggest challenges at helicopter design stage is estimating the helicopter flight dynamic characteristics. Generally these characteristics are obtained with flight tests at flight conditions within the operational envelopes of the platform. However, it is not efficient, feasible and possible to do flight tests for every critical conditions. Therefore, accurate analysis and simulations play essential role in filling the incomplete envelope. Accurate analyses and simulations require a good aerodynamics, dynamics and control system representations of the helicopter. Therefore it is essential for manufacturers and designers to have an accurate and modular shaped mathematical model which can be also easily modified so that complex and unusual configurations are modeled.

A helicopter flight dynamics mathematical model usually consists of a 6 degree of freedom rigid or elastic body equations of motions where force and moment contributions from each component are calculated individually. The model developed by Cvetkovic [1] can be a basic example of a mathematical model of a helicopter which is used in dynamic analyses of Mi-8 helicopter with the new composite main rotor blades designed at Belgrade Faculty of Mechanical Engineering. The mathematical model developed is built from simple 6 degrees of freedom rigid body equations of motions, where main rotor induced velocity is obtained from momentum theory with the assumption that helicopter rotor dynamics can be separated into longitudinal and lateral motions. However, although decoupling of longitudinal and lateral dynamics brings great simplification, helicopter longitudinal and lateral dynamics are strongly coupled and for accurate and reliable mathematical models it is not feasible to decouple them [2]. The nonlinear

mathematical model developed by Talbot et al. [3], includes a total force and moment model of a single main rotor helicopter, which also uses six degree of freedom rigid body equations of motion, with coupled longitudinal and lateral dynamics of the helicopter. Combined with six rigid body and the rotor rotational degree of freedom, coupled three rotor flapping degrees of freedom equations are solved simultaneously for piloted simulations. Another helicopter mathematical model, which calculates main rotor induced velocity from simple momentum theory, is the one developed by Salazar [4]. Coupled rotor flapping dynamics, only thrust generating tail rotor and classical six degree of freedom rigid body equations of motions are combined in order to obtain the linear and angular acceleration equations.

In order to understand the physical mechanism associated with helicopter specific problems such as rotor dynamics and aerodynamics in any flight conditions, mathematical models that defines both rotor and helicopter dynamic behaviors accurately are required. In that manner, the mathematical model developed by Takahashi M. D. [5] included rigid, hinge restrained rotor blades giving the flap, lag and torsion degree of freedoms to the blades. The induced velocity distribution over the rotor disc is calculated with three state nonlinear dynamic inflow models and the main rotor downwash effect on empennage surfaces and tail rotor is included. Except from all of these, a helicopter flight dynamic mathematical model, so called the Minimum Complexity Model, developed by Heffley and Mnych [6] have been commonly used in several studies for the last 20 years [7, 8, 9, 10, 11]. Minimum Complexity mathematical model, which is a buildup of individual vehicle components described by equations addressing the features associated with those components, enables user to be able to model the helicopter with only the basic data sources such as flight manuals or system component specifications. Computational delays, cost and inflexibility of the very sophisticated mathematical models are the main factors that were considered during the development of this model. As being an example of minimal complex helicopter mathematical model while requiring only basic data on helicopter to be modeled and the structure which allows improvements on any individual component made the minimum complexity mathematical model to be used extensively as a base model [7, 8, 9, 10, 11]. For example Hilbert revised the general minimum complexity mathematical model for

UH-60 helicopters to include fuselage aerodynamic force and moment equations that are specific to the UH-60, a canted tail rotor, a horizontal stabilizer with variable incidence and a pitch bias actuator [7]. Another update to the minimum complexity model is done by Yilmaz [8], in order to implement higher fidelity simulation components such as dynamic inflow model Peters-He [47, 48, 49], horizontal tail contribution, improved tail rotor model etc. The strength of mathematical models like minimum complexity lies beneath the opportunities of modifying or manipulating the fidelity of the model. The mathematical model developed by Munzinger [9] can be also an example for similar studies. It is based on the minimum complexity mathematical model however in order to increase the fidelity of the simulations, additional components like control rotor, actuator models and sensor models are added. Besides the minimum complexity mathematical model and its derivatives, a mathematical model for a model scale helicopter has been developed by Kim S. K. and Tilbury D. M. [12]. First principles and basic aerodynamics are used in order to derive the six degree of freedom equations of motion of the helicopter. The mathematical model developed is then used to analyze the flybar and main rotor blade interactions and investigate the effect of flybar on stability of the model helicopter. This study shows that mathematical models are important simulation, analyses and identification tools not only for piloted helicopters but also for model and unmanned rotorcrafts.

Except from helicopter flight dynamic characteristics, at both preliminary and detailed design stages of the helicopters, load analysis on helicopter components are also required. Analysis of aerodynamic force and moments, inertial loads or if exists centrifugal forces acting to the components of the helicopter, are essential in the design and assembly stages of both individual components and whole system. Besides also these detailed analyses are a required for critical flight conditions and maneuvers. Therefore mathematical models with higher fidelities and more sophisticated models, while having low computational costs are essential. With the advances in computation technologies, larger and more sophisticated mathematic models can be used. At this point, comprehensive rotorcraft codes including the content for flight dynamics analyses show their importance. FLIGHTLAB [13], which is built in a modular structure where each module corresponds to a physical or logical subsystem of the aircraft model, can be pointed as one of the well-known

low-cost, selective high fidelity, reconfigurable and high productivity simulation and analysis tool. Flight dynamics analyses, such as trim conditions, linear and nonlinear response of the helicopter can be studied with a selective fidelity level. Another example for comprehensive rotorcraft codes is CAMRAD [14, 15] developed by Johnson Aeronautics with the versions CAMRAD, CAMRAD/JA and CAMRAD II. CAMRAD, a comprehensive model of rotorcraft aerodynamics and dynamics, combines structural, inertial and aerodynamic models in order to analyze rotor and helicopter performance, loads and dynamic responses. Similar to FLIGHTLAB [13], variable fidelity models can be selected by the user.

The base mathematical model, developed in this study without the aerodynamic refinements can be placed between classical flight dynamics mathematical models such as Minimum Complexity Model [6] and more sophisticated comprehensive rotorcraft analysis codes such as FLIGHTLAB and CAMRAD [13, 14]. Similar to comprehensive rotorcraft tools, various fidelity models are implemented and built as selective structure and reconfigurable according to the platform. On the other hand, it is similar to the classical mathematical models [4, 6, 7] that are used in real time simulators whose fidelities are lower however overall calculations are much faster and just accurate enough to analyze the flight dynamic response of the platform.

2.2 Refined Main and Tail Rotor Aerodynamic Models

As stated by Heffley [6] desired features of a mathematical model from aerodynamic point view are accurate main rotor induced velocity computation, realistic power requirements calculations over desired flight envelope, correct transition from hover to forward flight and accurate first order flapping dynamics for main rotor (coupled or decoupled).

The blade dynamic response and aerodynamic force and moments generated by the helicopter rotor are strongly dependent to the induced velocity distribution. This was also stated by the study of Wheatley [15]. The conclusion of the study was “the blade motion is critically dependent upon the distribution of induced velocities over the rotor disc and cannot be calculated rigorously without the accurate

determination of the induced flow”. Therefore, as being dependent to the blade dynamic response, in order to calculate the aerodynamic force and moments generated by the rotor blades accurately, a good induced velocity prediction model is essential.

As the simplest approach, basic rotor performance can be analyzed by Rankine-Froude momentum theory [2, 19] which enable the derivation of first order rotor thrust and torque evaluation and derives the basics of higher fidelity induced flow models. Despite being a very basic inflow prediction model, the momentum theory can be effectively used in mathematical models especially with a lower fidelity aerodynamic model in which the main purpose is to have a general understanding of the dynamic response of the helicopter. In the study of Salazar [4] as an example, helicopter momentum theory for hover, climb and advance flying conditions were used to develop mathematical equations of the helicopter.

The reason why momentum theory is at the lowest fidelity level is because it suggests a uniform induced velocity distribution over the rotor disk. However, in reality the induced velocity is highly non-uniform, since because tip vortices trailed in helices from each blade which are the dominant factors in the rotor induced velocity, distort the uniformity of the induced velocity distribution over the disk and it is found that the uniform inflow assumption is far from satisfied with real rotors [2]. Therefore a non-uniform inflow model is essential for an accurate and reliable mathematical model.

Non-uniform inflow prediction over a helicopter rotor disc for both hover and forward flight conditions is an issue for which engineers have been working on for nearly a hundred years. One of the early models which is a simple first harmonic non-uniform inflow model proposed by Glauert in 1926 [17], was developed with combination of experimental results and uniform inflow model. The model developed at that time was for autogyros and the gradient coefficient value which gives non-uniformity to uniform inflow distribution was unspecified. After seven years the unspecified gradient coefficient was derived and correlated from autogyro flight test by Wheatley [15]. For hover flight cases, Prandtl proposed a function [19] that computes tip-loss effects which is built up on Betz tip-loss factor idea. Instead of assuming a value for tip loss factor, Prandtl offered a tip loss function having a

purpose “to approximately model the high induced losses produced by the trailing vortices generated from the tip and root side edges of the blade, flow physics that are included in the more advanced vortex wake model” [19]. The negligible cost of the method and being an effective tool for the preliminary analysis of spanwise distributions of air loads provoked Prandtl’s Tip Loss function to be used extensively in wind energy and helicopter field. [61, 62, 63, 64]

However for forward flight cases, the unsymmetrical flow conditions that blades encounter result in non-uniformity over both spanwise and azimuthwise induced flow distribution. Therefore non-uniformity of the inflow over azimuthwise direction has also to be considered. Therefore, using a wake geometry which is modified from Coleman’s simple cylindrical vortex wake, Drees [18, 19] has determined the gradient formula which depends on both wake skew angle and the advance ratio. Drees inflow model, which is also implemented to the main rotor aerodynamic model in this study, suggests coefficients that result in nonsymmetrical inflow distribution over both spanwise and azimuthwise directions and it is used extensively in literature [14, 21, 22, 23, 25]. Another inflow model implemented on this study is Mangler & Squire’s non-uniform inflow model [19] which is based on potential theory and valid for advance ratios greater than 0.1. However Bramwell [26] modified the initial induced velocity calculation which can be related with the Mangler & Squire model so that it can be also used for hover flight conditions. The usage of Mangler & Squire inflow model can be seen in the study of Gläßel et al. [33] which investigates blade vortex interactions, neural networks for blade vortex interaction, and system identification. One of the well-known studies done by Castles and De Leeuw [35] before the prescribed wake models and wake induced velocity were available with the advances in computation technologies presents a practical model for computing the approximate values of the normal component of the induced velocity. The wake is modeled as vortex rings and wake geometry consists of straight elliptic cylinder.

Another well-known and extensively used induced flow model was developed by Peters et al. [47] which expresses the induced velocity in Fourier series and Legendre functions. It is stated in the study presented in 1987 that “The theory implicitly includes dynamic inflow theory, the Prandtl/Goldstein static inflow

distribution and Theodorsen theory.”[47]. Then, 2 years after, Peters and He [48] validated the induced velocity model with a set of Laser-Doppler Velocimetry inflow measurements made by the ARMY Labs at NASA Langley. The results showed that the induced velocity model is also effective in forward flight. In addition also in the study of Peters and He [49] comparisons of finite state inflow model developed with vortex-filament methods and experimental data show good correlation for both hover and forward flights.

The configurable fidelity, computationally low cost and accuracy of the Peters-He inflow model [47, 48] resulted in being one of the most extensively used inflow models by the studies on rotor aerodynamics, rotor aerodynamic mathematical models, helicopter flight dynamics mathematical models that are also used in simulators and even in comprehensive rotorcraft codes which leave the option to select the inflow model from a bunch of different fidelity models to the user.[13, 14, 15, 50, 51, 52].

For flight dynamics and control applications, simple harmonic, finite state, non-uniform inflow models for induced velocity calculations have been used extensively. [27]. However, as the interest in more reliable, lighter and maneuverable helicopters increased, the interest in more accurate and reliable mathematical and aerodynamic models increased. Besides, with the advances in computational technologies, more sophisticated and complicated prescribed and free wake model codes became available. This can be interrelated with the increase in the mathematical models that use refined aerodynamic models in the last decades. The studies of Huh and Liu can be seen as examples for refined aerodynamic models for mathematical models. The study done by Huh [29] which is an aerodynamic mathematic model of a hovering helicopter rotor for which wake geometry and loading characteristics are analyzed using axisymmetric vortex sheet and free wake analysis. The study of Liu [30] is a comprehensive rotorcraft analysis with a new representation of wake vortex structure. Another example for refined aerodynamic model including wake geometry and wake induced velocity prediction for a flight dynamic mathematical model, is the coupled rotor-fuselage flight dynamic simulation model developed by Theodore [31] which includes maneuvering wake model and coupled flap-lag-torsion flexible blade representation. In addition, Reddy

K.R., Stewart C.J. [32] built the aerodynamic component of a simulation tool by using vortex sheet to represent near wake of the rotor and vortex rings to represent the intermediate and far wakes for which comparison and validation of the blade loadings with the published test data have been done.

For estimating the wake geometry, prescribed wake models are quite common [34]. Mostly, variables of prescribed wake models in the formulation of wake geometry are derived from wake flow visualization studies with several different rotor configurations. As a result, wake geometries are related to rotor parameters so that they are in generic structure that can be applied to any rotor if desired parameters are known.

The aerodynamic model [28] for the mathematical model developed in this study, consists of several non-uniform inflow models and vortex wake theory combined with prescribed wake models for both hover and forward flight conditions in a selective structure like comprehensive analysis codes [13, 14, 23, 24] Wake geometry for hover flight cases is predicted with Landgrebe's prescribed wake model [19, 54]. A set of parameters related with the rotor thrust values, rotor solidity and blade twist were determined with experiments by Landgrebe [53] and a set of equations are derived so that the wake geometry in hover flight condition is determined quickly. The vortex sheet geometry is described as vortex filaments when combined forming a linear sheet from tip to the root of the blade. The parameters which are all empirical constants are listed in the study of Egolf and Landgrebe [54]. Young's study [55] in which a method for calculating the performance of a helicopter in hover flight conditions was presented can be pointed as an example usage of Landgrebe's Wake model for hover. In addition Ramasamy's work [34] where Landgrebe's Wake Model is used to model and compare axial convection rates for untwisted and twisted blades is also an example of the usage of Landgrebe's Prescribed Wake Model.

On the other hand, for forward flight conditions two different prescribed wake models are implemented to the mathematical model developed in this study. The first one is Undistorted Wake Model [19, 56]. The undistorted wake model assumes that the wake forms a helical surface and is swept down by the average induced velocity of the rotor. Therefore it neglects the distortion, unsymmetrical circulation

distribution and vortex strengths and the blade vortex interactions. However, because of its simplicity it is assumed to be applicable for lower fidelity models or especially for high forward speeds. For more accurate aerodynamic modeling, a higher fidelity prescribed wake geometry model is implemented. The Beddoes Distorted Wake model [19, 57] divides the wake into regions according to the influence of the main rotor on vortex filaments. The distortion generated by the main rotor is then added to the wake geometry resulting in higher fidelity wake geometry model. It is stated in the study of Szymendera that “Beddoes model showed good agreement with free wake models but was considerably less computationally intensive” [59]. This shows the reason of extensively usage of Beddoes Prescribed Wake model which is a model for high resolution air load calculations [57, 60]. An example of the usage is the study where Lee et al. [58] developed an aerodynamic analysis module as a part of comprehensive rotorcraft program in which wake geometry is represented by Beddoes Wake Model. Another example is the study of Gläßel et al. [33] which investigates blade vortex interactions neural networks for blade vortex interaction system identification

Vortex wake theories generally use vortex sheets, vortex rings and trailing vortices in order to represent the wake behind a rotor [19]. Strong tip vortices, root vortices or the whole vortex sheet geometry is determined from wake geometry while the velocity induced on the rotor disc by the presence of wake is calculated from Biot-Savart’s law [19, 36]. Vortex filaments are generally divided into line or curved vortex elements and the induced velocity on the rotor disk is calculated from the integration of whole vortex elements’ inductions in the wake of the rotor to the point at which computation is done. In the formulation of Biot Savart’s law [19, 36], except from the wake geometry and vortex strengths, vortex core size and vertical structure appears to be one of the most dominant factors affecting the magnitude of the induced velocity. Besides, vortex core size has influence on rotor performance, noise, blade structural loads and rotorcraft vibration [37]. Therefore, it is essential to estimate the vortex core size of the vortices, especially tip vortex. As being an important factor on rotor performance, vortex core size has been studied extensively. It is stated in the study of Young [37] in which analytic expressions are derived for estimating the core size of tip vortices that the greater the rotor thrust, the larger the vortex core size and the more efficient a rotor the smaller the vortex

core size. In addition the study of Young [37] stated that “vortex core size initially decreases for low axial-flow advance ratios, but for large advance ratios core size asymptotically increases to a nominal upper limit”. Another study on vortex core size is done by Ramasamy et al. [38] on micro-rotors, proposes a value of apparent to actual viscosity ratio, so that calculated growth rate, fits well with the growth rate of the vortex core estimated from the measurements. In addition studies of Mahalingam and Komerath [39] and Wong et al. [40] both in which initial measurements of the near wake of a 2 bladed teetering, untwisted, square tipped rotor in forward flight are done by LDV techniques, a general characteristics and behavior of vortex core size and vortex core axial velocity are determined.

Vortex core model used in this study is developed with the combinations of Squire’s Core Growth model [38] and the observations of Mahalingam and Komerath [39] and Wong et al. [40]. In the developed model, wake is divided into three regions, so called near, roll-up and far wakes, and vortex core sized are calculated separately for each region which gives an increasing core size with wake age.

2.3 Tip Path Plane Dynamics

Since the phenomenon of increasing rolling moment generated by the main rotor with increasing forward flight is eliminated by Cierva by installing mechanical hinges that allows the blades to flap [42], modeling flapping dynamic response of the blades became one of the most challenging issues for rotor mathematical models. As aerodynamic force and moments generated by the rotor are affected by the tip path plane dynamics of the rotor [42, 44], for an accurate rotor mathematical model, it is essential to model the blade dynamic behavior efficiently [41]. As being strongly dependent on the aerodynamic force and moments, centrifugal and inertial forces in flapping equations are generally combined with the aerodynamic mathematic model of the rotor and are derived according to it. For instance in the study of Chen [41], the aerodynamic model is immersed to the flapping dynamics equations where aerodynamic force and moments equations are derived from simple analytical methods. Another example is the work of Talbot and Corliss [45] at which a mathematical model of UH-1H helicopter is developed for dynamic simulations. In

the main rotor mathematical model, the flapping equations contain force and moment coefficients from the rotor. As rotor flapping is dependent on the aerodynamic forces and aerodynamic forces are dependent to flapping dynamics, blade flap angles and blade aerodynamic force and moments should be solved simultaneously. This can be seen in the flapping dynamics equations derived by Padfield [46] or Prouty [42, 43] which contain aerodynamic force and moment terms so that the aerodynamic model and tip path plane dynamics models are merged together.

The flapping dynamics model developed in this study uses the coupled flapping equations derived by Chen [41, 44] however the aerodynamic model is separated from the flapping equations. Therefore aerodynamic force and moments are solved separately and implemented into the flapping equations. This enables the selective structure so that different aerodynamic models can be used without deriving new flapping equations for each of them, as long as aerodynamic force and blade flapping angles are exchanged between flapping dynamics module and aerodynamic module. The iteration between aerodynamic model and flapping dynamics model continues until longitudinal and lateral flapping angles converge.

CHAPTER 3

MATHEMATICAL MODEL

3.1 Introduction

The mathematical model developed in this study defines a helicopter and all helicopter components that are force and moment contributors to the system with empirical and analytical models, in order to describe rigid body dynamics of the helicopter. Helicopter components such as fuselage, horizontal tail, vertical tail, tail rotor and main rotor are mathematically modeled in order to formulate the whole helicopter system as a set of first order, coupled and non-linear differential equations.

The mathematical model is developed in a modular structure where each component model is independent from each other. Therefore, the module that is desired to be developed or altered can be replaced without changing others. The modules are developed with specific inputs and outputs, so that as long as the improved or altered replacement of the desired module has the same structure that ensures the definite input and outputs, the mathematical model would continue to work without any problems.

Several models with different complexity and fidelity are implemented for each helicopter component. These models are implemented in a selective structure so that according to the aim of the analyses, the complexity, fidelity and accuracy of the calculations can be chosen. The option to choose the fidelity, complexity and accuracy of the whole mathematical model, brings the ability to be used in a wide range of analyses. With higher fidelity and accurate models, the mathematical model developed can be used as a comprehensive analyses tool. Detailed aerodynamic force and moments generated from each helicopter component, main rotor and tail rotor blade load distributions and the locations on the blades where maximum and

minimum aerodynamic loadings occur, critical loads and locations of critical loads for main rotor under trimmed or maneuvering flight conditions can be determined. The analyses can be used at preliminary helicopter design stages, preliminary helicopter rotor sizing activities or blade structural design stage where radial and azimuthal aerodynamic load distributions are essential. On the other hand, low fidelity and accuracy model configurations are sufficient to study the overall dynamic behavior of the whole helicopter. Real time simulations or predefined simulation profiles can be modeled in order to analyze the dynamic response of the helicopter. For example the dynamic response of the helicopter to any pilot control inputs during a flight or maneuver case can be analyzed without calculating the detailed load distribution over the rotor.

When looked from the outside, the mathematical model developed is a coupled and non-linear system which can be represented with a vector ordinary differential equation such as;

$$\dot{x} = f(x, u, t) \tag{3-1}$$

where x is an array including the helicopter states which are desired to be controlled, \dot{x} is the time derivative of the helicopter states which are desired to be equated to zero in order to determine the trim condition or a predefined value in order to determine the dynamic trim condition which is mostly the case at maneuvering flights. The u term in the system represents the pilot inputs by which the helicopter states are controlled. Lastly the whole system depends on the simulation time which can be set to zero in order to calculate helicopter state derivatives and determine the trim condition or the time can be set to a predefined value in order to simulate helicopter dynamic behavior and response under the pilot controls inputted at any flight condition. The state time derivatives outputted from the mathematical model are also integrated in time domain in order to determine the helicopter states after a time step of simulation. The new states determined from time integration of the mathematical model outputs go back to be used as input

states for the next time step of simulation to determine time derivatives of the states at the next time step.

The helicopter states which are translational & rotational speeds and two attitude angles, and inputs of the mathematical model system are defined as;

$$x = \begin{Bmatrix} u_{xbody} \\ v_{ybody} \\ w_{zbody} \\ \phi \\ \theta \\ p \\ q \\ r \end{Bmatrix}$$

(3-2)

$$u = \begin{Bmatrix} \theta_0 \\ \theta_{1s} \\ \theta_{1c} \\ \theta_{tr} \end{Bmatrix}$$

(3-3)

The helicopter states are defined as velocity components of the system in body reference frame and Euler angles of the helicopter. The differential equations control the time derivatives of the states where for trim conditions the time derivatives of the system states are equated to zero. The initial states of the helicopter that are used to start the time integration for simulation or iteration for trim calculation are decided by the user. As the nature of the differential equations require good initial estimates for faster solutions, initial states of the helicopter shall be well defined in order to decrease the computation time for trim solution. For example, for complex maneuvers, states of a simpler maneuver may be used as initial states. The inputs of the system are the four pilot controls including collective, longitudinal and lateral cyclic inputs for the main rotor and collective for the tail rotor. For trim analyses, pilot controls are calculated by the trim model that uses the mathematical model, where the pilot controls determined assures the time derivative of the states to be equal to zero. On the other hand, for real time or pre-defined

simulations, pilot controls are inputs that are supplied by the user. Arbitrary pilot inputs can be supplied to the mathematical model and the dynamic response and behavior of the helicopter can be analyzed.

In conclusion, a helicopter mathematical model is developed in this study which can be used as both a comprehensive analyses tool and a flight dynamics simulation tool. The mathematical model is developed in a modular structure where each helicopter component that has force and moment contributions to the total helicopter system are modeled with different fidelity empirical and analytical models and option to select to fidelity and accuracy level of the model is left to the user. In this chapter, each of the helicopter component models is defined in detail. Starting from the coordinate systems that are essential for a system, implemented sub-systems such as; main rotor, refined main rotor, tail rotor, fuselage, horizontal tail and vertical tail models are explained in detail.

3.1.1 Flow Chart

A flow chart of the developed mathematical model is presented. As mentioned before, the mathematical model is developed in a modular structure where each module defines a helicopter component that has force and moment contributions to the total helicopter system. The flow chart of the whole mathematical model developed in MATLAB SIMULINK is given at Figure 3-1.

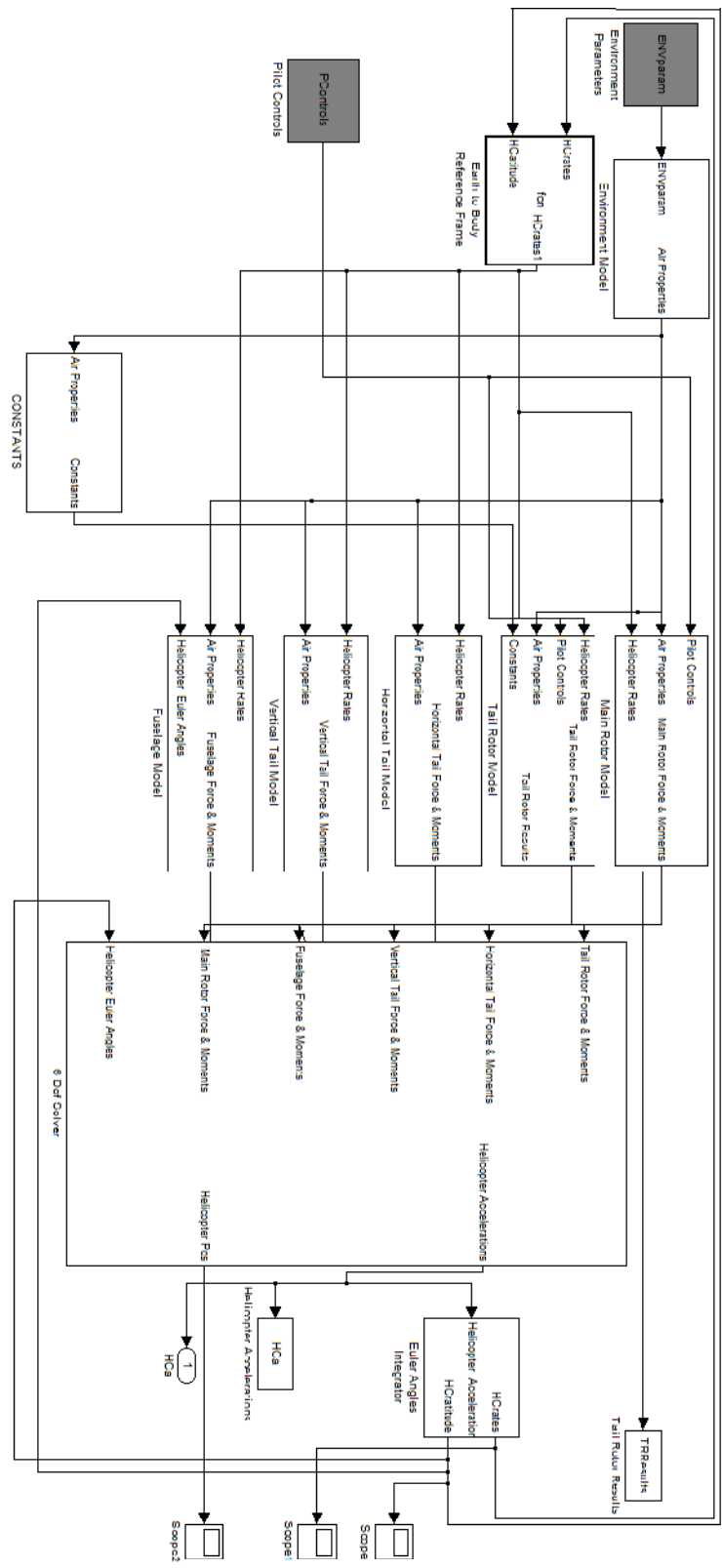


Figure 3-1 Matlab & Simulink model of the developed mathematical model

Environmental model calculates air properties and parameters that are used in the mathematical model changing with the altitude of the helicopter. In simulation analyses, during a flight condition the change in altitude (if exists) is taken into account in the environmental module.

Main rotor module is the force and moment model of the helicopter main rotor including aerodynamic, inertial and centrifugal components. As being the main force and moment source of a helicopter, the accuracy and fidelity of the main rotor model is important. Most of the computation effort is spent in this module where inflow distributions, blade dynamic behavior, wake geometry and total aerodynamic force and moments are predicted according to the desired detail.

Tail Rotor Module models the tail rotor of the helicopter with lower fidelity models. Tail rotor force and moment contribution to the total system is determined with blade element momentum methods.

Horizontal Tail Module models the pitching moment contribution from horizontal tail (if exists) to the total system. The lift of the horizontal tail is multiplied with the distance from horizontal tail aerodynamic center to the helicopter center of gravity in order to determine pitching moment contribution. The downwash of the main rotor to the horizontal tail is modeled with simple momentum theory with the assumption that main rotor wake is uniform; inflow does not change with position and time, and rotor wake does not rotate.

Vertical Tail Module, similar to horizontal tail module, models yawing moment and side force contribution of the vertical tail (if exists) to the total force and moments acting on the aircraft center of mass. Downwash effect of the tail rotor is taken into account similarly the downwash effect of the main rotor to the horizontal tail.

Fuselage Module, which is one of the important modules, defines the fuselage aerodynamic force and moments while taking main rotor downwash into account. Gravitational force is included in the fuselage module where gravitational acceleration is acted on the center of mass of the helicopter which is a point on the fuselage.

Total force and moments generated by each component of the helicopter are transformed into body reference frame and transferred to the center of mass of the total system from aerodynamic center of each component. The total force and moments acting on the helicopter center of gravity is determined in order to calculate helicopter states time derivatives that are going to be used by the trim model or used in the next time step of the simulation.

3.2 Reference Coordinate Systems

The mathematical model developed in this study like most of the mathematical models is both a component wise and total force & moment calculation tool. Force and moment vectors generated by each component are mathematically modeled and calculated. Because the load direction of each component is important when considering total force and moments acting on the system, it is crucial to calculate all force and moments generated by each helicopter component in the same coordinate system. On the other hand freestream air velocity that each force and moment contributor component encounter including the relative velocities because of the motion of the component itself or translational and rotational velocities of the whole system, is specific and varies for each component. Several coordinate systems are defined to make the analysis easier. While calculating the force and moments generated by each component a reference frame located at its aerodynamic center is used. Then these forces and moments are transformed to a global reference frame where the equations of motions for the whole system are written.

3.2.1 Inertial Reference Frame

The inertial reference frame is a fixed frame on earth without any translation or rotation. Helicopter position and velocities are defined in inertial reference coordinate system. z axis points upwards which is opposite to gravitational acceleration, while x is directed along with x axis of the vehicle carried reference frame and y is located according to the right hand rule.

3.2.2 Vehicle Carried Reference Frame

The vehicle carried reference frame is positioned on the center of gravity of the platforms and it translates but does not rotate with the helicopter. z axis points downwards, parallel to the gravity vector, x axis points to the nose of the helicopter and y axis points starboard direction of the helicopter when Euler angles are zero.

3.2.3 Body Axis Reference Frame

Similar to vehicle carried reference frame, body axis reference frame is located on the center of gravity of the helicopter and rotates and translates with it. Body axis coordinate system can be defined with rotation of vehicle carried reference frame with Euler Angles (φ , θ , ψ). The x axis points forward through the nose of the helicopter, y axis is directed to starboard side of the helicopter and z axis points downwards without any rotation.

Helicopter altitude and velocities are transformed from inertial axis reference frame to body axis reference frame. Total force and moments acting on helicopter's center of mass and translational and rotational accelerations are calculated in body axis reference frame and then transformed to inertial reference frame. Therefore instead of calculating each helicopter component force and moments and then transforming them to body and inertial reference frames, this procedure allows for calculating the total force and moments acting to the center of mass of the helicopter in body reference frame and determining total translational and rotational accelerations of the helicopter with only one transformation. Body to inertial and inertial to body reference frame transformation is done with the transformation matrices (3-4), (3-5).

$$L_{BI} = \begin{bmatrix} \cos\theta\cos\varphi & -\cos\theta\sin\varphi & -\sin\theta \\ -\sin\theta\sin\theta\cos\varphi - \cos\theta\sin\varphi & \sin\theta\sin\theta\sin\varphi - \cos\theta\cos\varphi & -\sin\theta\cos\theta \\ -\cos\theta\sin\theta\cos\varphi + \sin\theta\sin\varphi & \cos\theta\sin\theta\sin\varphi + \sin\theta\cos\varphi & -\cos\theta\cos\theta \end{bmatrix} \quad (3-4)$$

$$L_{IB} = L_{BI}^{-1} \quad (3-5)$$

3.2.4 Wind Axis Reference Frame

It is the coordinate system located at the center of gravity of the helicopter similar to the body reference frame. x axis of the wind axis reference frame is directed along the flight direction. The angle of attack (α) and sideslip (β) of the helicopter are defined as the angles between wind axis reference frame and body axis reference frames. Transformation is done from wind axis to body reference frame by the transformation matrix;

$$L_{BW} = \begin{bmatrix} \cos\alpha\cos\beta & -\cos\alpha\sin\beta & -\sin\alpha \\ \sin\beta & \cos\beta & 0 \\ \sin\alpha\cos\beta & -\sin\alpha\sin\beta & \cos\alpha \end{bmatrix} \quad (3-6)$$

3.2.5 Hub Axis Reference Frame

Total force and moments generated by the main rotor are calculated in hub reference frame and then transformed to body axis reference frame. Similar to body axis reference frame, hub reference frame is fixed to the helicopter and translates and rotates with it. z axis is directed upwards, which is just the opposite of body z axis, hub x axis is directed to the aft of the helicopter just as the opposite of body x axis, which is also the direction of freestream in leveled forward flight and y axis is positioned according to the right hand rule. Besides, the azimuth angle is defined in hub reference frame where it is the angle of rotation around positive z axis. The zero azimuth corresponds to the position of the blade when it coincides with positive x axis and points the aft of the helicopter. Ninety degrees azimuth angle is coincident with positive y axis, pointing starboard side of the helicopter. The orientation of the hub reference frame is given in Figure 3-2.

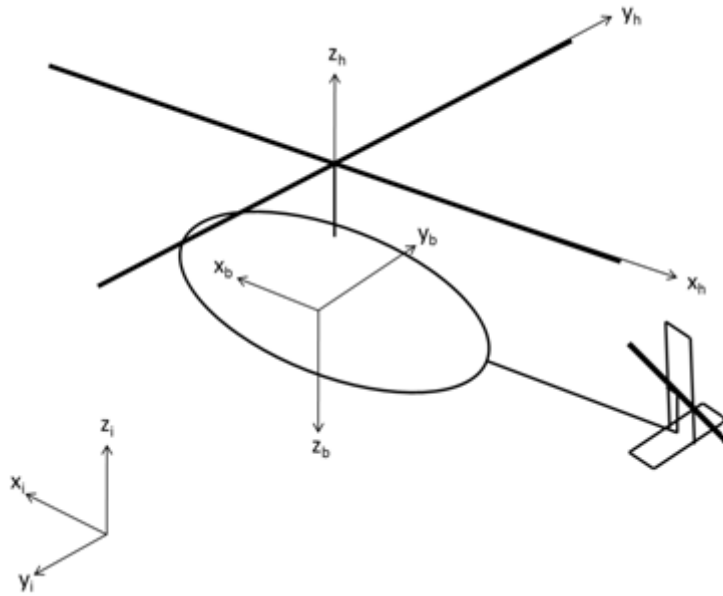


Figure 3-2 Hub reference frame coordinate system

Helicopter velocities that are resolved in body axis reference frame are transformed into hub reference frame with the transformation matrix (3-7).

$$L_{HB} = \begin{bmatrix} -\cos\alpha_{shaft} & 0 & -\sin\alpha_{shaft} \\ 0 & 1 & 0 \\ \sin\alpha_{shaft} & 0 & -\cos\alpha_{shaft} \end{bmatrix}$$

(3-7)

Total aerodynamic, inertial and centrifugal force and moments generated by the main rotor are integrated in hub reference frame and then transformed to body axis reference frame in order to determine the contribution of the main rotor to helicopter dynamics. The transformation matrix from hub to body reference frame is done with equation (3-8).

$$L_{BH} = L_{HB}^{-1}$$

(3-8)

3.2.6 Blade Reference Frame

Blade individual total force and moments are calculated and integrated in blade reference frame which is fixed at blade roots and rotates with blades. Each blade has its own blade reference system located at its root for which z axis points upwards, parallel to z axis of hub reference frame, x axis points from root to the tip of the blades and y is oriented according to right hand rule. Force and moments generated by each blade element are calculated in blade element reference frame and transformed to blade reference frames according to which force and moments are integrated along the blade span. Total force and moments generated by the blade are integrated in blade reference frame and then transformed to hub reference frame with the transformation matrix (3-9). Ψ notation in the equations is no longer yaw angle of the helicopter but azimuth angle of the blades which is the rotation angle about shaft.

$$L_{HBL} = \begin{bmatrix} \cos\varphi & -\sin\varphi & 0 \\ \sin\varphi & \cos\varphi & 0 \\ 0 & 0 & 1 \end{bmatrix}$$

(3-9)

3.2.7 Blade Element Reference Frame

Blade element reference frame is the coordinate axis located at each blade elements aerodynamic center, while z axis pointing the lift direction, x axis pointing the drag direction and y lies in radial direction. Blade element reference frame which can also be called deflected or deformed reference frame contains the flap angle of the blade, collective, longitudinal and lateral cyclic, twist and inflow information of each individual blade element. Throughout this study, blades are assumed rigid. Therefore, deflection angle of each blade element is calculated from the flap angle information of the blades. In addition, for convenience, blade element reference frame deflects with the blade around flap hinge; however blade reference frame does not. Therefore, the aerodynamic forces generated by the each blade element are transformed to blade reference frame by both effective angle of attack and flap angle. Angle of attack of each blade element and generated lift, drag and aerodynamic moments and blade element positions are defined and calculated in

blade element reference frame. The aerodynamic forces calculated in blade element reference frame are transformed to blade reference frame where they are integrated along the blade in order to determine total force and moments generated by the single blade. The transformation matrix from blade element reference frame to blade reference frame is given by (3-10);

$$L_{BL \leftarrow Bref} = \begin{bmatrix} \cos\beta & 0 & -\sin\beta \\ -\sin\alpha\sin\beta & \cos\alpha & -\sin\alpha\cos\beta \\ \sin\alpha\sin\beta & \sin\alpha & \cos\alpha\cos\beta \end{bmatrix}$$

(3-10)

The α angle in the transformation matrix represents the effective angle of attack, where β represents the flap angle of the rigid blade. Blade reference frame, blade element reference frame, effective angle of attack and flapping angle are visualized in Figure 3-3 and Figure 3-4, for convenience.

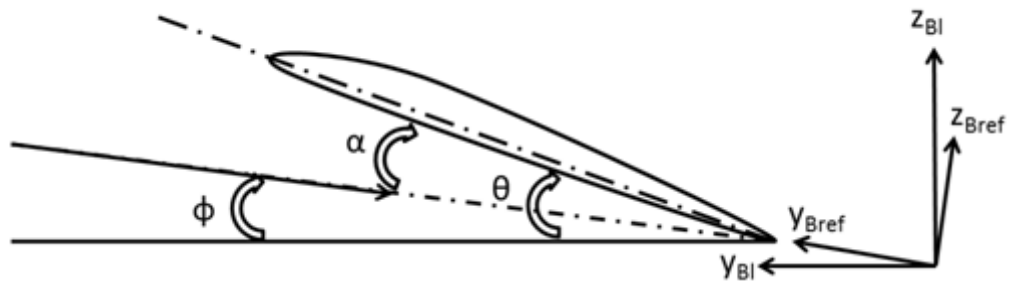


Figure 3-3 Blade and Blade Reference Frame systems

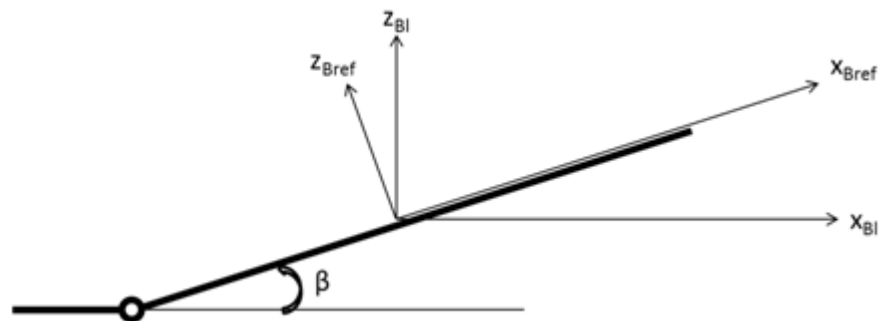


Figure 3-4 Blade and Blade Reference Frame systems

- θ : blade element incidence
- φ : blade element inflow angle
- α : blade element effective angle of attack
- β : blade flapping angle

Blade element incidence angle is calculated while taking pilot controls such as collective, longitudinal and lateral cyclic and blade twist. Inflow angle contains the induced velocity, freestream velocity that is normal to hub plane, relative freestream velocity because of flapping and relative velocities because of the body rotational motion information. As represented in Figure 3-3, blade element reference frame is oriented according to local effective angle of attack; therefore each blade element has its own coordinate system which changes repeatedly during a flight condition or maneuver. On the other hand, because the blades are assumed rigid, each blade element along the same blade has same flap angle which is used in the transformation matrix.

3.2.8 Tail Rotor Reference Frame

It is the coordinate axis located on the hub of the tail rotor without rotating with the tail rotor. z axis is parallel to the body y axis, which is also parallel to the tail rotor thrust vector. x axis, similar and parallel to main rotor hub reference system x axis, points the aft of the helicopter and y axis is oriented according to the right hand rule. Aerodynamic force and moments generated by the tail rotor are integrated and calculated according to the tail rotor reference system. Since, tail rotor hub type is

assumed to be hingeless, and tail rotor blades are assumed to be rigid, there is no flapping dynamics, therefore any net inertial and centrifugal force and moments acting to the hub of the tail rotor. Therefore only aerodynamic loads are considered. Force and moments generated by the tail rotor are determined in tail rotor reference system and then transformed into body reference system in order to obtain the contribution to the total force and moments acting on the helicopter center of gravity, by using the transformation matrix (3-11).

$$L_{BTR} = \begin{bmatrix} 1 & 0 & 0 \\ 0 & 0 & 1 \\ 0 & -1 & 0 \end{bmatrix}$$

(3-11)

3.2.9 Horizontal Tail Reference Frame

Aerodynamic force and moments generated by horizontal tail component of helicopter are calculated in Horizontal Tail Coordinate system which is located on horizontal tail aerodynamic center. Axes of the horizontal tail coordinate system are equivalent to the axes of the body reference frame.

3.2.10 Vertical Tail Reference Frame

Similar to the horizontal tail reference system, vertical tail reference system is equivalent to the body reference frame but located at vertical tail aerodynamic center. Aerodynamic force and moments generated by vertical tail are calculated in vertical tail reference system and then transformed into body reference system.

3.3 Main Rotor Model

As being the most dominant contributor to the helicopter total force and moment, an accurate and reliable main rotor mathematical model is essential. On the other hand, for flight dynamic activities, lower fidelity mathematical models which are computationally much more efficient are mostly desired. Therefore, a selective structured, main rotor model which enables the user to select the fidelity, accuracy

and computational cost of the model is developed. In this section, each of the models with different fidelities is explained in detail.

3.3.1 Main Rotor Blade Model

As mentioned before, for both main rotor and tail rotor models, blade element method is implemented. Although, different inflow models with different fidelity and accuracy are included in the mathematical model, aerodynamic radial force and moment distributions are always calculated from blade element method independent from the inflow or wake model. Blade element method, a powerful analytical method, can calculate aerodynamic force and moments distributions along the blades accurately depending on the inflow model.

The essence of the blade element method is to divide the blade into sections, where each section is called as a blade element. In the developed mathematical model, blades are assumed to be rigid. Therefore, blade element allocation is done according to aerodynamic aspects only. The accuracy of the rotor aerodynamic load prediction depends on the accurate prediction of the strong tip vortices [19, 28]. Therefore in order to resolve the strong tip vortex accurately, blades are divided into blade elements denser at the locations near tip whereas near root of the blades where aerodynamic loads are approximately linearly changing with radial location, blades are divided with larger intervals. For blade segmentation, a stretching function is used in order to determine radial locations of the blade elements which are denser at locations near blade tip and contrarily infrequently located at the locations near blade root. In Figure 3-5, an example of the blade segmentation is shown which is getting denser at the locations near tip.

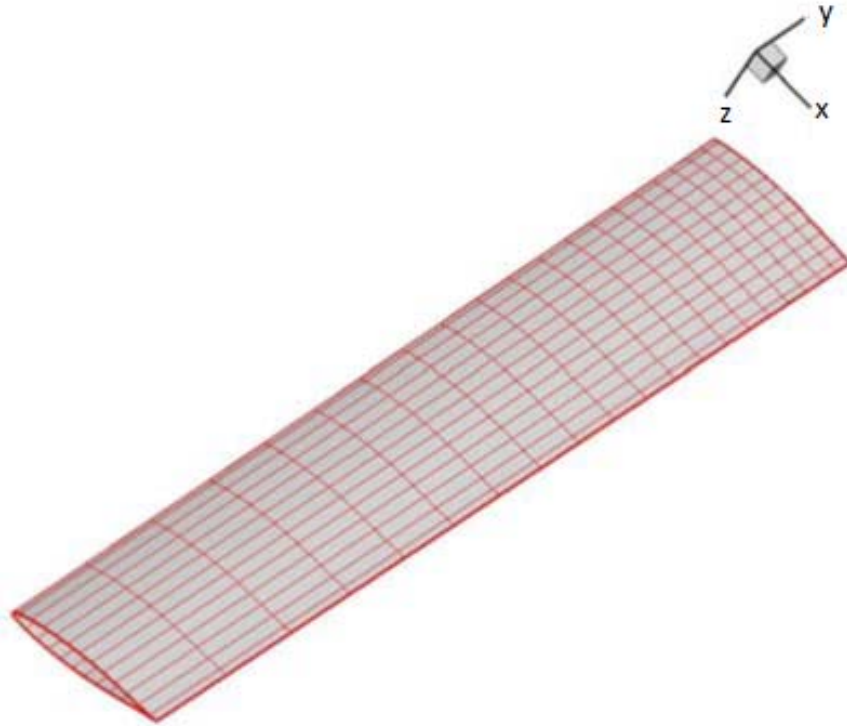


Figure 3-5 Example blade segmentation of the developed mathematical model

After blade elements are located along the blade, parameters that are used in the calculations by several models are determined for each blade element. One parameter that is determined for aerodynamic calculations is pitch angle of each blade element. Pitch angle of each blade element contains the information of the pilot controls such as collective, longitudinal and lateral cyclic and twist of the blade. Blade pitch angle changes with both radial and azimuthal direction because of the cyclic controls and twist of the blade. Local angle of attack of each blade element is calculated as;

$$\theta_i = \theta_0 - \theta_{1c} \cos \psi - \theta_{1s} \sin \psi + r_i \theta_t, i = 1, 2 \dots, N$$

(3-12)

Θ_0 is the collective angle that is controlled by the pilot, θ_{1c} and θ_{1s} are the cyclic controls. Θ_t is the twist angle (if exists) and when multiplied with the non-dimensional blade element location, r , local effect of the twist is determined. N represents the total blade element number on the blade. Pitch angle of each blade element is determined by superposition of all the contributions. As pilot controls change with both iteration and simulation processes, the pitch angle of each blade element is calculated with every iteration or time step.

Another parameter that is determined for aerodynamic calculations is chord length of each blade element. Blade taper ratio is taken in account when dealing with the chord length distribution along the blade and chord length of each blade element is calculated.

One other parameter calculated is the width of each blade element, which is used in aerodynamic calculations also.

In conclusion, blades are represented by blade elements located all along the blade. Geometrical parameters that are used in the main rotor aerodynamic model are determined before the performance calculations start. Blade element locations along the blade, pitch angle, chord length and width of each blade element are predetermined before the aerodynamic model starts to process.

3.3.2 Initial Inflow Model

For the initial mathematical model which is modified with the implementation of a refined aerodynamic model later, blade element momentum theory is used in order to determine main rotor aerodynamic force and moments. The method used is a combination of blade element method by which rotor air loads are calculated and momentum theory by which perpendicular freestream air velocity at the rotor disk is calculated.

Starting from the treatment of rotor performance in both forward and hover flights developed by Glauert, a formula for inflow ratio over the rotor disk is derived. For rotors in forward flight, neglecting the non-symmetric induced velocity distribution over the rotor disk is indeed a critical assumption that deviates the model accuracy from reality. However, the simplicity and computational cost efficiency that

momentum theory offers are useful especially for low fidelity mathematical models. Besides, the initial mathematical model is modified with a refined aerodynamic model where higher fidelity inflow models are implemented. Therefore, the momentum theory can be considered as a starting point for the mathematical model development which afterwards is replaced with a more accurate model.

The solution for the induced velocity ratio is given by, [19];

$$\lambda = \mu \tan \alpha + \frac{C_T}{2\sqrt{\mu^2 + \lambda^2}} \quad (3-13)$$

where; μ is the advance ratio and λ is the inflow ratio and they both non-dimensionalized with blade tip speed.

Possible roots of the equation are calculated with simple fixed point iteration method with a damping factor of 0.5. Usually the method converges in 5-10 iterations with an error of %0.01. It can be seen from the equation that, momentum theory can be used for both hover and forward flight cases. For hover analyses, the advance ratio μ comes as zero as there is no forward velocity and leads the equation to be dependent on only thrust coefficient.

It is worthwhile to consider the inflow distribution calculated from momentum theory only as an approximate value. As can be seen from the inflow model equation, the mean inflow calculated from momentum theory depends on the thrust value of the rotor which has to be supplied to the momentum theory. However, without knowing the inflow distribution accurately, thrust value of the rotor cannot be determined accurately. This leads to an important assumption here. For inflow values calculated from momentum theory, a thrust coefficient value for the rotor is assumed. In order to assume a sensible initial thrust coefficient value of the rotor, thrust of the rotor is calculated for hover flight condition where thrust is equated to the weight of the helicopter. Following equations addresses the assumption made for momentum theory.

$$T \cong W \tag{3-14}$$

$$C_T \cong \frac{Mg}{\rho\pi R^2(\Omega R)^2} \tag{3-15}$$

3.3.3 Aerodynamic Load Model

As mentioned in blade model part, blade element method is used for main rotor aerodynamic model. Blades are divided into blade elements as explained in the blade model section. What aerodynamic model does is that, it calculates the dynamic inflow contribution to the total inflow from each of the blade elements, aerodynamic lift, drag and moments and combines them with centrifugal and gravitational force and moments of each blade element, integrates blade element loads along the blade in order to calculate blade total force and moments that are transferred to the hub. All these calculations are done for each blade element at each azimuth angle. Effective angle of attack, inflow angle, local pitch angle, local vertical and tangential velocities, blade element lift, drag, normal force definitions are given in Figure 3-6.

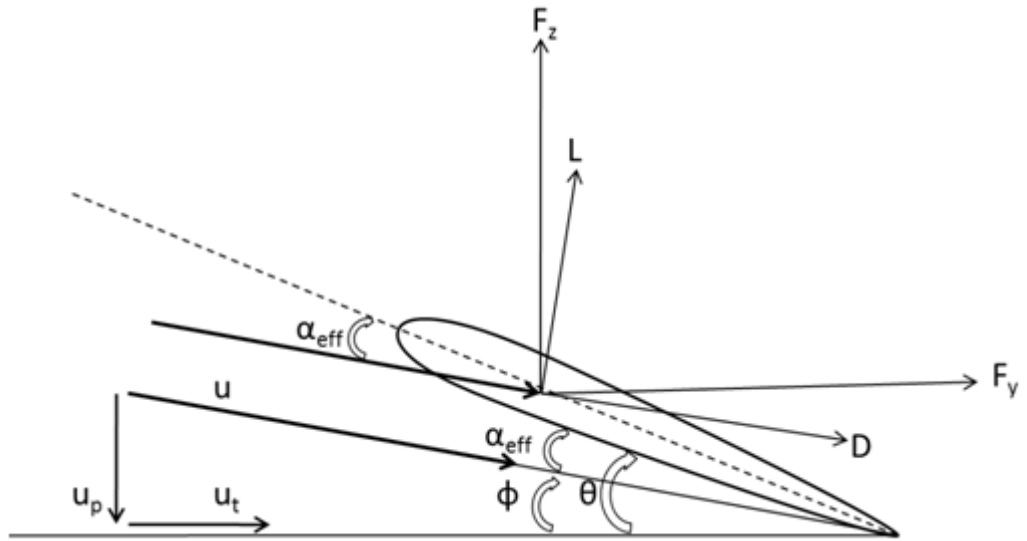


Figure 3-6 Blade element force and angle definitions

Lift and drag forces of each blade element are calculated from aerodynamic relations where these forces are integrated along the blade in order to determine total force and moment generated by a single blade at a specified azimuth angle. In order to determine aerodynamic force of each blade element, local velocity components and pitch angle are required. Pitch angle of each blade element is determined from blade model where pilot controls such as collective, longitudinal and lateral cyclic angles and blade twist are taken into account.

The tangential local velocity component that each blade element encounters is calculated by superposing the rotational velocity of the blades and helicopter translational and rotational motion. u_t , tangential velocity, calculated with equation below;

$$u_{t_{rotation}} = \Omega r$$

(3-16)

$$u_{t_{advance\ ratio}} = \mu(\Omega R) \sin \psi \cos(\theta_{shaft} + \alpha_{TPP}) \quad (3-17)$$

$$u_{t_{relative}} = -qz_{hub} \sin \psi \quad (3-18)$$

$$u_t = f(r, \psi, \mu, q, \theta_{shaft}) = u_{t_{rotation}} + u_{t_{advance\ ratio}} u_{t_{relative}} \quad (3-19)$$

α_{TPP} is defined in hub reference frame.

Similarly, perpendicular velocity, u_p , is also calculated from superposition of contributions. One perpendicular velocity contribution comes from helicopter translational motion such as climb, descent or forward flight where helicopter pitch angle or rotor shaft angle is arbitrary. Another and main contribution to local perpendicular velocity comes from the induced velocity distribution over the rotor disk. Prediction of induced velocity distribution is explained in inflow model part, in detail. A third and one of the dominant perpendicular velocity contributions come from the blade flapping motion. As the blade flaps up and down about flapping hinge during its rotation, relative freestream velocity develops on the blade which is called dynamic inflow throughout the study. For convenience, dynamic inflow development is shown in the Figure 3-7.

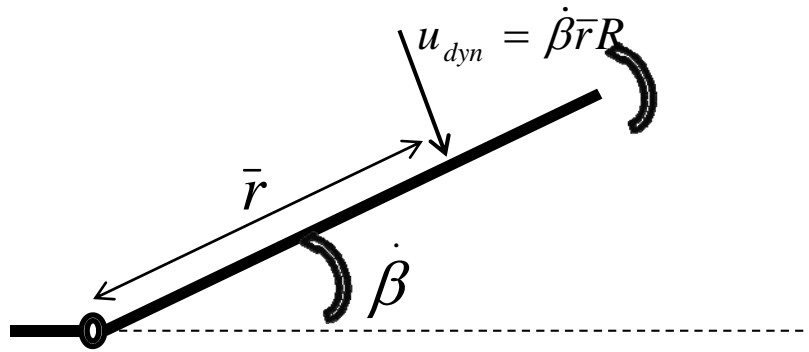


Figure 3-7 Dynamic inflow development

Blade flapping dynamics is modeled and explained in the blade dynamic part of the study. Flap angle information at each azimuth angle that aerodynamic analysis is going to be done, is determined from the blade flapping dynamics model and transferred to the aerodynamic model. Flap angle distribution along the azimuth angle is used in order to determine the time derivative of the flapping angle. The time derivative of the flapping angle is multiplied with the dimensional blade element radial position in order to determine the dynamic inflow contribution to the total perpendicular velocity of the blade element. Time derivative of the flap angle is calculated with the difference between the flap angles at two adjacent azimuth locations and the time for the blade to travel over the angular distance between those adjacent azimuth angles. Time derivative of the flapping angle is calculated with the equation below;

$$\dot{\beta}_n = \frac{(\beta_{n+1} - \beta_n)}{\frac{2\pi}{N\Omega}} \quad (3-20)$$

where n is azimuth step number, N is total azimuth steps which are user defined input to the mathematical model.

All inflow contributions are superposed in order to determine the total perpendicular velocity that each blade element encounters. The total perpendicular velocity component that each blade element encounters at each azimuth step is calculated with the equations below;

$$u_{p_{advance\ ratio}} = \mu(\Omega R)\sin(\theta_{shaft} + \alpha_{TPP}) \quad (3-21)$$

$$u_{p_{climb\ \&\ descent}} = \lambda_c \quad (3-22)$$

$$u_{p_{dynamic\ inflow}} = \dot{\beta}r \quad (3-23)$$

$$u_{p_{induced\ velocity}} = \lambda_i \quad (3-24)$$

$$\begin{aligned} u_p &= f(r, \psi, \mu, \lambda_i, \lambda_c, \beta, \dot{\beta}) \\ &= u_{p_{advance\ ratio}} + u_{p_{climb\ \&\ descent}} + u_{p_{dynamic\ inflow}} + u_{p_{induced\ velocity}} \end{aligned} \quad (3-25)$$

Total perpendicular and tangential velocity components of the total velocity that each blade element encounters are used to determine the inflow angle of each blade element.

The inflow angle which is basically the angle between perpendicular velocity and tangential velocity that each blade element encounters at each azimuth location, is defined as,

$$\phi_{r,\psi} = \text{atan2}(u_p, u_t) \quad (3-26)$$

The local pitch angle of the blade element information comes from the blade model. As aerodynamic force and moments generated by each blade element depends on the effective angle of attack, the pitch angle and inflow angles are superposed in order to determine effective angle of attack. Aerodynamic coefficient tables depend on angle of attack and Mach number. The effective angle of attack is determined with equation (3-27) and local Mach number is determined with the division of total freestream velocity that blade element encounters by speed of sound at the flight condition which is calculated by environmental module.

$$\alpha_{eff.} = \theta_r - \phi_{r,\psi} \quad (3-27)$$

$$M_{r,\psi} = \sqrt{u_p^2 + u_t^2} / a \quad (3-28)$$

Blade profile aerodynamic coefficients are interpolated for the effective angle of attack and local Mach numbers, and are used in blade element lift and drag calculations. The assumption here is that the sectional aerodynamic properties are uniformly distributed and constant along the blade element and aerodynamic loads are acting on the aerodynamic center of the blade element. This actually decreases the accuracy and fidelity of the method however increasing the blade element number along the blade act oppositely and increases accuracy especially at the locations near tip. How the blade element number affects accuracy of the method is investigated in the validation chapter of the study. Sectional lift and drag values are multiplied with blade element width in order to determined total aerodynamic force

and moments generated by the blade element. The lift, drag and moment calculations are done with equations (3-29) to (3-31);

$$dL_{r,\psi} = 1/2\rho V_{r,\psi}^2 C_{l_{r,\psi}} \quad (3-29)$$

$$dD_{r,\psi} = 1/2\rho V_{r,\psi}^2 C_{d_{r,\psi}} \quad (3-30)$$

$$dM_{r,\psi} = 1/2\rho V_{r,\psi}^2 C_{m_{r,\psi}} c_r \quad (3-31)$$

Because blade are assumed to be rigid and only permitted to deflect about flapping hinge, aerodynamic moment of the blade elements become useless for the calculations. However, for comprehensive or main rotor detailed analysis applications, aerodynamic torsional moment generated by the blades may be required to be calculated. Therefore, moment calculations remain in the method.

Other than the aerodynamic loads, centrifugal and gravitational forces act on each of the blade elements which are also transferred to the hub. Centrifugal and gravitational forces, acting on the blade elements are individually calculated and superposed with aerodynamic loads in order to determine the resultant force acting on each of the blade elements. Centrifugal and gravitational forces are calculated in blade reference frame whereas aerodynamic forces are calculated in blade element reference frames. Therefore, aerodynamic forces are transformed to blade reference frame from blade element reference frame before calculating the resultant forces. Each of the force components acting on the blade elements are shown in the Figure 3-8.

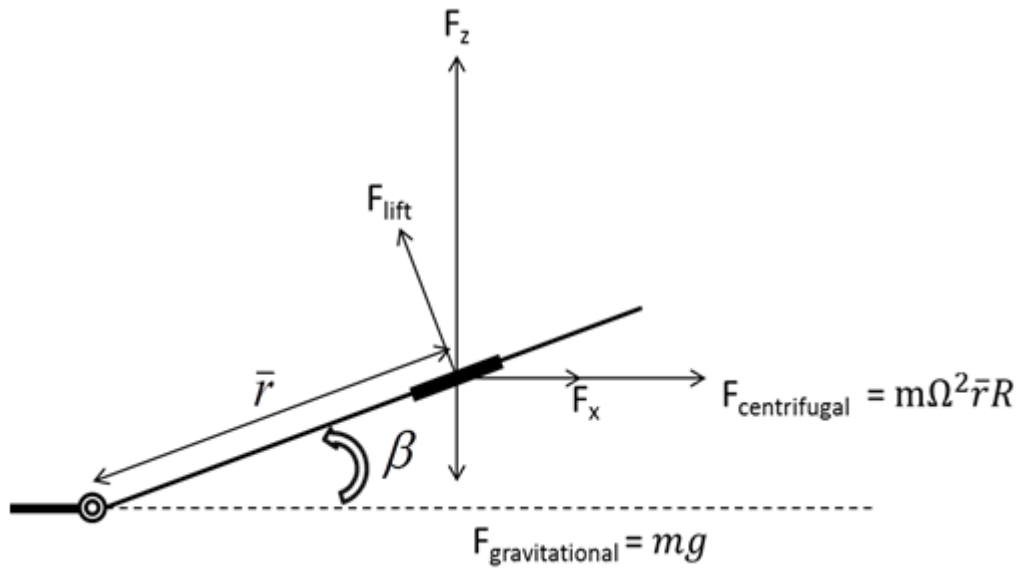


Figure 3-8 Force components acting on each blade element

Aerodynamic, centrifugal and gravitational forces are resolved into their components in blade reference frame and summed up for resultant force components. In order to determine blade total force and moments at the blade root, resultant force components of each blade element are integrated along the blade. The integration equations are given as;

$$dF_z(r, \psi) = dL_{r,\psi} \cos\phi \cos\beta - dD_{r,\psi} \sin\phi \cos\beta - m_r g \quad (3-32)$$

$$dF_x(r, \psi) = -dL_{r,\psi} \cos\phi \sin\beta + m_r \Omega^2 r g \quad (3-33)$$

$$dF_y(r, \psi) = -dL_{r,\psi} \sin\phi - dD_{r,\psi} \cos\phi \quad (3-34)$$

$$F_z(\psi) = \int_{\text{root cut-out}}^R dF_z c_r dr = \sum_{n=1}^N dF_{z_n} c_n dr_n \quad (3-35)$$

$$F_x(\psi) = \int_{\text{root cut-out}}^R dF_x c_r dr = \sum_{n=1}^N dF_{x_n} c_n dr_n \quad (3-36)$$

$$F_y(\psi) = \int_{\text{root cut-out}}^R dF_y c_r dr = \sum_{n=1}^N dF_{y_n} c_n dr_n \quad (3-37)$$

$$M_y(\psi) = eF_z(\psi) \quad (3-38)$$

The existence of flapping hinge eliminates the moments around y-axis of the blade reference frame. Therefore the force and moments transferred to the hub are simplified. Besides, the force parallel to x-axis of blade reference frame depends on the azimuth when transferring to the hub reference frame therefore; it is resolved into its harmonics. Transformation matrix from blade reference frame to hub reference frame given in the coordinate systems chapter of the study is used in order to transform the blade total force and moments generated to the hub. The transformation matrix is given as;

$$L_{HBL} = \begin{bmatrix} \cos\varphi & -\sin\varphi & 0 \\ \sin\varphi & \cos\varphi & 0 \\ 0 & 0 & 1 \end{bmatrix} \quad (3-39)$$

Multiplication of the transformation matrix with the total force and moments generated by the blade at blade reference frame system results in force and moments that are transferred to the hub and so to the fuselage.

On the other hand, the force and moments transferred to the hub are changing with azimuth and unless an azimuth position of the blade is specified, loads that are transferred to the hub cannot be determined. In order to eliminate this obligation of specifying an exact azimuth location, average of the total force and moments generated by the blade are taken in azimuth direction. The equations for average total force and moments transferred to the hub and to the fuselage are given as;

$$\bar{T} = \frac{(\sum_{i=1}^{N_A} F_z(\psi))}{N_A} N_b \quad (3-40)$$

$$\bar{\tau} = \frac{(\sum_{i=1}^{N_A} \sum_{n=1}^N dF_{y_n} c_n r_n dr_n)}{N_A} N_b \quad (3-41)$$

$$\bar{F}_z = \frac{(\sum_{i=1}^{N_A} F_z(\psi))}{N_A} N_b \quad (3-42)$$

$$\bar{F}_x = \frac{(\sum_{i=1}^{N_A} F_x(\psi))}{N_A} N_b \quad (3-43)$$

$$\bar{F}_y = \frac{(\sum_{i=1}^{N_A} F_y(\psi))}{N_A} N_b \quad (3-44)$$

$$\bar{M}_y = \frac{(\sum_{i=1}^{N_A} M_y(\psi))}{N_A} N_b \quad (3-45)$$

The average total force and moments that are calculated in blade reference frame are then transformed to hub reference frame with the transformation matrix.

3.3.4 Blade Dynamics & Hub Model

Initially blades dynamic behaviors are modeled with the flapping equation derived by Chen [44] which is in the same fidelity level with the initial inflow model. However in order to develop a main rotor model in which blade dynamic model and aerodynamic model are compatible with each other, Chen's flapping equation is modified. The complete flapping equation is resolved into its components and then the aerodynamic moment component is replaced with the one calculated by the mathematical model developed. As a result, a generic blade dynamic behavior model is derived where aerodynamic moment around the flapping hinge is calculated independently of the flapping equation. Besides, on the other hand, with the refined main rotor model, starting from basic equations of motion [2], another flapping dynamics equation is derived and implemented as another selective option for user, Appendix B.

It shall be noted that throughout the study, articulated hub with only flapping dynamics is modeled for main rotor. Addition of lead-lag hinges and other hub types such as teetering, hingeless are left for future study.

Blade's dynamic behavior is determined by summing all moments acting to the blade at blade flap hinge. It shall be stated at this point that, throughout the study, articulated hub type with only flapping dynamics enabled is modeled as main rotor hub. The total moment around the hinge leading to the flap angle which is the

only deflection of the rigid blade and dependent to azimuth angle is resolved into its contributor components. The general form of the flapping equation is given by [44];

$$M_A + M_{CF} + M_I + M_{Cor.} + M_R + M_{BA} + M_{BL} + M_w = 0 \quad (3-46)$$

As the moments are written in blade reference frame axis, signs of moments that try to lift the blade up, increase the flap angle are positive whereas signs of the moments that try to decrease the flap angle are negative.

The term M_{CF} is the moment term due to centrifugal force. It is the moment depends on the centrifugal force generated because of the rotational velocity of the blade around the shaft and depends on the flap angle. Centrifugal force and moment is calculated with the formula stated below;

$$M_{CF} = -\Omega^2 [I_\beta \cos\beta + eM_\beta] \sin\beta \quad (3-47)$$

Two terms occur in the centrifugal moment about the flapping hinge because of the possible existence of the hinge offset. The complete equation represents the moment generated because of the centrifugal force of a rotating blade with at a flap angle about a flap hinge which is not coincident with the rotation axis but has an offset.

M_I term is the moment term due to blade inertia. It contains the information of double derivative of flapping angle, which is mostly neglected because of the negligible moment contribution. Besides second order terms in flapping equations brings difficulties to solve. The tradeoff between accuracy contribution and the effort in order to solve second order differential equations usually end with decision of neglecting the double derivative.

$$M_I = -I_\beta \ddot{\beta} \quad (3-48)$$

M_{cor} is the moment contribution related with the Coriolis acceleration. It is generated because of both blade rotation around its shaft and helicopters angular velocities. Moment due to Coriolis acceleration is calculated with the formula below;

$$M_{Cor.} = 2[I_{\beta} + eM_{\beta}](p\Omega\cos\psi - q\Omega\sin\psi) \quad (3-49)$$

M_r is the restraint moment if a torsional spring exists on the flapping hinge, and calculated with simple basic moment equation of spring.

$$M_R = -K_{\beta}\beta \quad (3-50)$$

M_{BA} and M_{BL} are the moments due to helicopter translational and rotational accelerations. As helicopter maneuvers generate flapping moment for the blade, these contributions should be included in the flap equation. The moment contributions are calculated by;

$$M_{BA} = I_{\beta}(\dot{p}\sin\psi + \dot{q}\cos\psi) \quad (3-51)$$

$$M_{BL} = M_{\beta}(\dot{w} - uq + pv) \quad (3-52)$$

Except from the centrifugal moment, one of the dominant moment contributions is generated by the gravitational acceleration and blade mass. Weight moment of the blade about flapping hinge is calculated as follows;

$$M_W = -M(1 - e)R/2 \quad (3-53)$$

Lastly, M_A term in the total moment equation refers to the aerodynamic moment generated by the blades. Normally in the flapping equation derived by Chen [44] the aerodynamic force equations exist. However, because blade flaps under the aerodynamic forces and aerodynamic forces are strongly coupled with the blades flap motion, the aerodynamic model that is used to calculate the load distribution over the rotor disk and is used to determine the flap angles should be identical for accurate mathematical models. Therefore, the flap equation derived by Chen is resolved into its components as the given formula above and the aerodynamic moment contribution is calculated individually. The total aerodynamic moment about the flapping hinge is calculated with the integration of the moments of each blade element around flapping hinge along the blade span.

$$M_A(\psi) = \int_e^R F_z dr = \sum_1^N F_z r$$

(3-54)

The coupling between aerodynamic forces and flapping angles are obtained with a loop between the aerodynamic model where forces are calculated depending on flap angles, and the blade dynamic model where flap angles are calculated under the aerodynamic loading.

As a result, a complete flapping equation is derived and a loop between aerodynamic model and blade dynamic model is built in order to calculate blade dynamic behavior under any flight condition.

$$\sum_1^N F_z r - \Omega^2 [I_\beta \cos\beta + eM_\beta] \sin\beta + 2[I_\beta + eM_\beta] (p\Omega \cos\psi - q\Omega \sin\psi) - K_\beta \beta + I_\beta (\dot{p} \sin\psi + \dot{q} \cos\psi) + M_\beta (\dot{w} - uq + pv) - \frac{M(1-e)R}{2} = I_\beta \ddot{\beta}$$

(3-55)

The complete flapping equation which is azimuth angle dependent is solved for β . At each azimuth angle, the equation is solved individually and flap angle variation with azimuth angle is determined.

3.4 Re-Fined Main Rotor Model

As being the main force and moment contributor to the whole helicopter system, main rotor in a mathematical model shall be modeled accurately. On the other hand, the more accurate and at higher fidelity a model is the more complex it is and inefficient on computational cost issue. Therefore a trade off is done between accuracy and computation cost. As a result, main rotor is modeled with several sub models with different fidelities, accuracy and complexity. The option to select to model that is going to be used in the analyses is left to the user. The main rotor model in the initial mathematical model is then replaced with the refined main rotor model. The following chapters describe the inflow models for hover and forward flight conditions at different fidelity and complexities, the wake prediction methods and models that are implemented into the mathematical model and methods for calculating wake induced velocities for both hover and forward flight cases.

3.4.1 Hover Inflow Model

Momentum theory which neglects the tip losses and assumes uniform inflow distribution in both radial and azimuthal direction was implemented in the initial mathematical model. On the contrary, in the refined aerodynamic model two different inflow models are implemented and the option to select is left to the user.

The first model implemented for the refined aerodynamic model is the combination of momentum and blade element theory modified with Prandtl's Tip Loss Function [19]. This model also supplies initial conditions for the higher fidelity second inflow model. Prandtl's tip loss function provides a solution to model the inflow distribution while taking blade tip losses into account. Instead of assuming a constant tip loss factor value which is mostly used in Wind Turbines as Betz constant [20], a formula is derived by Prandtl [19] so that loss factor varies with blade number, radial position of the blade element and local induced inflow angle. The main effect of the factor is to increase the induced velocity near tips of the

blades so that the lift generated locally is decreased. The correction factor that is included in the quadratic formula of the inflow distribution is determined by the formulas; (3-56) to (3-58).

$$F = \left(\frac{2}{\pi}\right) a \cos(e^{-f}) \quad (3-56)$$

$$f = \frac{N_b}{2} \left(\frac{1-r}{r\phi}\right) \quad (3-57)$$

$$\phi = \frac{\lambda(r)}{r} \quad (3-58)$$

The tip loss factor determined is used in the inflow distribution formula derived by equating incremental thrust coefficients from the momentum and blade element theories [2, 19]. The radial inflow distribution equation is given as (3-59) and is solved with simple fixed point iteration method while the convergence can be determined rapidly.

$$\lambda(r) = \frac{\sigma C_{l\alpha}}{16F} \left(\sqrt{1 + \frac{32F}{\sigma C_{l\alpha}} \theta r} - 1 \right) \quad (3-59)$$

The second inflow model implemented with the refined aerodynamic model is vortex theory, which predicts the wake geometry, calculates the wake induced velocity on the rotor disk and total inflow velocity distribution for hover and axial flight cases. The initial values calculated with Prandtl's tip loss function or purely momentum theory is used in order to calculate the initial circulation distribution over

the rotor disk. The first hover wake geometry is predicted with the initial values then with an iterative process wake geometry is calculated repeatedly until induced velocity iteration converges.

3.4.2 Hover Wake Model

For hover flight cases, the distortion in the wake geometry can be neglected. Therefore Landgrebe's wake model which is developed with experimental methods and includes the effect of rotor thrust, blade effective twist, and blade number on wake geometry, is accurate enough to predict the wake model [53, 54]. In the developed mathematical model, wake is modeled up to ten revolutions of the rotor with higher resolution in near wake and lower resolution in the far wake. In Landgrebe's prescribed wake model, the tip vortex and the remaining vortex sheet is modeled separately while the sudden change in axial velocity because of the consecutive blade passing by sudden changes in factors used in the formulation. The tip vortex geometry is described by the equations (3-60) to (3-69) [19, 53 and 54].

Landgrebe's Prescribed Wake Model

$$\frac{z_{tip}}{R} = \begin{cases} k_1 \psi_w & \text{for } 0 \leq \psi_w \leq 2\pi/N_b \\ \left(\frac{z_{tip}}{R}\right)_{\psi_w=2\pi/N_b} + k_2 \left(\psi_w - \frac{2\pi}{N_b}\right) & \text{for } \psi_w \geq 2\pi/N_b \end{cases} \quad (3-60)$$

$$\frac{y_{tip}}{R} = r_{tip} = A + (1 - A)e^{(-\Delta\psi\omega)} \quad (3-61)$$

$$k_1 = -0.25 \left(\frac{C_T}{\sigma} + 0.001\theta_{tw} \right) \quad (3-62)$$

$$k_2 = -(1.41 + 0.0141\theta_{tw}) \sqrt{\frac{C_T}{2}} \approx -(1 + 0.01\theta_{tw}) \sqrt{C_T} \quad (3-63)$$

$$A = 0.78, \Delta = 0.145 + 27C_T \quad (3-64)$$

The remaining vortex sheet is described with a set of equations for the very outer and inner vortex filaments where the sheet at intermediate parts is determined by linear interpolation. The outer and inner vortex geometries are determined with the following equations where again the sudden change in the axial velocity in the rotor wake is modeled with sudden change in geometry factors.

The outer and inner end of the vortex sheets are calculated by different formulas. The outer end of the sheet is represented by;

$$\left(\frac{z}{R}\right)_{r=1} = \begin{cases} K_{1,r=1}\psi_w & \text{for } 0 \leq \psi_w \leq 2\pi/N_b \\ K_{1,r=1}\left(\frac{2\pi}{N_b}\right) + K_{2,r=1}\left(\psi_w - \frac{2\pi}{N_b}\right) & \text{for } \psi_w \geq 2\pi/N_b \end{cases} \quad (3-65)$$

$$\left(\frac{z}{R}\right)_{r=0} = \begin{cases} 0 & \text{for } 0 \leq \psi_w \leq 2\pi/N_b \\ K_{2,r=0}\left(\psi_w - \frac{2\pi}{N_b}\right) & \text{for } \psi_w \geq \pi/2 \end{cases} \quad (3-66)$$

$$K_{1,r=1} = -2.2 \sqrt{\frac{C_T}{2}} \quad (3-67)$$

$$K_{2,r=1} = -2.7 \sqrt{\frac{C_T}{2}}$$

(3-68)

$$K_{1,r=0} = \left[\frac{\theta_{tw}}{128} (0.45\theta_{tw} + 18) \right] \sqrt{\frac{C_T}{2}}$$

(3-69)

In addition to whole vortex sheet solution, the prescribed wake geometry model is modified so that the whole rotor wake is divided into regions according their influence strength on the rotor disk. Whole rotor wake is divided into three regions. The first region which is generally up to 90 degrees of azimuth following-up the blade that the vortices are trailed and called near wake. In the near wake, wake has the highest influence on induced velocity on the rotor disk therefore whole vortex sheet is taken into account. The second region, where the tip and root vortices start to roll and form up, called the roll-up wake. The last and the least effective on wake induced velocity region is far wake where the whole vortex sheet is represented with only one strong tip vortex filament. In the Figure 3-9 whole vortex sheet (right) and the roll-up tip vortex with inner vortices represented by the vortex sheet (left) are shown [28]. More study and validation with experimental data on Landgrebe's prescribed wake geometry can be found at Leishman's "Principles of Helicopter Aerodynamics" [19]. Comparison of wake geometries calculated by prescribed wake and free wake models with the experimental data is presented in the Figure 3-10.

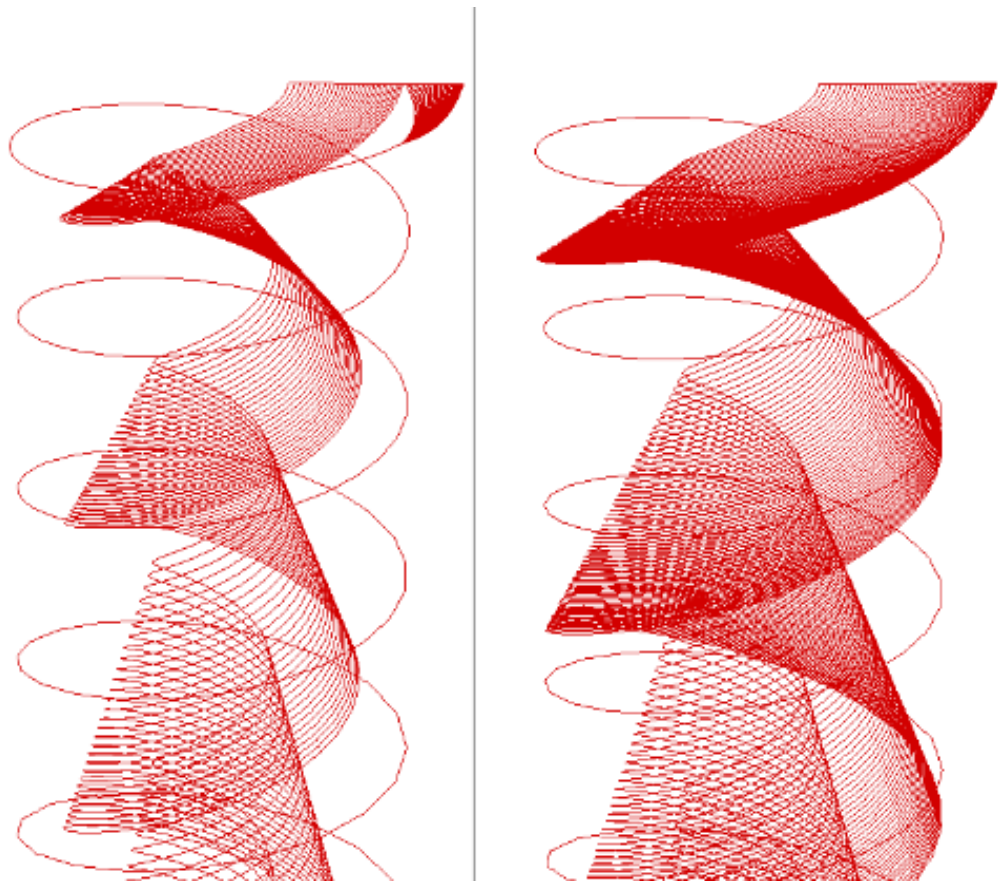


Figure 3-9 Landgrebe's Prescribed Wake Model (with/without rolling-up tip vortex)

Dividing the wake into regions and decreasing the vortex filaments at roll-up and far wake regions decreases the computational cost of the wake induced velocity calculation process while it also decreases accuracy. The choice to use whole vortex sheet model or modified wake model is left to the user.

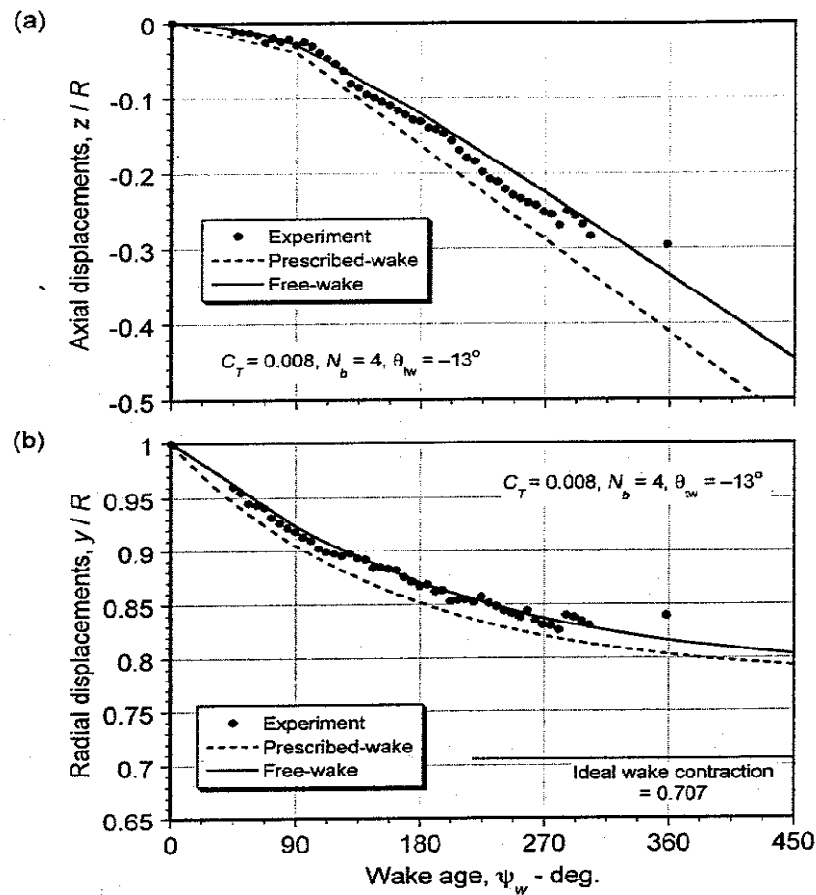


Figure 3-10 Comparison of prescribed and free wake methods with experimental measurement. [19]

3.4.3 Hover Wake Induced Velocity Model

Wake induced velocity is calculated with the multiplication of influence matrix and circulation distribution. The circulation distribution which depends on local lift coefficient and dynamic pressure is calculated during aerodynamic load calculation. For hover flight cases, the circulation distribution is embedded into an array which is multiplied with the influence matrix in order to determine the total wake induced velocity. On the other hand, influence matrix which contains the information of each vortex filament induction on each blade element at each azimuth angle, is calculated by the help of Biot-Savart law [36].

In order to determine the influence matrix, each vortex filament in the wake geometry, is divided into vortex elements. The lengths of these vortex elements are taken smaller in the near wake in order to capture the curvatures of the vortex filament and the induction done by the vortex filament accurately; while lengths of the vortex elements get longer at far wake in which induction influence is weakest. Then influence of each vortex element from each vortex filament to each blade element is calculated by Biot-Savart's law [36]. The influence of a vortex element on a point in space is calculated with the equation (3-70);

$$\begin{Bmatrix} V_x \\ V_y \\ V_z \end{Bmatrix} = \frac{\Gamma_i}{4\pi} \frac{h}{(r_c^{2n} + h^{2n})^{1/n}} (\cos\theta_1 - \cos\theta_2) \begin{Bmatrix} e_x \\ e_y \\ e_z \end{Bmatrix} = \sigma_{ij}\Gamma_i \quad (3-70)$$

Where h defines a normal vector to the vortex element from the point that the influence of the vortex element is desired to be determined and r_c is the vortex core size.

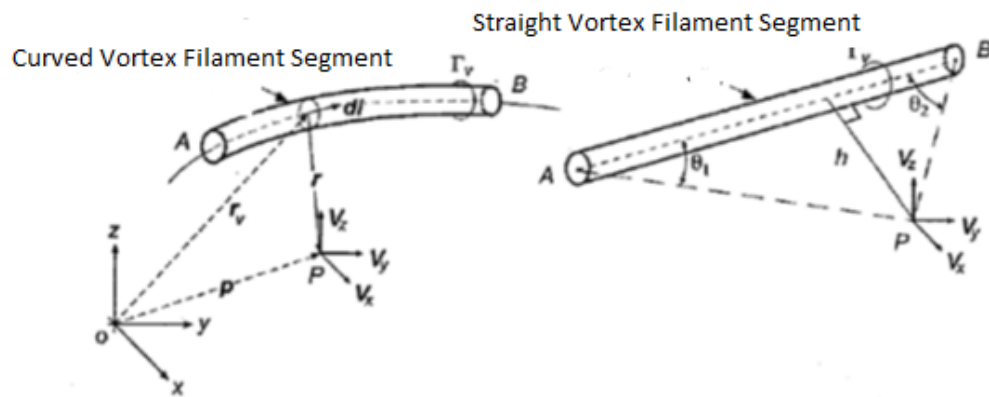


Figure 3-11 Biot-Savart's Law for curved and straight vortex filament segments [19]

If the number of blade elements is represented by n and the number of vortex elements is represented by m , then a matrix with a size of $n \times m$ including the influence coefficients can be built. Besides, similar vortex filaments are trailed from each blade of the rotor. Therefore, there will be an influence matrix for each blade of the rotor.

In order to determine the induced velocity distribution over a single blade, the influence matrices, containing influence coefficients, from each blade are multiplied with the circulation distribution of each blade. As a result, induction done by each vortex element from each vortex filament from each blade on each blade element of a single blade is determined. This process is repeated for each blade at each azimuth angle so that wake induced velocity distribution over the rotor disk is obtained. The induced velocity calculation is done with the following formula where influence matrix including wake's effect is multiplied with circulation distribution in order to determine induced velocity distribution.

$$v_i = \sum_{j=1}^{n+1} \sigma_{ij} \gamma_j \quad (3-71)$$

$$\gamma_j = \Gamma_{j-1} - \Gamma_j \quad (3-72)$$

$$v_i = \sum_{j=1}^n (\sigma_{i,j+1} - \sigma_{ij}) \Gamma_j \quad (3-73)$$

3.4.4 Forward Flight Inflow Models

Similar to hover, different inflow models are implemented with different fidelities. According to the aim of the analysis or simulation that is going to be done,

proper inflow model could be selected by the user. With the forward flight, the axial symmetry of the inflow distribution over the rotor disk starts to distort. The non-symmetric tangential velocity that blades encounter at advancing and retreating sides result in non-symmetric and complex aerodynamic load and inflow distribution on the rotor disk. Therefore unlike hover flight cases, for forward flight cases, inflow models which are able to define this non-symmetry are implemented.

Drees Linear Inflow Model

Inflow prediction over a helicopter rotor disc for both hover and forward flight conditions is an issue for which engineers have been working on for nearly a hundred years. One of the first inflow models was proposed by Glauert which was firstly only a time-averaged longitudinal inflow [17, 18, 19].

$$\lambda_i = \lambda_0 \left(1 + k_x \frac{x}{R} \right) = \lambda_0 (1 + k_x r \cos \psi)$$

(3-74)

where;

$$\lambda_{mean} = \lambda_0 = \frac{C_T}{2\sqrt{\mu^2 + \lambda_{mean}^2}}$$

(3-75)

Then the non-symmetry in lateral direction suggested to be considered by Glauert, resulting in the most general form of inflow model which is a variation of the first equation proposed. Both longitudinal and lateral variation in the inflow is modeled by Glauert which can be considered as the most general linear inflow distribution equation over the rotor disk, by the following formula [17, 18, 19];

$$\lambda_i = \lambda_0 \left(1 + k_x \frac{x}{R} + k_y \frac{y}{R} \right) = \lambda_0 (1 + k_x r \cos \psi + k_y r \sin \psi)$$

(3-76)

Starting from the time Glauert first proposed the inflow model; several attempts have been made to calculate the gradient coefficients. Drees inflow model, which is the lowest fidelity inflow model implemented in the mathematical model developed, suggests gradient formula which depends on both wake skew angle and the advance ratio. Besides, Drees model also suggests a first harmonic inflow coefficient formula for lateral inflow. Drees coefficients for the Glauert formula are determined by [18, 28];

$$k_x = \frac{4}{3} \left(\frac{1 - \cos\chi - 1.8\mu^2}{\sin\chi} \right) \text{ and } k_y = -2\mu \quad (3-77)$$

$$\chi = \tan^{-1} \left(\frac{\mu_x}{\mu_z + \lambda_i} \right) \quad (3-78)$$

When similar studies on inflow gradient are investigated, it can be stated that, “Drees, Payne and Pitt & Peters models are found to give the best representation of the inflow gradients as functions of the wake skew angle and the advance ratio when compared to the experimental evidence.” [19]. for convenience, various estimated values of first harmonic inflow gradient coefficient formulas are given at the Table 1. It should be noticed that, only Drees’s inflow model deals with lateral inflow distribution.

Table 1 Estimated values of first harmonic inflow gradient coefficient formulas [19]

Author(s)	k_x	k_y
Coleman et al. (1945)	$\tan(\chi/2)$	0
Drees (1949)	$\frac{4}{3} \left(\frac{1 - \cos\chi - 1.8\mu^2}{\sin\chi} \right)$	-2μ
Payne (1959)	$\frac{4}{3} \left[\frac{\mu}{L\lambda} / (1.2 + \mu/\lambda) \right]$	0
White & Blake (1979)	$\sqrt{2}\sin\chi$	0
Pitt & Peters (1981)	$\left(\frac{15\pi}{23} \right) \tan\left(\frac{\chi}{2}\right)$	0
Howlett (1981)	$\sin^2\chi$	0

The assumption of linear radial inflow distribution over the blades, means neglecting the tip and root losses which differs the inflow solution from reality dramatically. However for certain applications or analysis done with the mathematical model developed at which lower inflow fidelity is acceptable, computationally efficient Drees model can be selected by the user. In addition comparison between the inflow distribution determined by Drees inflow model and experimental results are given in Figure 3-12 and Figure 3-13.

Mangler & Squire Inflow Model

A higher fidelity inflow model studied in this study which uses incompressible, linearized, Euler equations in order to relates the pressure distribution across the rotor disk to inflow distribution, is Mangler & Squires 's nonuniform inflow model. Inflow is described by the Fourier series;

$$\lambda_i = \left(\frac{2C_T}{\mu}\right) \left[\frac{c_0}{2} + \sum_{n=1}^{\infty} (-1)^n c_r(r, \alpha) \cos n\psi \right] \quad (3-79)$$

The coefficients in the Fourier series are determined by the linear combination of two types of inflow forms for which the linear combination weights are decided by the user. Type-1, which gives an elliptical loading and consistent with Glauert's high-speed approximation, coefficients are calculated with;

$$c_0 = \frac{3}{4}v \quad (3-80)$$

$$c_1 = -\frac{3\pi}{16} \sqrt{1-v^2} \left(\frac{1-\sin\alpha}{1+\sin\alpha} \right)^{1/2} \quad (3-81)$$

Where $v^2=1-r^2$. For even values of n equal or bigger than two,

$$c_n = (-1)^{\frac{n-2}{2}} \left(\frac{3}{4}\right) \left(\frac{v+n}{n^2-1}\right) \left(\frac{1-v}{1+v}\right)^{n/2} \left(\frac{1-\sin\alpha}{1+\sin\alpha}\right)^{n/2} \quad (3-82)$$

And for odd values of n equal or bigger than three, c_n is directly equated to zero.

Type-3, which gives a load distribution vanishing at the edges and center of the rotor disk, coefficients are calculated by;

$$c_0 = \frac{15}{8}v(1-v^2) \quad (3-83)$$

$$c_1 = -\frac{15\pi}{256} (5 - 9v^2) \sqrt{1 - v^2} \left(\frac{1 - \sin\alpha}{1 + \sin\alpha} \right)^{1/2} \quad (3-84)$$

$$c_3 = \frac{45\pi}{256} (1 - v^2)^{3/2} \left(\frac{1 - \sin\alpha}{1 + \sin\alpha} \right)^{3/2} \quad (3-85)$$

For even values of n equal or bigger than two,

$$c_n = (-1)^{\frac{n-2}{2}} \left(\frac{15}{8} \right) \left[\left(\frac{v+n}{n^2-1} \right) \left(\frac{9v^2+n^2-6}{n^2-9} \right) + \left(\frac{3v}{n^2-9} \right) \left(\frac{1-v}{1+v} \right)^{n/2} \left(\frac{1-\sin\alpha}{1+\sin\alpha} \right)^{n/2} \right] \quad (3-86)$$

On the other hand, for odd values that n are equal or greater to five, c_n is equated to zero.

Then the linear combination of the Type-1 and Type-3 loadings is determined by the formula below;

$$\Delta p = \omega_1 \Delta p_1 + \omega_3 \Delta p_3, \quad \omega_1 + \omega_3 = 1 \quad (3-87)$$

The iteration loop that uses Mangler & Squire inflow model requires an initial thrust value of the rotor in order to start the iterative procedure. Besides, a good starting point decreases the computational effort for the iteration loop. Therefore, rotor thrust coefficient is determined by Drees inflow model and used as an initial value for Mangler & Squire inflow model.

The inflow distribution results taken by both Mangler & Squire inflow model with a linear combination of half by half and Drees inflow model are compared with the experimental data in the Figure 3-12 and Figure 3-13. [28];

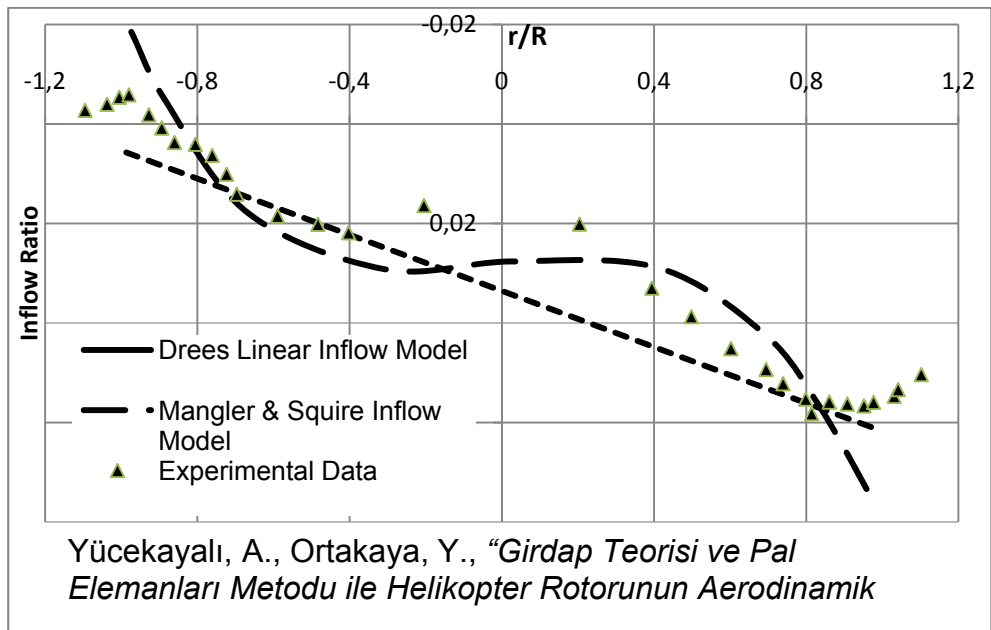


Figure 3-12 Drees and M&S inflow distribution comparison with experimental results [28]

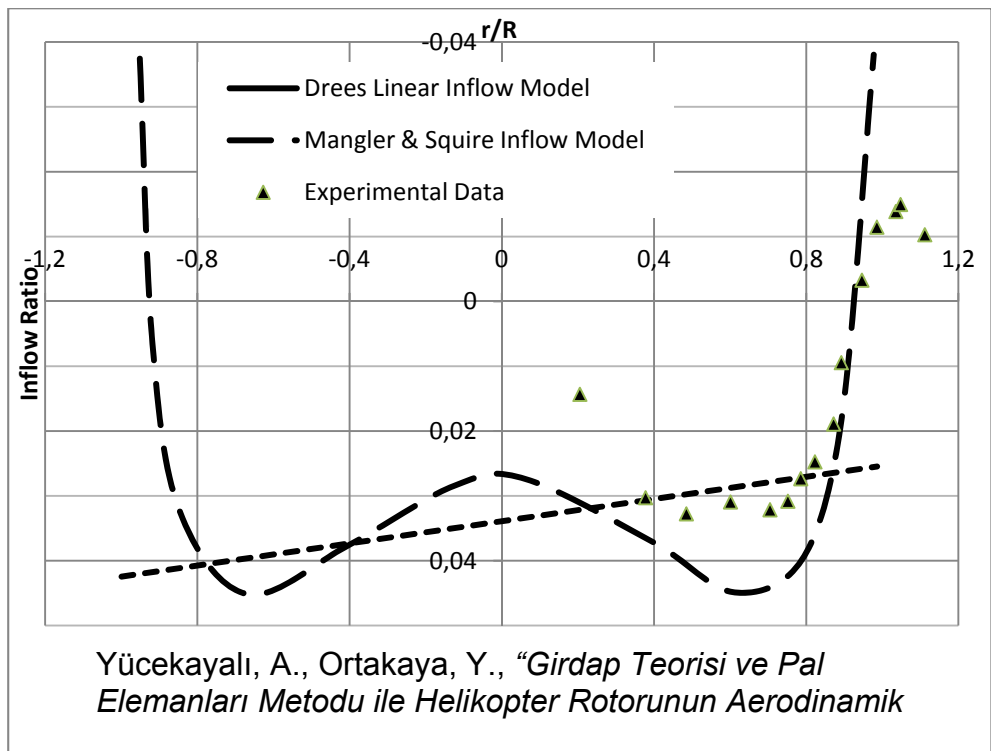


Figure 3-13 Drees and M&S inflow distribution comparison with experimental results [28]

3.4.5 Forward Flight Wake Models

Unlike hover flight cases, forward flight wake geometry is non-uniform and axial symmetry does not exist. Non-uniform aerodynamic load distribution is generated over the rotor disk while resulting in non-uniform and non-symmetric induced velocity and downwash distribution. Rotors downwash is non-uniformly interacts with the wake trailed from each blade and vortex filaments interacts self or mutually with each other therefore wake geometry for forward flight is highly distorted. On the other hand, in high advance ratios, vortex filaments trailed are getting away from the blades rapidly, while decreasing the influence on the blade. Therefore two prescribed wake geometry models, an undistorted and a distorted, are implemented into the mathematical model developed. The undistorted prescribed wake model represents the simplicity and low fidelity; on the other hand the distorted prescribed wake model represents higher fidelity solutions for wake induced velocity over the rotor disk which is desirable when accurate rotor aerodynamic load predictions are required. Besides, both wake models implemented are prescribed wake models, which are always considered a modeling option in any form of the rotor analysis with the relative simplicity and the computation efficiency which is at least two orders of magnitude less expensive [19].

Undistorted Wake Model (Rigid Wake Model)

The undistorted wake model assumes the wake of the rotor is uniform in which induced velocity does not change with time or position [19]. Vortex filaments geometries are defined according to the flight conditions and momentum theory. The thrust coefficient existing in the undistorted wake model equations is initially determined with simple momentum theory whereas within the iteration loop, the thrust coefficient is calculated repeatedly with the inflow model selected by the user. As mentioned, in forward flight cases the importance of the wake geometry decreases with increasing forward flight velocity when compared with the hover flight cases. Although undistorted wake model is far different from the real wake geometry, the model is sufficient enough to determine the primary effects of the wake over inflow distribution over the rotor disk [19]. Therefore, undistorted wake model is a useful wake geometry prediction method where high accuracy on rotor

aerodynamic loads is not required. Undistorted wake geometry is modeled with the equations (3-88) to (3-96);

$$\frac{\delta \vec{r}}{\delta \psi_b} + \frac{\delta \vec{r}}{\delta \psi_w} = \mu \hat{i} + \lambda_i \hat{k} \quad (3-88)$$

$$\psi_b: r(\psi_b, \psi_w) = r(\psi_b + 2\pi, \psi_w) \quad (3-89)$$

$$\psi_w: r(\psi_b, 0) = r_v \cos \psi_b \hat{i} + r_v \sin \psi_b \hat{j} \quad (3-90)$$

$$\vec{r}(\psi_b, \psi_w) = (\mu \psi_w + r_v \cos(\psi_b - \psi_w)) \hat{i} + r_v \sin(\psi_b - \psi_w) \hat{j} + \lambda_i \psi_w \hat{k} \quad (3-91)$$

$$\frac{x_{tip}}{R} = \dot{x}_{tip} = \cos(\psi_b - \psi_w) + \mu \psi_w \quad (3-92)$$

$$\frac{y_{tip}}{R} = \dot{y}_{tip} = \sin(\psi_b - \psi_w) \quad (3-93)$$

$$\frac{z_{tip}}{R} = \dot{z}_{tip} = \lambda_i \psi_w = -\mu \psi_w \tan \chi_{TPP} \quad (3-94)$$

$$\chi_{TPP} = \text{atan}\left(\frac{\lambda_i}{\mu}\right)$$

(3-95)

$$\lambda_i = \mu \tan \alpha_{TPP} + \frac{\kappa C_T}{2\sqrt{\mu^2 + \lambda_i^2}}$$

(3-96)

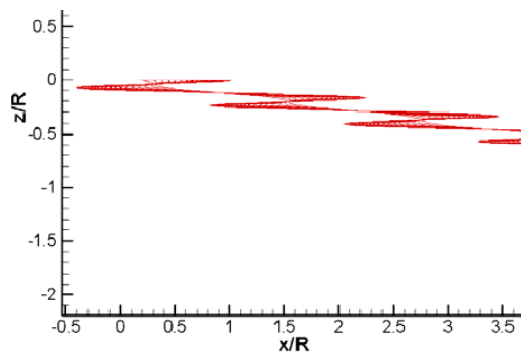


Figure 3-14 Undistorted Prescribed Wake Model

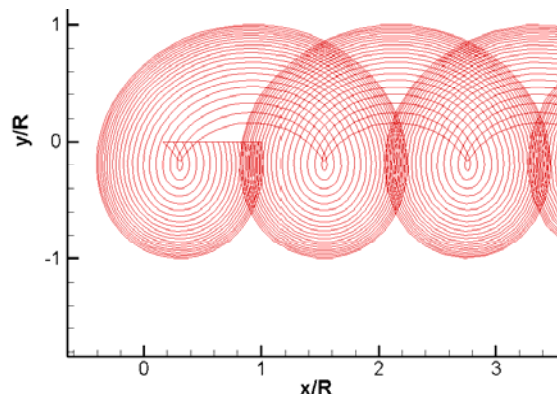


Figure 3-15 Undistorted Prescribed Wake Model

Beddoes's Generalized Wake Model

The second wake model implemented into the mathematical model is Beddoes's Generalized Wake Model which is a distorted wake model while taking non-uniform induced velocity distribution into account [57]. Although it is a prescribed wake model developed by empirical and experimental methods, it is found to be very effective in predicting the rotor wake geometry [57]. The self or mutual interactions of vortex filaments, distortion because of the rotor downwash and non-uniformity of the induced velocity in the rotor wake effects are included in this prescribed wake model. As being implemented into the mathematical model developed as default wake model for forward flight, according to the aim of the analysis, undistorted wake model can also be selected for calculations.

Beddoes's prescribed wake geometry is determined with the equations below for which an example of the wake geometry prediction is given in Figure 3-16;

$$\lambda_i = \lambda_0 (1 + E\dot{x} - E|(\dot{y})^3|) \quad (3-97)$$

$$\lambda_i = 2\lambda_0(1 - E|(y'_{Np})^3|) \quad (3-98)$$

$$\dot{z} = -\mu_z\psi_w + \int_0^{\psi_w} \lambda d\psi_b \quad (3-99)$$

If $\dot{x} < -\cos(\psi_b - \psi_w)$; then no convection of the vortex filament above the rotor disk. In this case;

$$\int_0^{\psi_w} \lambda d\psi_b = \lambda_0(1 + E(\cos(\psi_b - \psi_w) + 0.5\mu\psi_w - |(\dot{y})^3|))\psi_w \quad (3-100)$$

If, $\cos(\psi_b - \psi_w) > 0$; then vortex filament element is always in the downwash of the rotor and in this case;

$$\int_0^{\psi_w} \lambda d\psi_b = -2\lambda_0(1 - E|(\dot{y})^3|)\psi_w \quad (3-101)$$

If both cases are not satisfied, than the vortex filament element spends its time half in rotor disk and half in the downwash way of the rotor. In this case the geometry of the vortices in the helicopter wake are calculated as;

$$\int_0^{\psi_w} \lambda d\psi_b = -2\lambda_0 \dot{x} \frac{(1 - E|(\dot{y})^3|)}{\mu_z} \quad (3-102)$$

$$\mu_z = V_\infty \cos \alpha_{TPP} / (\Omega R) \quad (3-103)$$

$$\frac{x}{R} = \dot{x} = r_v \cos(\psi_b - \psi_w) + \mu\psi_w \quad (3-104)$$

$$\frac{y}{R} = \dot{y} = r_v \sin(\psi_b - \psi_w) \quad (3-105)$$

$$\frac{z}{R} = -\mu_z \psi_w + \int_0^{\psi_w} \lambda d\psi_b \quad (3-106)$$

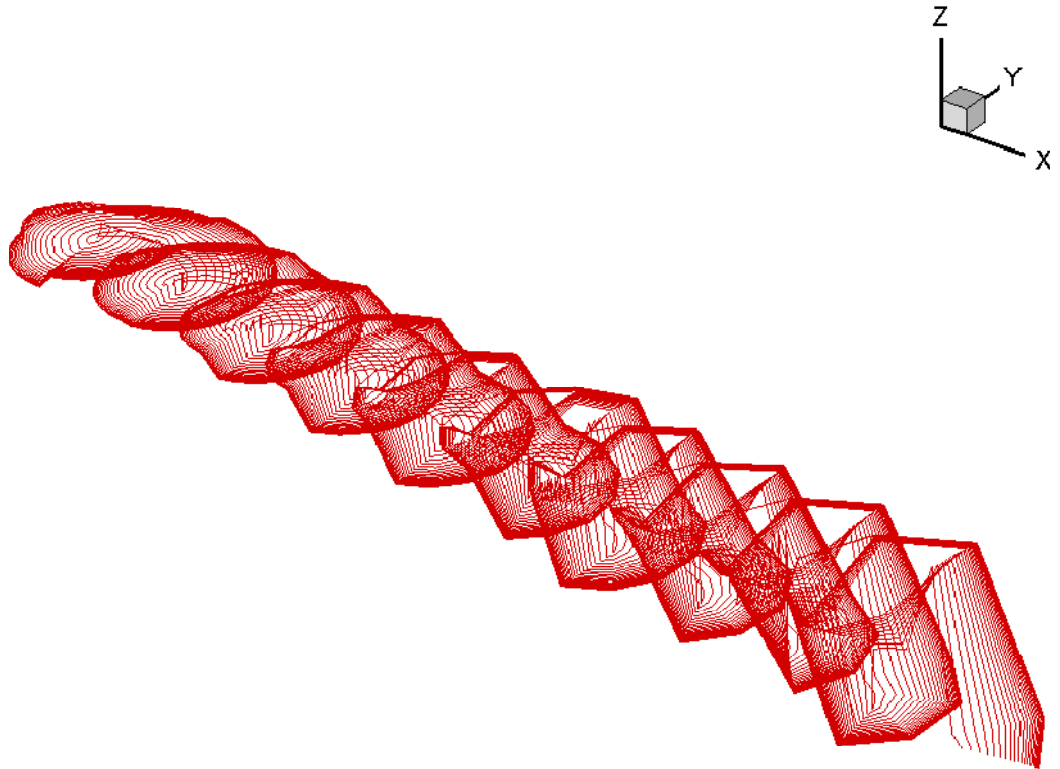


Figure 3-16 Beddoes' Prescribed Wake Model

3.4.6 Forward Flight Wake Induced Velocity Model

Similar to the hover wake induced velocity calculation, Biot-Savart's Law is used which is explained in wake induced velocity for hover flight cases part of this study. For forward flight cases, similar to hover, the induced velocity distribution over a single blade, the influence matrices, containing influence coefficients, from each blade are multiplied with the circulation distribution of each blade. As a result, induction done by each vortex element from each vortex filament from each blade on each blade element of a single blade is determined. This process is repeated for each blade at each azimuth angle so that wake induced velocity distribution over the rotor disk is obtained. However, for forward flight conditions, circulation distribution over the rotor disk is not axis-symmetric. Unlike hover, as the aerodynamic loads generated by each blade element changes with azimuth, the circulation and trailed vortices strengths changes also with azimuth angle. Therefore, the vortex strength term in the formulation of influence matrix now depends on both radial location and wake age. The wake induced velocity formulation is then modified and derived as;

$$v_i = \sum_{j=1}^{n+1} \sigma_{ij} \gamma_j \quad (3-107)$$

$$\gamma_j = \Gamma_{j-1} - \Gamma_j \quad (3-108)$$

$$v_i = \sum_{j=1}^n (\sigma_{i,j+1} - \sigma_{ij}) \Gamma_j \quad (3-109)$$

The comparison of the aerodynamic load distributions over the rotor disk determined by Drees and Mangler & Squire's inflow models and vortex theory are done and given at Appendix C. Besides, aerodynamic load distribution over the rotor

disc determined by vortex theory at various forward flight speeds and control angles are given at Appendix C.

3.5 Tail Rotor Model

Throughout this study, tail rotor is considered as only two dimensional force contributor to the whole helicopter system. When compared with the main rotor, except from the thrust and drag components, the force and moments generated by the tail rotor may be neglected [6]. This is also validated at mathematical model validation part of this study. Therefore, lower fidelity aerodynamic models are implemented for tail rotor analysis.

3.5.1 Tail Rotor Hub & Blade Model

Similar to main rotor procedure, blade element method is used to calculate aerodynamic force and moment distributions on the tail rotor disk. Tail rotor blades are divided into ten elements (the default value, however it can be altered as desired by the user) for each of which aerodynamic force and moments are calculated individually. Blades are assumed to be rigid therefore blades do not deform under any loading. Besides, tail rotor blades are not permitted to flap or deflect at any direction. This leads inertial and centrifugal terms in the total force and moment equations of the tail rotor to drop.

For tail rotor, unlike the main rotor, only collective control is available in the developed mathematical model which is mostly the case in helicopters. Without flapping dynamics, deformation or deflection and cyclic control, tail rotor model reduces to a rotor model with thrust control only. Besides, throughout the study, tail rotor hub type is assumed to be hingeless hub type with collective control only which does not allow the blade off-plane motion.

As mentioned, tail rotor blades are divided into blade elements, generally equal widths, for each of which local incidences are calculated. For each blade element, local incidence is calculated taking collective control and twist (if exists) into account. For each blade element, the pitch angle is computed as;

$$\theta = \theta_0 + \bar{r}\theta_t$$

(3-110)

Where θ_0 is the collective angle which is controlled by the pilot or the trim model, r is the non-dimensional blade radial position on the blade, θ_t is the blade twist angle (if exists). Incidence calculated for each blade element is used by the aerodynamic model where with the inflow information and effective angle of attack the aerodynamic force and moments generated by the each blade element is calculated.

3.5.2 Inflow Model

The most important force component of the tail rotor is assumed to be the thrust. Therefore an inflow model with which only the thrust generated is predicted accurate enough is required. Besides, tail rotor blades are assumed to be rigid and hub is assumed to be hingeless. This eliminates blade flapping, deformation or any deflections while clearing off total centrifugal and inertial force and moments transferred to the hub of the tail rotor. In addition, when total force and moments acting to the center of mass of the whole system and the respectively big moment arm of the tail rotor, tail rotor thrust values are considered to be at second importance in this study. On the other hand, helicopters have the ability to make a yaw or coordinated turn maneuver to both sides. This brings the necessity of tail rotor thrusts to be able to change in a range from negative values to positive values which would provide the moment required for the desired maneuver. Therefore tail rotor control ranges usually includes negative and positive collective values, which requires tail rotor inflow models to be still able to work with negative collective inputs. As a conclusion, inflow models which are at low fidelity levels however accurate enough to be able to model the helicopter behavior properly, computationally cost efficient so that the main computation effort could be spend for main rotor, and reliable which conformable to work under a wide range of collective inputs including negative and positive values are assigned for tail rotor mathematical model.

Similar to main rotor, different inflow models are implemented for tail rotor alternative to each other and the selection of the model is left to the user. For flight conditions for which tail rotor can be considered as a hovering rotor, momentum theory which depends on collective control, solidity and lift curve slope parameters of the tail rotor and Prandtl's tip loss function combined with momentum theory which captures tip losses decently are implemented.

As mentioned in main rotor inflow models for hover, Prandtl tip loss function modifies the momentum theory. Prandtl's tip loss function equations are already been mentioned at Main Rotor Inflow Models section of this study.

The Prandtl's tip loss function is implemented in momentum theory and blade element theory. Radial inflow distribution determined from blade element momentum theory modified with Prandtl's tip loss function for hover flight conditions is calculated by;

$$\lambda(r) = \frac{\sigma C_{l\alpha}}{16F} \left(\sqrt{1 + \frac{32F}{\sigma C_{l\alpha}} \theta r} - 1 \right) \quad (3-111)$$

For flight conditions for which the total freestream velocity including relative velocities and body translational velocity, can be considered as forward flight, momentum theory and Drees inflow models are implemented for tail rotor inflow models.

Inflow distribution from momentum theory is determined by;

$$\lambda_i = \mu \tan(\alpha_{Tpp}) + \frac{C_T}{2\sqrt{\mu^2 + \lambda_i^2}} \quad (3-112)$$

On the other hand, Drees inflow model which is in general a method for determining the longitudinal and lateral inflow distribution coefficients of the Glauert's inflow distribution formula is implemented with the following equations;

The Glauert's general inflow model;

$$\lambda_i = \lambda_0 \left(1 + k_x \frac{x}{R} + k_y \frac{y}{R} \right) = \lambda_0 (1 + k_x r \cos \psi + k_y r \sin \psi) \quad (3-113)$$

The coefficients of the Glauert's general inflow model are determined from Drees's approximations as;

$$k_x = \frac{4}{3} \left(\frac{1 - \cos \chi - 1.8 \mu^2}{\sin \chi} \right) \text{ and } k_y = -2\mu \quad (3-114)$$

Where wake skew angle is calculated from;

$$\chi = \tan^{-1} \left(\frac{\mu_x}{\mu_z + \lambda_i} \right) \quad (3-115)$$

Option to select any of the inflow models implemented in the mathematical model developed is left to the user. According to the aim of the analyses, proper inflow model should be selected.

3.5.3 Aerodynamic Model

For tail rotor, similar to main rotor, blade element method is implemented in order to determine aerodynamic force and moment distribution on the rotor disk. The induced velocity or inflow distribution that blade element method requires is calculated from empirical methods that are explained in tail rotor inflow model part in detail.

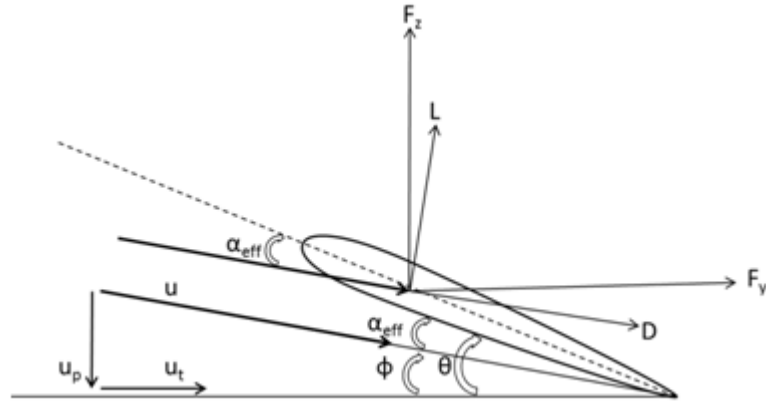


Figure 3-17 Blade element force and angle definitions

The absence of flapping dynamics and cyclic controls, leads simplifications in the both inflow model and aerodynamic model. For aerodynamic calculation, effective angle of attack is determined from equation (3-116).

$$\alpha_{\text{effective}} = \theta - \phi \quad (3-116)$$

where θ is local pitch angle including blade twist and collective control and ϕ is the local inflow angle which is the angle between normal and tangential components of the local freestream air velocity. Local velocities are determined by the tail rotor inflow model where helicopter translational and rotational motions that are generating relative velocities for tail rotor are taken into account. The inflow angle for each blade element on the tail rotor blades are calculated as follows;

$$\phi_{r,\psi} = \text{atan2}(u_p, u_t) \quad (3-117)$$

Perpendicular and tangential freestream velocities that each tail rotor blade element encounters are determined from superposition of velocity contributions.

Tangential velocity contributions are defined as tail rotor rotation, helicopter translational velocities and relative velocities generated because of helicopter rotational velocities.

$$u_{t_{\text{rotation}}} = \Omega r \quad (3-118)$$

$$u_{t_{\text{advance ratio}}} = \mu(\Omega R) \quad (3-119)$$

$$u_{t_{\text{relative}}} = -qZ_{\text{hub}} \cos \psi \quad (3-120)$$

$$u_t = f(r, \psi, \mu, q) = u_{t_{\text{rotation}}} + u_{t_{\text{advance ratio}}} u_{t_{\text{relative}}} \quad (3-121)$$

Perpendicular velocity contributions for each tail rotor blade element are defined as the induced velocity, relative velocity because of the helicopter rotational velocities and helicopter translational velocity in body y axis direction.

$$u_{p_{\text{climb \& descent}}} = V_{\text{helicopter}} \quad (3-122)$$

$$u_{p_{\text{relative}}} = -rX_{\text{hub}} - pZ_{\text{hub}} \quad (3-123)$$

$$u_{p_{\text{induced velocity}}} = \lambda_i(\psi) \quad (3-124)$$

$$u_p = f(r, \psi, \lambda_i, r, p) = u_{p_{\text{climb \& descent}}} + u_{p_{\text{relative}}} + u_{p_{\text{induced velocity}}} \quad (3-125)$$

Aerodynamic force and moment coefficients are determined by table look-up where coefficient tables depend on local angle of attack and Mach number. Angle of attack is determined from the difference between local incidence of the blade elements and the inflow angle where local Mach number is calculated from the ratio of total blade element velocity to speed of sound.

$$\alpha_{\text{eff.}} = \theta_r - \phi_{r,\psi} \quad (3-126)$$

$$M_{r,\psi} = \sqrt{u_p^2 + u_t^2} / a \quad (3-127)$$

As the aerodynamic coefficients are interpolated with table look-up method, the lift and drag forces that each blade element generate changing in both radial and azimuthal direction is determined with the equations below;

$$dL_{r,\psi} = 1/2 \rho V_{r,\psi}^2 C_{l_{r,\psi}} \quad (3-128)$$

$$dD_{r,\psi} = 1/2 \rho V_{r,\psi}^2 C_{d_{r,\psi}} \quad (3-129)$$

Lift and drag forces generated are transformed into tail rotor hub reference frame with the help of the trigonometric relations as defined below;

$$dF_z(r, \psi) = dL_{r,\psi} \cos\phi - dD_{r,\psi} \sin\phi \quad (3-130)$$

$$dF_x(r, \psi) = dL_{r,\psi} \sin\phi + dD_{r,\psi} \cos\phi \quad (3-131)$$

The forces generated by tail rotor in tail rotor hub reference frame are azimuth averaged and transformed into body reference frame system with the transformation matrix defined in Coordinate Systems chapter. The averaged x and z component forces are calculated as follows;

$$\bar{F}_x = \frac{(\sum_{i=1}^{N_A} F_x(\psi))}{N_A} N_b \quad (3-132)$$

$$\bar{F}_z = \frac{(\sum_{i=1}^{N_A} F_z(\psi))}{N_A} N_b \quad (3-133)$$

3.6 Fuselage Model

Fuselage aerodynamic force and moment are calculated from aerodynamic coefficient table of the fuselage which is in wind axis reference frame. Aerodynamic center of the fuselage and mass center of the helicopter does not have to be coincident therefore aerodynamic offset option is available in the developed mathematical model. Aerodynamic force and moments generated by the fuselage acting on the aerodynamic center of the fuselage are transferred to the mass center of the helicopter and combined with the gravitational forces in order to determine total force and moments acting on the fuselage.

The total air velocities that fuselage encounter at its aerodynamic center are calculated from superposition of flight velocities at body axis reference frame, the relative velocities formed from rotational rates of the helicopter and the downwash of the main rotor.

Freestream velocity is defined in body axis reference frame which is also fuselage coordinate system.

$$u_{F_{freestream}} = u_B \quad (3-134)$$

$$v_{F_{freestream}} = v_B \quad (3-135)$$

$$w_{F_{freestream}} = w_B \quad (3-136)$$

Relative velocities occur because of the helicopter rotational rates and offset between fuselage aerodynamic center and mass center of the helicopter. The offset vector is given by;

$$\vec{R}_{F_{a.c.}} = \vec{i}x_{F_{a.c.}} + \vec{j}y_{F_{a.c.}} + \vec{k}z_{F_{a.c.}} \quad (3-137)$$

In order to calculate relative velocities that fuselage encounter because of the helicopter rotational rates, offset vector and helicopter p, q, r rates are cross multiplied.

$$u_{F_{relative}} = -z_{F_{a.c.}}q + y_{F_{a.c.}}r \quad (3-138)$$

$$v_{F_{relative}} = -x_{F_{a.c.}}r + z_{F_{a.c.}}p \quad (3-139)$$

$$w_{F_{relative}} = -y_{F_{a.c.}}p + x_{F_{a.c.}}q \quad (3-140)$$

In addition, in most of the flight cases in the flight envelope of the helicopter, fuselage operates under the effect of main rotor. The downwash of the main rotor changes dynamic pressure and angle of attack of the fuselage. In this study, the rotational velocities in the rotor wake are neglected resulting in two dimensional downwash effects on the fuselage.

$$X_{TPP} = atan\left(-\frac{\lambda_i}{\mu}\right) \quad (3-141)$$

λ_i term in the skew angle equation is the total mean inflow through the rotor disk. It is normally calculated in main rotor aerodynamic model, where aerodynamic force and moment generated by main rotor are determined. However, an option is implemented which lets the mathematical model to approximate the inflow through the rotor disk by using advance ratio and thrust coefficient of the main rotor. The mean inflow of the main rotor is calculated with the equation (3-142);

$$\lambda_i = \mu tan\alpha_{TPP} + \frac{C_T}{2\sqrt{\mu^2 + \lambda_i^2}} \quad (3-142)$$

With an iterative process, mean inflow through the main rotor is approximately calculated rapidly. The main assumption for this is that main rotor is modeled with momentum theory and main rotor downwash does not change in

position and does not rotate. Therefore, the inflow calculated is directly added as downwash to the fuselage.

$$u_F = u_{F_{Freestream}} + u_{F_{Relative}} - \lambda_i \sin X_{TPP} \quad (3-143)$$

$$v_F = v_{F_{Freestream}} + v_{F_{Relative}} \quad (3-144)$$

$$w_F = w_{F_{Freestream}} + w_{F_{Relative}} + \lambda_i \cos X_{TPP} \quad (3-145)$$

Aerodynamic force and moments generated by the fuselage are calculated from aerodynamic coefficient tables which depend on angle of attack and sideslip of the fuselage and from dynamic pressure over the fuselage. Total air velocity components that fuselage encounter are used to calculate angle of attack, sideslip and dynamic pressure.

$$\alpha_{Fus.} = \text{atan2}(w_F, u_F) \quad (3-146)$$

$$\beta_{Fus.} = \text{atan2}(v_F, u_F) \quad (3-147)$$

$$q_{Fus.} = 1/2 \rho \left(\sqrt{u_F^2 + v_F^2 + w_F^2} \right)^2 \quad (3-148)$$

Aerodynamic force and moments generated by the fuselage are acting on the aerodynamic center of the fuselage and in wind axis reference frame. Therefore, aerodynamic loads are converted to body axis reference frame from wind axis reference frame with the transformation matrix [Appendix A]. The offset between mass center of the helicopter and aerodynamic center of the fuselage is used to transfer the loads to the center of gravity of the helicopter and combine with the gravitational force in order to determine total force and moments generated by the fuselage and acting on the mass center of the helicopter.

Aerodynamic force and moment generated by the fuselage are computed with the following equations;

$$F_{x_w} = q_{Fus} \cdot S_{ref} \cdot c_x \quad (3-149)$$

$$F_{y_w} = q_{Fus} \cdot S_{ref} \cdot c_y \quad (3-150)$$

$$F_{z_w} = q_{Fus} \cdot S_{ref} \cdot c_z \quad (3-151)$$

$$M_{x_w} = q_{Fus} \cdot S_{ref} \cdot c_{mx} l_{ref}. \quad (3-152)$$

$$M_{y_w} = q_{Fus} \cdot S_{ref} \cdot c_{my} l_{ref}. \quad (3-153)$$

$$M_{z_w} = q_{Fus} \cdot S_{ref} \cdot c_{mz} l_{ref}. \quad (3-154)$$

Where reference length is taken as diameter and reference area is the main rotor disk area;

$$S_{ref.} = \pi R_{MR}^2 \quad (3-155)$$

Then the force and moments calculated in wind axis reference frame are transformed into body axis reference frame with the wind to body reference frame transformation matrix;

$$L_{BW} = \begin{bmatrix} \cos\alpha\cos\beta & -\cos\alpha\sin\beta & -\sin\alpha \\ \sin\beta & \cos\beta & 0 \\ \sin\alpha\cos\beta & -\sin\alpha\sin\beta & \cos\alpha \end{bmatrix} \quad (3-156)$$

$$\vec{F}_{Fus.aero} = \begin{Bmatrix} Fx_{Fus.aero} \\ Fy_{Fus.aero} \\ Fz_{Fus.aero} \end{Bmatrix} = \begin{bmatrix} \cos\alpha\cos\beta & -\cos\alpha\sin\beta & -\sin\alpha \\ \sin\beta & \cos\beta & 0 \\ \sin\alpha\cos\beta & -\sin\alpha\sin\beta & \cos\alpha \end{bmatrix} \begin{Bmatrix} Fx_w \\ Fy_w \\ Fz_w \end{Bmatrix} \quad (3-157)$$

$$\vec{M}_{Fus.aero} = \begin{Bmatrix} Mx_{Fus.aero} \\ My_{Fus.aero} \\ Mz_{Fus.aero} \end{Bmatrix} = \begin{bmatrix} \cos\alpha\cos\beta & -\cos\alpha\sin\beta & -\sin\alpha \\ \sin\beta & \cos\beta & 0 \\ \sin\alpha\cos\beta & -\sin\alpha\sin\beta & \cos\alpha \end{bmatrix} \begin{Bmatrix} Mx_w \\ My_w \\ Mz_w \end{Bmatrix} \quad (3-158)$$

Besides, gravitational force acting on the whole helicopter is computed as a fuselage force, acting on the center of the mass of the helicopter. Therefore, gravitational force is added to fuselage total force and moments. Gravitational acceleration is transformed from inertial to body reference frame with the transformation matrix and multiplied with the total mass of the helicopter in order to calculate the gravitational force acting on the helicopter center of mass in body axis coordinate system.

$$\begin{aligned}
& \begin{Bmatrix} F_{X_{Fus.Grav}} \\ F_{Y_{Fus.Grav}} \\ F_{Z_{Fus.Grav}} \end{Bmatrix} \\
& = \begin{bmatrix} \cos\theta\cos\varphi & -\cos\theta\sin\varphi & -\sin\theta \\ -\sin\theta\sin\theta\cos\varphi - \cos\theta\sin\varphi & \sin\theta\sin\theta\sin\varphi - \cos\theta\cos\varphi & -\sin\theta\cos\theta \\ -\cos\theta\sin\theta\cos\varphi + \sin\theta\sin\varphi & \cos\theta\sin\theta\sin\varphi + \sin\theta\cos\varphi & -\cos\theta\cos\theta \end{bmatrix} \begin{Bmatrix} 0_I \\ 0_I \\ -9.81_I \end{Bmatrix} M
\end{aligned}
\tag{3-159}$$

Finally, total force equation for the fuselage is derived as;

$$\vec{F}_{Fus.} = \vec{F}_{Fus.aero} + \vec{F}_{Fus.Grav}
\tag{3-160}$$

Taking the aerodynamic offset of the fuselage, the total moments acting to the center of mass by the fuselage are determined as the summation of aerodynamic moments and moment due to aerodynamic forces and aerodynamic offset of the fuselage;

$$\vec{R}_{F_{a.c.}} = \vec{i}_{F_{a.c.}} + \vec{j}_{F_{a.c.}} + \vec{k}_{F_{a.c.}}
\tag{3-161}$$

$$\vec{M}_{Fus.} = \vec{R}_{F_{a.c.}} \times \vec{F}_{Fus.aero} + \vec{M}_{Fus.aero}
\tag{3-162}$$

3.7 Horizontal Tail Model

As component built up method enables to calculate loads generated by each component separately and then superpose them, aerodynamic force and moments generated by horizontal tail are calculated at its own aerodynamic center and then transferred to the center of mass of the whole aircraft. Total air velocities that horizontal tail encounters are calculated from superposition of body, relative and

downwash velocities. Angle of attack and local Mach number are calculated from geometric relations between total freestream velocity components and aerodynamic coefficients are determined from look-up tables which are also angle of attack and Mach number dependent. The horizontal tail reference system is shown in Figure 3-18 according to which aerodynamic force and moments generated are calculated.

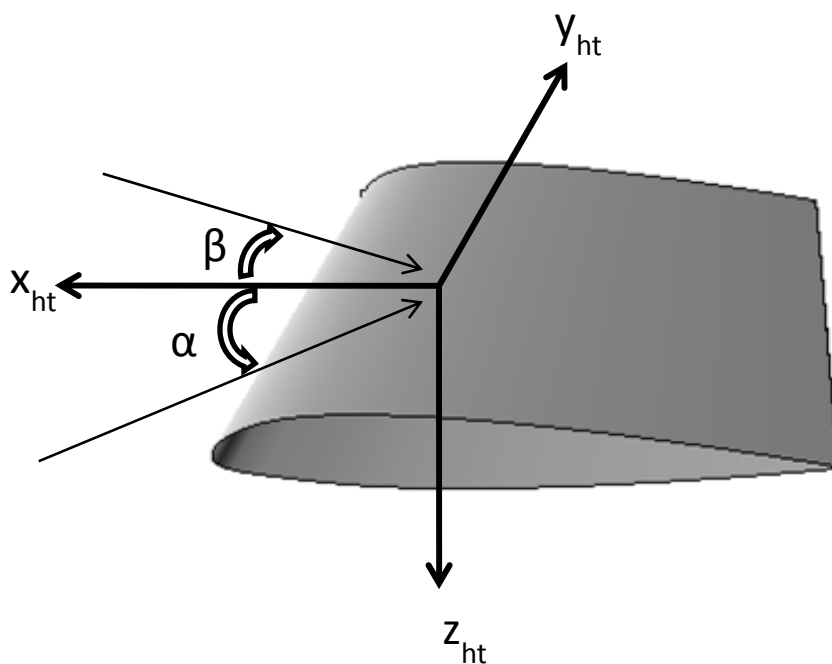


Figure 3-18 Horizontal tail reference system and angle definitions

As body reference frame and horizontal tail reference frames are equivalent, there is no need for any transformation. Therefore, the freestream air velocity vector for horizontal tail is same with one for helicopter body.

$$u_{ht\text{freestream}} = u_B \quad (3-163)$$

$$v_{ht\text{freestream}} = v_B \quad (3-164)$$

$$w_{ht\text{freestream}} = w_B \quad (3-165)$$

Relative velocity components occur because of the helicopter rotational velocities are calculated with the cross product of aerodynamic offset vector which is the vector from aerodynamic center of the horizontal tail to the center of gravity of the helicopter with helicopter body rotational velocities.

$$\vec{R}_{ht\text{a.c.}} = \vec{i}x_{ht\text{a.c.}} + \vec{j}y_{ht\text{a.c.}} + \vec{k}z_{ht\text{a.c.}} \quad (3-166)$$

$$u_{ht\text{relative}} = -z_{ht\text{a.c.}}q + y_{ht\text{a.c.}}r \quad (3-167)$$

$$v_{ht\text{relative}} = -x_{ht\text{a.c.}}r + z_{ht\text{a.c.}}p \quad (3-168)$$

$$w_{ht\text{relative}} = -y_{ht\text{a.c.}}p + x_{ht\text{a.c.}}q \quad (3-169)$$

Main rotor downwash on horizontal tail is calculated by using total induced vertical velocity through the main rotor and wake skew angle. The skew angle interval in which main rotor downwash effect would be included in horizontal tail velocity components is an input parameter and is specific to helicopter. The main assumption in calculating the main rotor downwash effect on horizontal tail, similar to the fuselage model, is that main rotor inflow across the rotor disk does not change in time and position. Besides, main rotor wake is assumed to be uniform and none rotating. Skew angle is determined by;

$$X_{TPP} = \text{atan}\left(-\frac{\lambda_i}{\mu}\right) \quad (3-170)$$

Similar to the downwash effect calculation of fuselage, normally for inflow through the rotor disk is calculated by aerodynamic model of the main rotor. However, another option which approximates the main rotor inflow ratio by using momentum theory is implemented. The downwash of the main rotor is then calculated from momentum theory with the equation below;

$$\lambda_i = \mu \tan \alpha_{TPP} + \frac{C_T}{2\sqrt{\mu^2 + \lambda_i^2}} \quad (3-171)$$

Total velocity on horizontal tail is calculated from superposition of all velocity components. The downwash of the main rotor is directly added to the total velocity encountered by horizontal tail.

$$u_{ht} = u_{ht_{Freestream}} + u_{ht_{relative}} - \lambda_i \sin X_{TPP} \quad (3-172)$$

$$v_{ht} = v_{htFreestream} + v_{htRelative} \quad (3-173)$$

$$w_{ht} = w_{htFreestream} + w_{htRelative} + \lambda_i \cos X_{TPP} \quad (3-174)$$

Horizontal tail angle of attack, sideslip, dynamic pressure are calculated from the components of total velocity that horizontal tail encounters.

$$\alpha_{ht} = \alpha_{inc.} - \text{atan2}(w_{ht}, u_{ht}) \quad (3-175)$$

$$\beta_{ht} = \text{atan2}(v_{ht}, u_{ht}) \quad (3-176)$$

$$q_{ht} = 1/2 \rho \left(\sqrt{u_{ht}^2 + v_{ht}^2 + w_{ht}^2} \right)^2 \quad (3-177)$$

α_{inc} term in the angle of attack equation is the horizontal tail incidence at which it is assembled on the fuselage and is an input parameter which is specific to helicopter.

The force and moment contribution of horizontal tail to the total system at center of gravity of the total system is determined by transferring the aerodynamic force and moments generated at the aerodynamic center of the horizontal tail to the center of gravity of the helicopter.

When compared with the force and moments transferred to the fuselage by main rotor and other main load contributors, most of the force and moments

generated by tail rotor are found to be negligible. The drag and aerodynamic moment generated at tail rotor aerodynamic center are therefore neglected. Besides, horizontal tail is assumed to be symmetric along the x-z plane of the helicopter; therefore no rolling moment contribution to the whole system is calculated. As a result, horizontal is modeled as being only a pitching moment contributor to the helicopter. The lift generated is multiplied with the aerodynamic offset vector of the horizontal tail in order to determine the total pitching moment generated by horizontal tail and acting on the center of mass of the helicopter.

For the aerodynamic force and moment coefficients that horizontal tail model requires, two methods are implemented. One method uses lift curve slope of the airfoil of the horizontal tail while assuming linear lift coefficient slope. The other method, similar to fuselage model, uses table look up method where aerodynamic coefficient tables which depends on angle of attack and sideslip, are supplied as input to the mathematical model.

Aerodynamic lift force generated at horizontal tail aerodynamic center is calculated by;

$$F_{z_{ht}} = -q_{ht} S_{ht} c_l \cos(\alpha_{ht}) \quad (3-178)$$

Aerodynamic offset of the horizontal tail relative to center of mass of the helicopter is;

$$\vec{R}_{ht_{a.c.}} = \vec{i}x_{ht_{a.c.}} + \vec{j}y_{ht_{a.c.}} + \vec{k}z_{ht_{a.c.}} \quad (3-179)$$

Pitching moment contribution of horizontal tail to the total system is then calculated by;

$$\vec{M}_{ht} = \vec{R}_{ht_{a.c.}} \times F_{z_{ht}} \vec{k} \quad (3-180)$$

3.8 Vertical Tail Model

Similar to horizontal tail, aerodynamic force and moments generated by vertical tail (vertical stabilizer) are calculated at its own aerodynamic center of and transferred to the center of mass of the helicopter for its contribution to total force and moments of the helicopter. Aerodynamic coefficients that lead to aerodynamic loads generated by the vertical tail are determined from look-up tables which are angle of attack and local Mach number dependent. Aerodynamic coefficients are interpolated for the angle of attack and freestream velocity that vertical tail encounters. Total air velocity that vertical tail encounters are calculated on vertical tail reference frame shown in Figure 3-19 which is superposition of helicopter body velocities, relative velocities because of the rotation of the helicopter and downwash of the tail rotor.

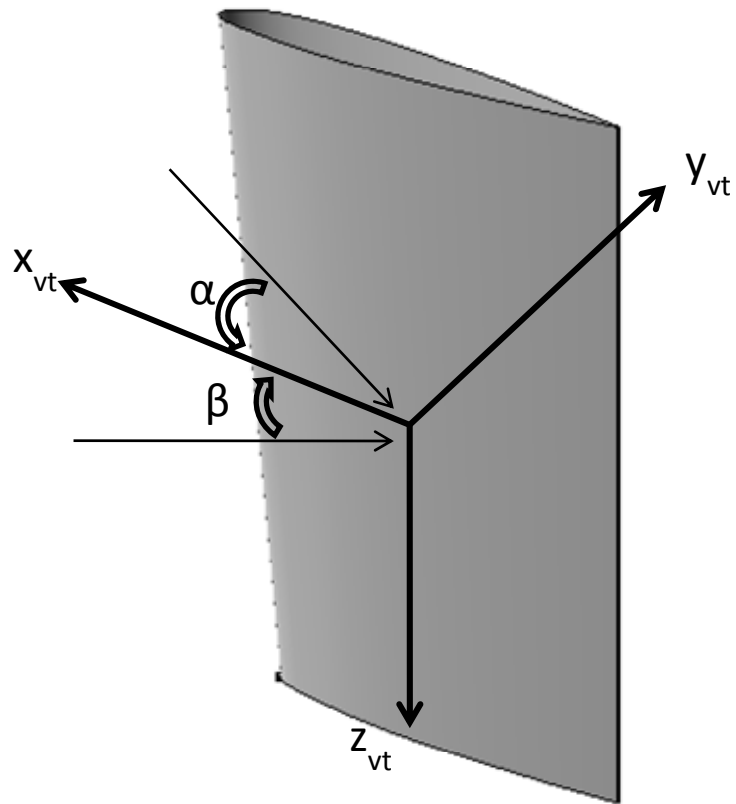


Figure 3-19 Vertical tail reference system and angle definitions

As body reference frame and vertical tail reference frames are equivalent, there is no need for any transformation. Therefore, the freestream air velocity vector for vertical tail is same with one for helicopter body

$$u_{vt_{freestream}} = u_B$$

(3-181)

$$v_{vt_{freestream}} = v_B \quad (3-182)$$

$$w_{vt_{freestream}} = w_B \quad (3-183)$$

Relative velocities because of the helicopter rotational velocities are calculated from cross product of offset vector from vertical tail aerodynamic center to mass center of the helicopter with body rotation vector of the aircraft. Besides, transformation matrix is again used in order to transform relative velocities calculated in body axis reference frame to vertical tail reference frame.

$$\vec{R}_{vt_{a.c.}} = \vec{i}x_{vt_{a.c.}} + \vec{j}y_{vt_{a.c.}} + \vec{k}z_{vt_{a.c.}} \quad 3-184$$

$$u_{vt_{relative}} = -z_{vt_{a.c.}}q + y_{vt_{a.c.}}r \quad (3-185)$$

$$v_{vt_{relative}} = -x_{vt_{a.c.}}r + z_{vt_{a.c.}}p \quad (3-186)$$

$$w_{vt_{relative}} = -y_{vt_{a.c.}}p + x_{vt_{a.c.}}q \quad (3-187)$$

In addition, tail rotors downwash effect on vertical tail is directly added into to total velocity formula. Normally, the downwash of the tail rotor which can be approximated to the inflow on the tail rotor disk is calculated by tail rotor aerodynamic model. However, a simple momentum theory equation is used in order

to calculate the downwash effect of tail rotor to vertical tail. The assumption here is, the wake of the tail rotor is uniform and none rotating. The downwash is determined by;

$$\lambda_i = \frac{C_T}{2\sqrt{\mu^2 + \lambda_i^2}} \quad (3-188)$$

Total velocity on horizontal tail is calculated from superposition of all velocity components. The downwash of the main rotor is directly added to the total velocity encountered by horizontal tail.

$$u_{vt} = u_{htFreestream} + u_{vtrelative} \quad (3-189)$$

$$v_{vt} = v_{vtFreestream} + v_{htRelative} - \lambda_i \quad (3-190)$$

$$w_{vt} = w_{vtFreestream} + w_{vtRelative} \quad (3-191)$$

The angle of attack of the vertical tail is defined by the angle between x and y component of the total velocity, as shown in the Figure 3-19. Similarly, the sideslip angle is defined as the angle between x and z components of the total velocity that vertical tail encounters. Angle of attack, sideslip and dynamic pressure that vertical tail encounters are calculated by;

$$\alpha_{vt} = \alpha_{inc.} - atan2(v_{vt}, u_{vt}) \quad (3-192)$$

$$\beta_{vt} = \text{atan2}(w_{vt}, u_{vt}) \quad (3-193)$$

$$q_{vt} = 1/2 \rho \left(\sqrt{u_{vt}^2 + v_{vt}^2 + w_{vt}^2} \right)^2 \quad (3-194)$$

α_{inc} term in the angle of attack equation represents the incidence at which vertical tail is assembled to the fuselage. It is an input parameter and specific to helicopter.

Similar to horizontal tail, some of the force and moments generated by vertical tail are neglected. When compared with the force and moment contribution to the helicopter coming from other main load sources, the drag and aerodynamic moment generated at vertical tail aerodynamic center are assumed to be negligible. Therefore only lift force that is in the body-y direction, generated by vertical tail is computed.

For the aerodynamic force and moment coefficients that vertical tail model requires, two methods are implemented. One method uses lift curve slope of the airfoil of the vertical tail while assuming linear lift coefficient slope. The other method, similar to fuselage and horizontal tail model, uses table look up method where aerodynamic coefficient tables which depends on angle of attack and sideslip, are supplied as input to the mathematical model.

Aerodynamic lift force generated at vertical tail aerodynamic center is calculated by;

$$Fy_{vt} = -q_{vt} S_{vt} c_l \cos(\alpha_{vt}) \quad (3-195)$$

Aerodynamic offset of the vertical tail relative to center of mass of the helicopter is;

$$\vec{R}_{vt.a.c} = \vec{i}x_{vt.a.c} + \vec{j}y_{vt.a.c} + \vec{k}z_{vt.a.c} \quad (3-196)$$

Pitching moment contribution of vertical tail to the total system is then calculated by;

$$\vec{M}_{vt} = \vec{R}_{vt.a.c} \times Fy_{vt}\vec{j} \quad (3-197)$$

3.9 6-DOF Solver

Six degree of freedom equations of motion module computes translational & rotational accelerations with the total force and moments acting on the helicopter center of mass. Force and moments generated by each helicopter components are individually calculated in each components aerodynamic center and then transformed into body reference frame coordinate system. Each component's transformed force and moments are transferred to the center of gravity of the whole system in order to determine the resultant loads acting on the helicopter at the center of mass of the helicopter. All force and moments contributions from each of the helicopter components are superposed at helicopter center of mass and resultant force and moment vectors are determined.

$$\vec{F}_{TOTAL} = \vec{F}_{MAIN ROTOR} + \vec{F}_{TAIL ROTOR} + \vec{F}_{FUSELAGE} + \vec{F}_{HORIZONTAL TAIL} + \vec{F}_{VERTICAL TAIL} \quad (3-198)$$

$$\begin{aligned}
\vec{M}_{TOTAL} = & \vec{M}_{MAIN ROTOR} + \vec{M}_{TAIL ROTOR} + \vec{M}_{FUSELAGE} + \vec{M}_{HORIZONTAL TAIL} \\
& + \vec{M}_{VERTICAL TAIL} + \vec{r}_{MAIN ROTOR} \times \vec{F}_{MAIN ROTOR} \\
& + \vec{r}_{TAIL ROTOR} \times \vec{F}_{TAIL ROTOR} + \vec{r}_{FUSELAGE} \times \vec{F}_{FUSELAGE} \\
& + \vec{r}_{HORIZONTAL TAIL} \times \vec{F}_{HORIZONTAL TAIL} + \vec{r}_{VERTICAL TAIL} \times \vec{F}_{VERTICAL TAIL}
\end{aligned}$$

(3-199)

Total force and moments determined at center of mass of the helicopter are then used to calculate helicopter translational and rotational accelerations. Total forces in body reference frame are divided with helicopter total mass in order to calculate 3 translational accelerations, and total moments in body reference frame are divided with helicopter inertias in order to calculate 3 rotational accelerations. The coupling terms coming from the rotations are ignored at this step but planned as future work.

$$a_x = \frac{F_{xTOTAL}}{m_{TOTAL}}$$

(3-200)

$$a_y = \frac{F_{yTOTAL}}{m_{TOTAL}}$$

(3-201)

$$a_z = \frac{F_{zTOTAL}}{m_{TOTAL}}$$

(3-202)

$$\dot{p} = \frac{M_{zTOTAL}}{I_{xx}}$$

(3-203)

$$\dot{q} = \frac{M_{yTOTAL}}{I_{yy}}$$

(3-204)

$$\dot{r} = \frac{M_{zTOTAL}}{I_{zz}}$$

(3-205)

Translational and rotational accelerations are used either by trim the model or just by the integrator module. If a trim flight condition is desired which may be either static or dynamic trim condition, then the trim model uses the accelerations calculated by the 6-dof solver module and tries to neutralize them by optimizing the trim variables. On the other hand, if a simulation is desired, then the accelerations calculated by 6-dof solver are used by the integrator module where translational and rotational accelerations are time based integrated in order to determine helicopters new states which are used as inputs to the mathematical model for the next time step.

3.10 Environmental Model

The time integration of the developed mathematical model results in change in the position of the helicopter in inertial reference frame. The integral of translational and rotational velocities are taken in order to determine the change in position and attitude of the helicopter in a single time step. Besides integration over a time interval with time steps predefined, motion and dynamic behavior of the helicopter during a maneuver or flight condition are calculated. According to the calculated path of the helicopter during a simulation or analysis, air properties change with the change in atmospheric temperature or altitude of the helicopter. Therefore air

properties that are used in the calculations are modeled in a different module, which takes altitude and temperature difference between standard air temperature and the temperature that the analyses desired to be done at, as input. Outputs of the environmental model are pressure, air density, viscosity and speed of sound at the flight or analysis altitude.

Air pressure at analysis or simulation altitude is calculated or updated with the equation (3-206)

$$P = 100 * \left(\frac{44331.514 - z}{11880.516} \right)^{1/0.1902632} \quad P = [\text{Pa}], z = [\text{m}] \quad (3-206)$$

Atmospheric standard temperature is calculated by;

$$T = T_1 + a(h - h_1) \quad T = [^\circ\text{C}], h = [\text{km}] [\text{Kansas}] \quad (3-207)$$

$$a = -6.5 \text{ } ^\circ\text{C}/\text{km} \text{ (up to 11 km of altitude)} \quad (3-208)$$

If T_1 and h_1 are taken air parameters at sea level, which mean zero altitude and 15° C temperature, and then the temperature formula leads the standard atmosphere temperature at the flight altitude. The ISA+ parameter in the inputs, defined the temperature that will be added on the standard air temperature, which would have effect on air density, viscosity and air speed values. The slope parameter “a” in the temperature equation is a standard values for atmosphere regions.

Air density which directly affects the helicopter performance is calculated with ideal gas assumption while the pressure and temperature values which are included in the formulation of density from above equations.

$$\rho = \frac{P}{RT}, \quad R = 287.05 \left[\frac{J}{kg} * degK \right]$$

(3-209)

Air viscosity value is required in vortex core calculation which also directly affects the rotor performance. For viscosity calculation, Sutherland's Law is implemented, in which viscosity is represented and calculated according to a reference value;

$$\mu = \mu_{ref} \left(\frac{T}{T_{ref}} \right)^{3/2} \frac{T_{ref} + S}{T + S}$$

(3-210)

Table 2 Sutherland's Law Coefficients for air

$\mu_0 \left[\frac{kg}{ms} \right]$	$T_0 [K]$	$S [K]$	$C_1 \left[\frac{kg}{ms\sqrt{K}} \right]$
1.716×10^{-5}	273.15	110.4	1.458×10^{-6}

As airfoil aerodynamic coefficient tables are angle of attack and Mach number dependent, local Mach number, so the speed of sound, is another dominant factor that directly affects the helicopter and helicopter rotor performance. Speed of sound is calculated with the following equation;

$$a = \sqrt{\gamma RT}, \gamma = 1.4$$

(3-211)

CHAPTER 4

MATHEMATICAL MODEL VALIDATION

In this chapter, the mathematical model developed (HELCOMAS, Helicopter Comprehensive Modeling, Analysis and Simulation Tool) is validated with both flight test data of various helicopters and with the comprehensive rotorcraft analysis tools CAMRAD/JA and FLIGHTLAB. Different fidelity sub models of the main rotor aerodynamic model are used for both hover and forward flight cases and results are compared with the validation data.

4.1 WESSEX VALIDATION WITH EXPERIMENTAL DATA

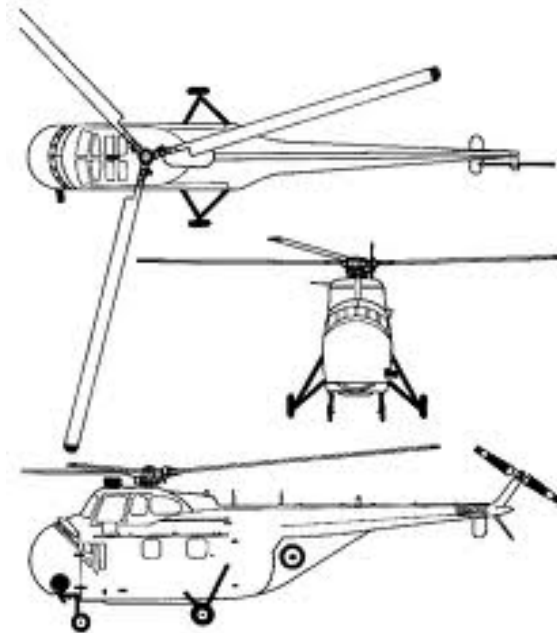


Figure 4-1 Westland Wessex [69]

The refined aerodynamic model of the developed mathematical model (xBEM) is validated with the flight test data of the Wessex [Figure 4-1] helicopters for hovering flight conditions. The flight test data of the Wessex helicopters are taken from Young's work [37] done in 1976 on developing a hover rotor performance model. The experimental data on Wessex helicopters presented on the Young's work are the measurements taken during free flight tests at RAE Bedford. The Wessex helicopter main rotor configuration is given at Table 3.

Table 3 Wessex Helicopter main rotor parameters [37]

Main Rotor Parameters	
Number of Blades	4
Rotor radius (m)	8.53
Blade Root Cut-Out (%)	16
Chord Length (m)	0.417
Tip speed (m/s)	205
Rotor RPM	229.6
Flapping Hinge Position (%)	3.5
Precone Angle (deg)	0
Blade Twist (deg)	-8
Shaft Tilt (deg)	0
Blade Profile	NACA 0012

It is mentioned in the Young's study that, "The experimental results were obtained on three different days with the rotor thrust coefficient varied mainly by changing the altitude and mass of the aircraft". The change of torque coefficient with thrust coefficient data were extracted from the flight test.

Analyses were done with different sub models of the vortex wake method implemented with the xBEM. The option to decide whether to represent the rotor wake with only a strong tip vortex or with the vortices that roll-up and form strong tip vortex or with the whole vortex sheet where each vortex filament that are trailed from each blade element are modeled for ten rotations of the blade, was implemented into the aerodynamic model and left to the user. In order to validate each of the option and compare the accuracy of the results taken with each wake representation method with each other, analyses with all options have been done and compared with the flight test data. The change of torque coefficient with the thrust coefficient is given in Figure 4-2.

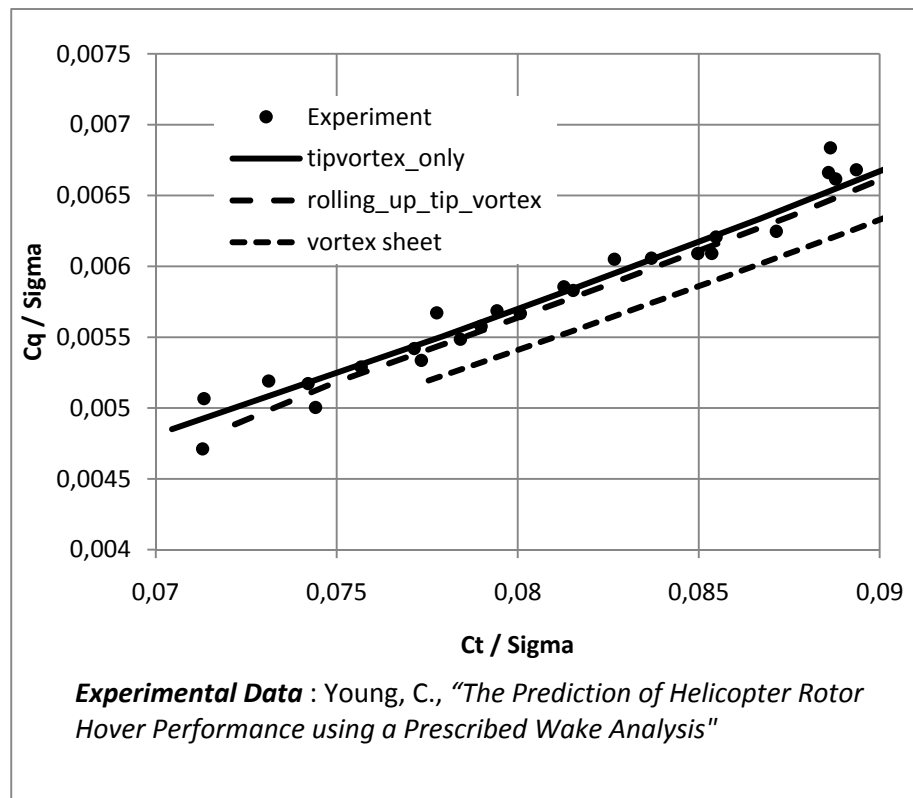


Figure 4-2 Wessex Helicopter Ct&Cq validation with experimental data

From Figure 4-2, it can be deduced that from the all three options presented in the main rotor aerodynamic model, the wake representation with only a strong tip vortex gives the best accuracy. Although all three options are thought to be accurate enough for aerodynamic load analyses, the option with wake representation with only a tip vortex is used in order to investigate the effect of the radial section number on the accuracy of the analyses. More analyses have been done with 20, 40 and 60 blade elements and results are compared in order to investigate the accuracy change with the change of radial section number. Results taken are given in Figure 4-3.

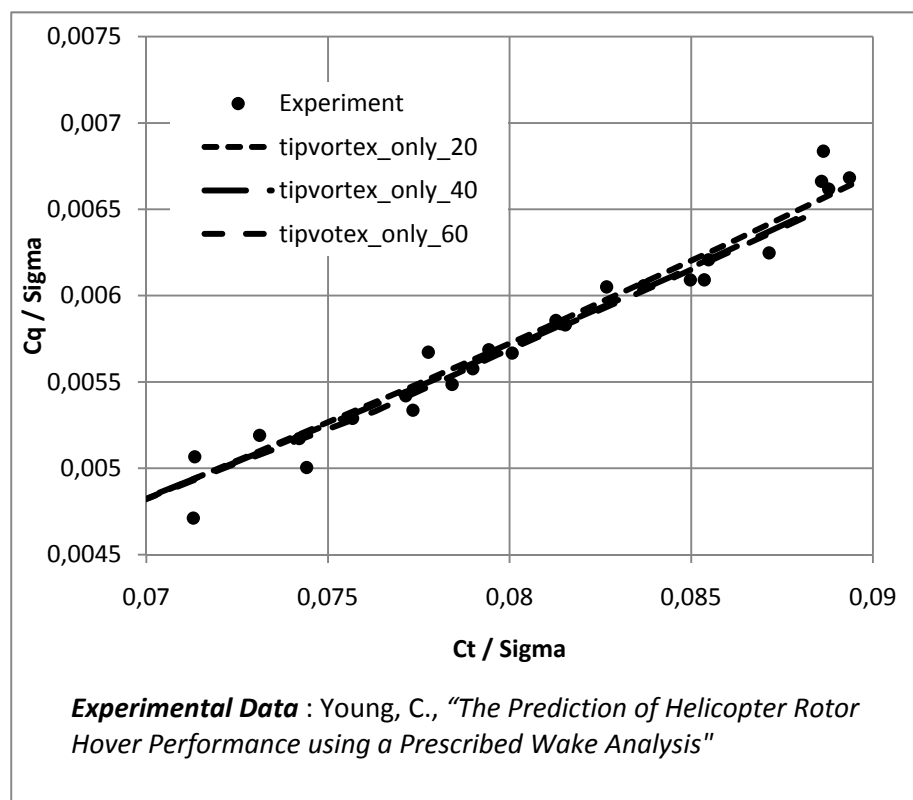


Figure 4-3 Effect of blade element number on accuracy of the results

From the analyses results and the comparison with the flight test data, it is found that, with the increasing blade element number, results are changing slightly. On the other hand, it is evaluated that the change in the results with the increasing blade element number is negligible whereas the computation time increases dramatically. For example, it takes maximum 30 seconds to converge with 20 blade elements, 54 seconds with 40 elements and 71 seconds with 60 blade elements. Therefore, it is decided that 20 blade elements gives the best trade of between accuracy and computational efficiency and throughout the study 20 blade elements are used. Contrarily, analyses are done with lesser blade elements and it is evaluated that the results got worsen rapidly as the blade element number decreases.

4.2 OH-58 VALIDATION WITH FLIGHT TEST DATA

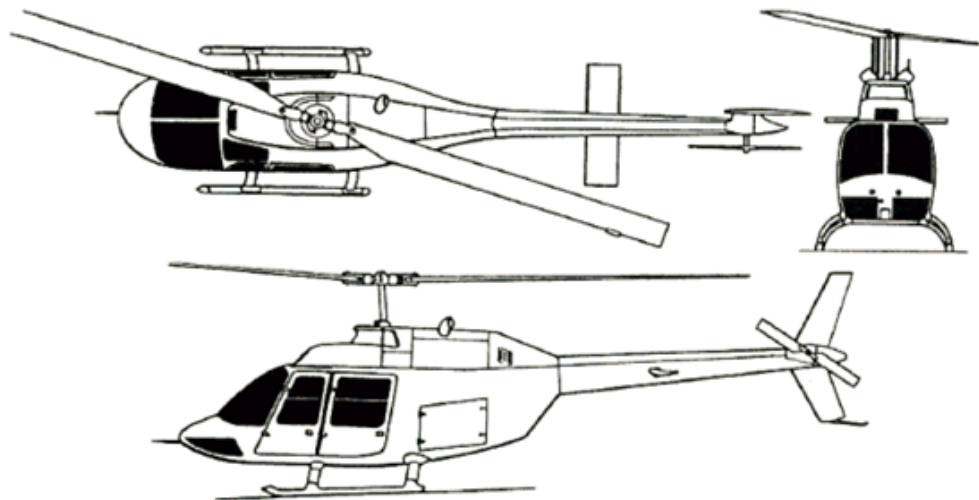


Figure 4-4 OH-58 / Kiowa [72]

In addition to validation with Wessex helicopters, main rotor aerodynamic model is validated with the flight test data of the OH-58 helicopter, Figure 4-4. OH-58 is a two bladed helicopter with a maximum takeoff weight of 1500 kg. The flight test data of the OH-58 helicopter is extracted from the work of Hoffrichter [66] from Boeing Vertol Company, where new composite main rotor blade preliminary design investigations were conducted. Several flight test data such as hover flight at 4000 feet altitude and 35 °C atmosphere temperature is presented in the study of Hoffrichter. The experimental data of OH-58 helicopter is compared with the analysis results determined by the refined aerodynamic model developed and implemented into the mathematical model. The helicopter main rotor configuration that is used in the analyses is given the Table 4.

Table 4 OH-58 Main Rotor Parameters [66]

Main Rotor Parameters	
Number of Blades	2
Rotor Radius (m)	5.38
Blade Root Cut-Out (%)	18.86
Chord Length (m)	0.345
Tip speed (m/s)	200
Rotor RPM	355.17
Flapping Hinge Position (%)	5
Precone Angle (deg)	0
Blade Twist (deg)	-10.6
Blade Taper Ratio (%)	30 @ $r/R = 0.9$
Shaft Tilt (deg)	0
Blade Profile	vr7 - vr8

The change of power required coefficient of the main rotor with thrust coefficient is analyzed at 4000 feet altitude and 35 °C atmosphere temperature and

results are compared with the flight test data. Analyses were done with vortex wake method while modeling the rotor wake for ten revolutions. From the results taken with the developed mathematical model, it is evaluated that the results show good agreement with experimental data, Figure 4-5.

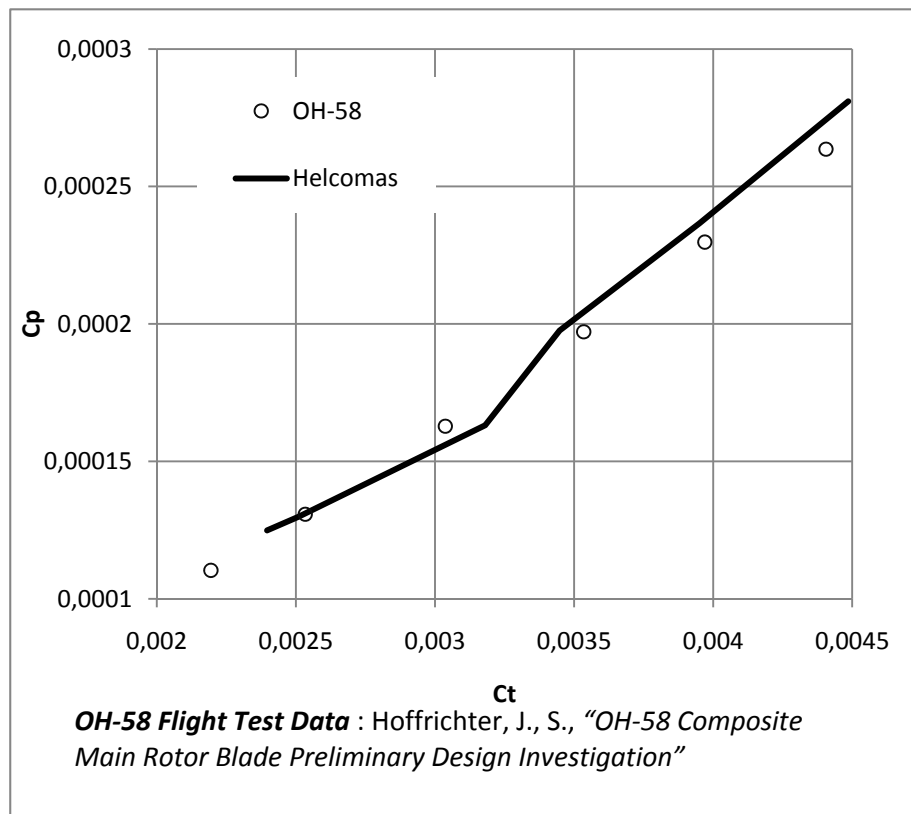


Figure 4-5 Validation with OH-58 Ct&Cp experimental data

In addition to the main rotor power required coefficient versus thrust coefficient comparison, sectional load validation study was also done. At hover flight condition, the sectional load which corresponds to the thrust of the blades is analyzed in detail. The thrust distribution over the rotor blade is determined and

validated with the flight test data. In the Figure 4-6, the change of thrust with non-dimensional radial location is compared with the test data.

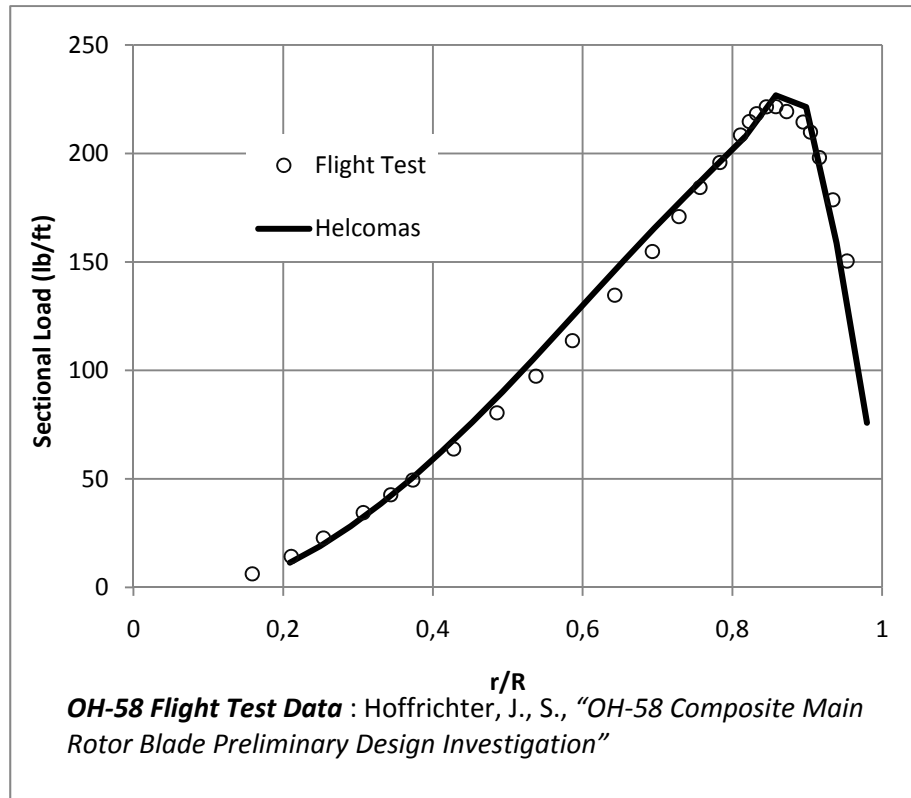


Figure 4-6 Validation with OH-58 radial thrust distribution experimental data

Because of the absence of the detailed flight test data for forward flight cases, a similar sectional load distribution along the blade analysis was not done. However, the total power required of the main rotor at advance ratios 0.04, 0.08 and 0.12 flight test data exists [66]. The required power curve for the main rotor at forward flight is determined by the aerodynamic model developed and compared with the flight test results in order to validate forward flight part of the aerodynamic model also. Analyses were done with vortex wake methods, for which wake is

modeled with Beddoes wake model for ten revolutions. The main rotor power required calculations are compared with the flight test data in the Figure 4-7 where the change in main rotor power required with the advance ratio and thrust can be investigated.

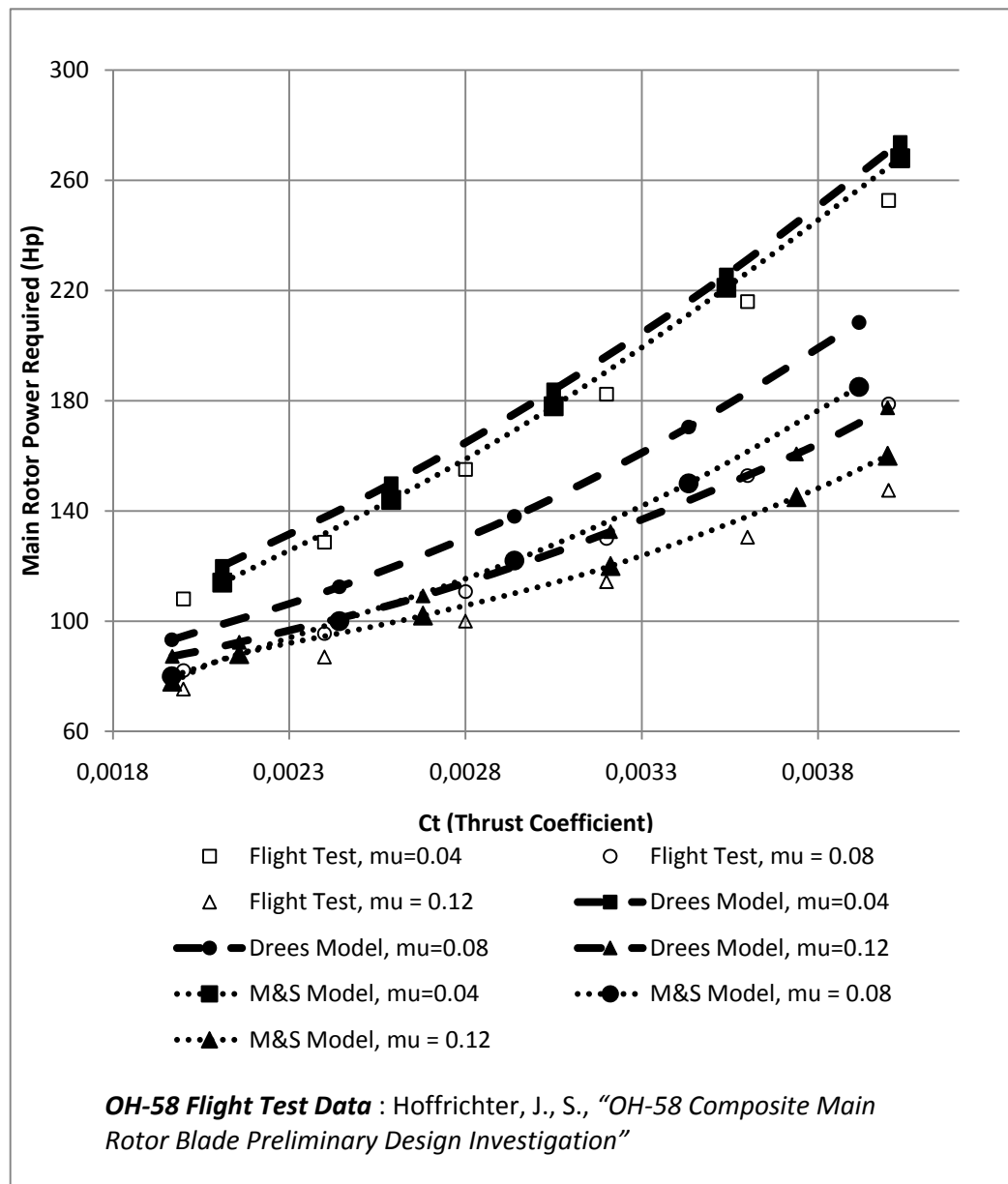


Figure 4-7 Validation with OH-58 main rotor power & thrust coefficient with experimental data

The difference between the flight test data and the calculated values of the main rotor required power at different advance ratios and thrust coefficients is believed to be related with the unknown flapping angles of the main rotor during the specified flight conditions. The analyses were done with the approximated flap dynamics model, which is believed to be the source of the error between flight test data and analyzed values.

4.3 SA-349 / GAZALLE VALIDATION WITH CAMRAD

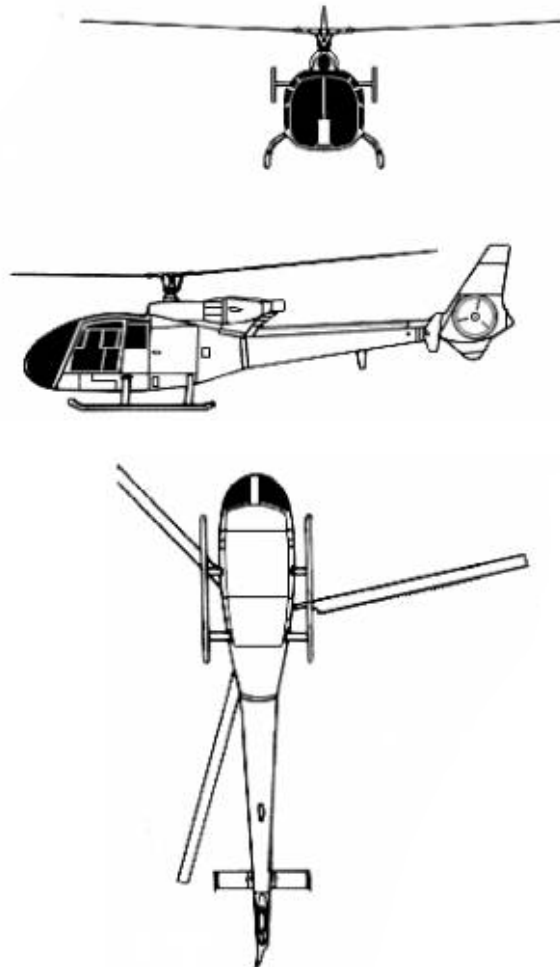


Figure 4-8 SA-349 / Gazalle [73]

The Aerospatiale SA-349/2 Gazelle helicopter, Figure 4-8, was analyzed in CAMRAD/JA and the xBEM. In order to validate developed main rotor mathematical model in forward flight conditions, Gazelle helicopter is modeled with CAMRAD and

analyses at different forward flight including high advance ratios are done. Rotor performances, such as thrust and torque values, and effective angle of attack distribution over the rotor disk at several forward flight conditions are determined by both tools and compared with each other. The results presented in this study determined by the mathematical model developed and comprehensive rotorcraft analysis tool CAMRAD, showed good consistency.

The SA-349/2 Gazelle rotor employs three Grande Vitesse blades with a linear twist, constant chord and single airfoil. The main rotor blade geometry is presented in the Figure 4-9 [67].

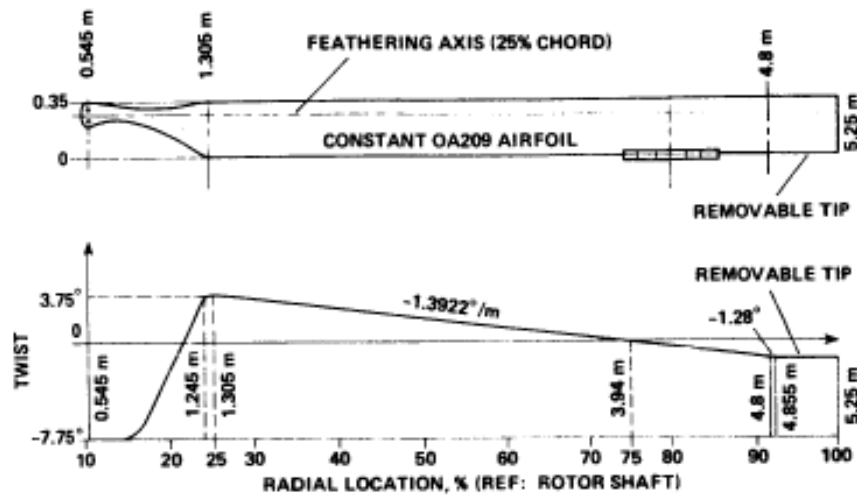


Figure 4-9 Gazelle's main rotor blade geometry [67]

Table 5 Gazalle/SA349 Main rotor parameters [67]

MAIN ROTOR	
Blade Number	3
Rotor Radius (m)	5.25
Chord Length (m)	0.35
Rotor Solidity	0.0637
Rotational Speed (RPM)	387
Tip Speed (m/s)	212
Blade Profile	OA209

Main rotor properties are given in Table 5.

CAMRAD/JA MODEL

Gazalle helicopter main rotor is modeled with non-uniform inflow model and for the wake representation, free wake model is selected. For the first 22.5° of azimuth, wake is modeled as near wake, from 22.5° to 45° wake is represented as rolling-up wake. Starting from 45° of azimuth up to four revolution of the wake, wake is represented with far wake model. Tip vortex radial position is defined as 0.98 (non-dimensional). 19 blade radial sections are defined for CAMRAD/JA model which are getting denser near to blade tip. Leaving all other parameters as default, Gazalle analyses are conducted with the built CAMRAD/JA model.

HELCOMAS - xBEM MODEL

Vortex wake theory which is evaluated as the highest fidelity inflow model is used for Gazalle analyses. Near, rolling-up and far wake regions are defined similar to the CAMRAD model in order to have similar fidelity models. 20 blade radial

sections are defined and whole vortex sheet is modeled. Vortex core radius and tip vortex location calculations are done automatically by the developed mathematical model

ANALYSIS RESULTS

Main rotor of the Gazelle helicopter is analyzed in forward flight conditions with both xBEM and CAMRAD. The changes in total rotor thrust and torque with the change in forward flight velocity are studied. The objective was to validate main rotor aerodynamic model (xBEM) of the developed mathematical model. Therefore only main rotor module of HELCOMAS is used throughout this validation study. At each forward flight speed, at which comparison is done, pilot trim controls are inputted to the main rotor aerodynamic model. Pilot trim controls are determined from Gazelle's full helicopter model built in CAMRAD. Main rotor total thrust and torque values, which are determined by developed aerodynamic model, are compared and validated with CAMRAD results. In the Figure 4-10, Figure 4-11 and Figure 4-12, thrust coefficient versus forward velocity, torque coefficient versus forward velocity and thrust coefficient versus torque coefficient variations are given.

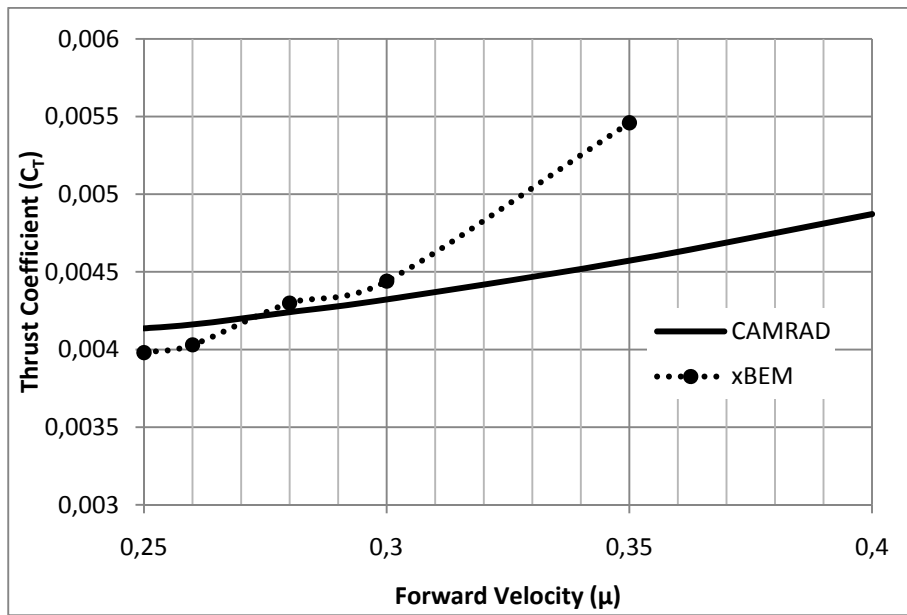


Figure 4-10 C_t vs Advance Ratio validation with CAMRAD

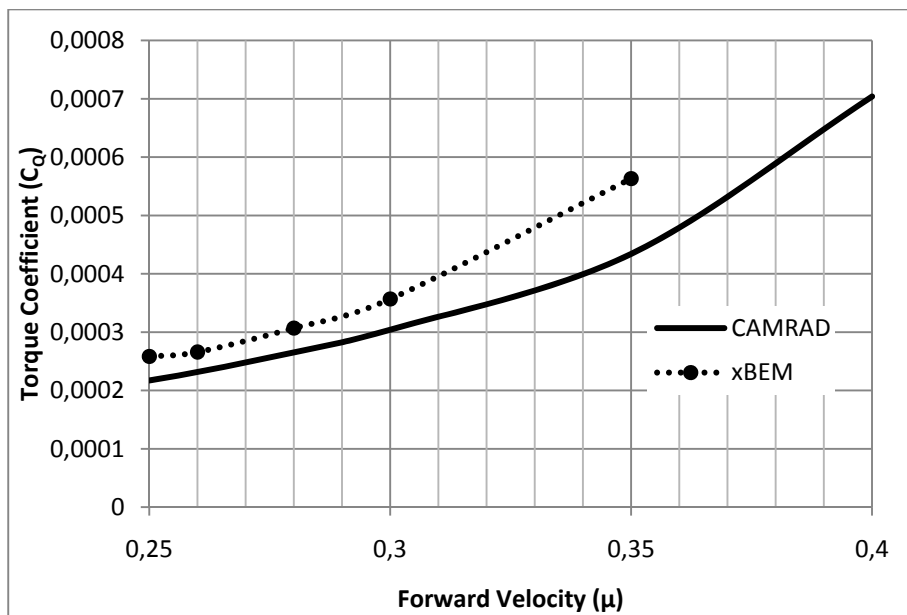


Figure 4-11 C_q vs Advance Ratio validation with CAMRAD

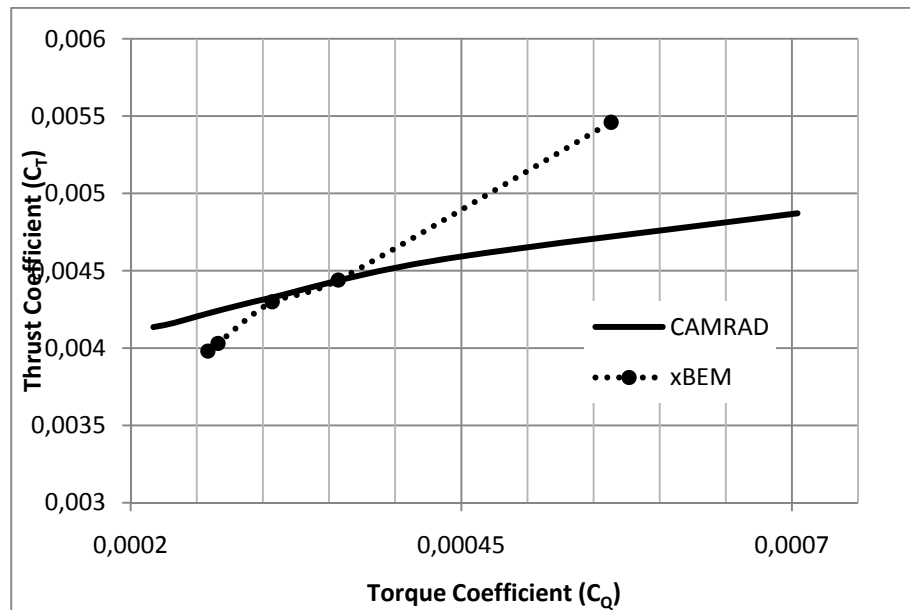


Figure 4-12 C_t vs C_q validation with CAMRAD

As seen from Figure 4-10, Figure 4-11 and Figure 4-12, total thrust and torque values of the rotor are consistent with each other up to 0.3 advance ratio. After advance ratios of 0.3, which correspond to high forward speeds, results taken with xBEM start to deviate. Maximum freestream air velocity that blades at advance ratios higher than 0.3 are more than 0.8 mach. It is evaluated that the reason of the increase in the differences between CAMRAD and xBEM results at advance ratios higher than 0.3 is related with the different inflow distribution calculation techniques implemented in each tools.

In addition to total thrust and torque analyses, effective angle of attack distributions over the rotor disk are compared. For advance ratio of 0.26 and 0.30, effective angle of attack sweep over the azimuth angle are studied. In the Figure 4-13 to Figure 4-20 angle of attack change with changing azimuth at non-dimensional radial locations of 0.28, 0.59, 0.79, 0.87 calculated by both tools are plotted.

105 knots forward flight ($\mu = 0.26$)

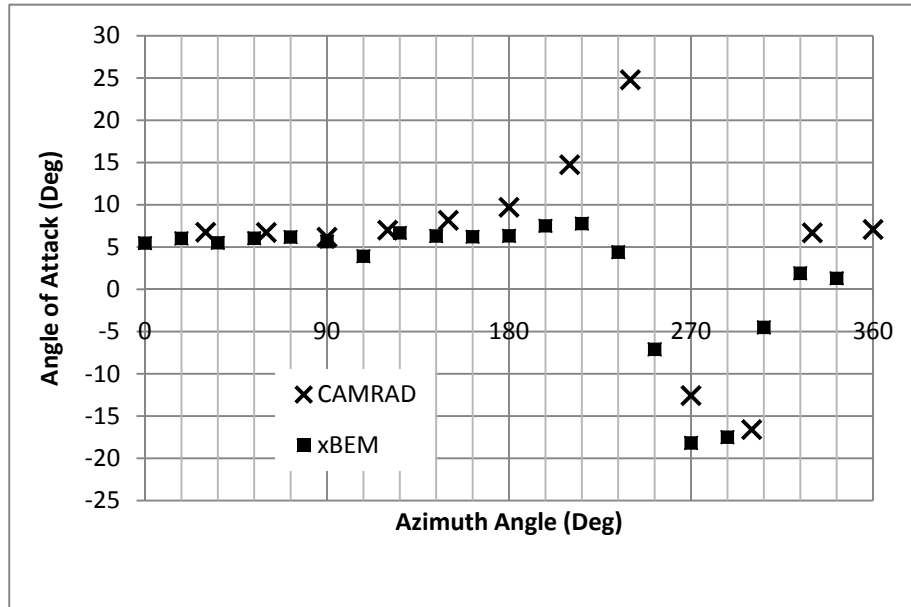


Figure 4-13 Aoa vs Azimuth angle at $r/R = 0.28$ (105 kts)

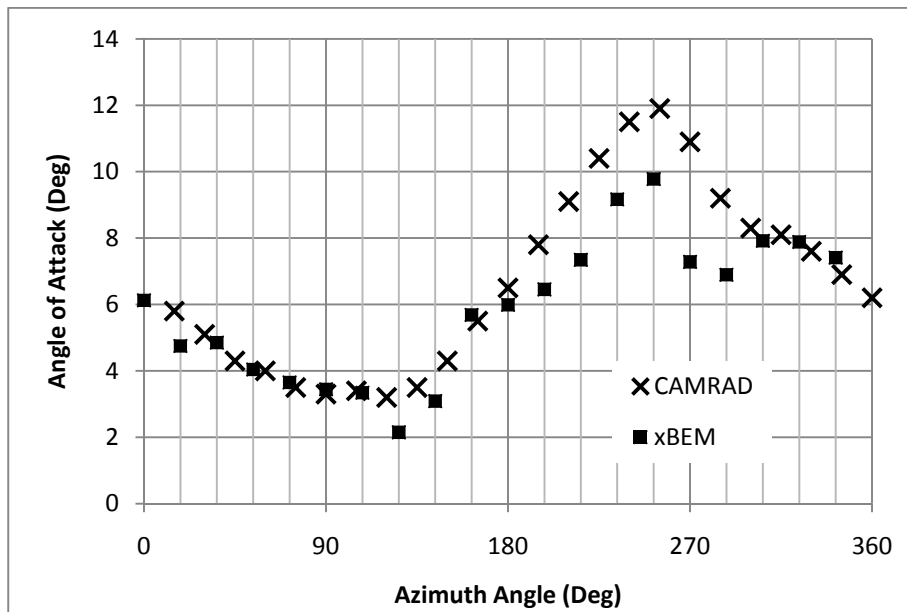


Figure 4-14 Aoa vs Azimuth angle at r/R = 0.59 (105 kts)

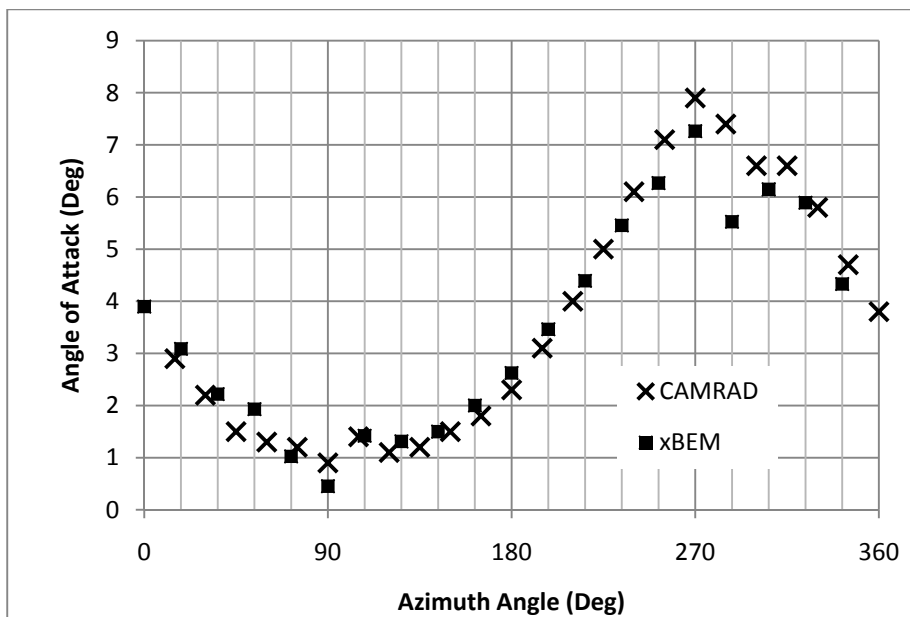


Figure 4-15 Aoa vs Azimuth angle at r/R = 0.79 (105 kts)

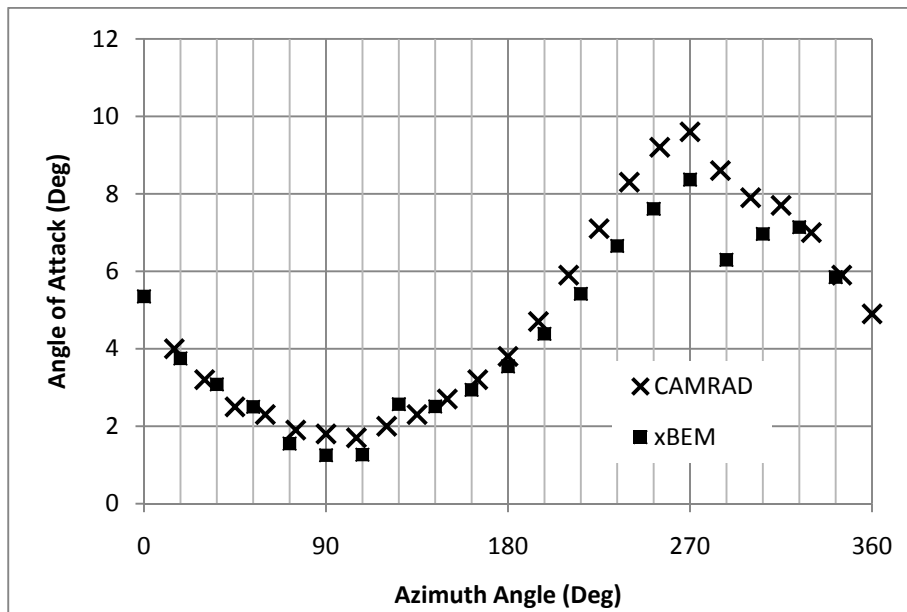


Figure 4-16 Aoa vs Azimuth angle at r/R = 0.87 (105 kts)

125 knots forward flight ($\mu = 0.3$)

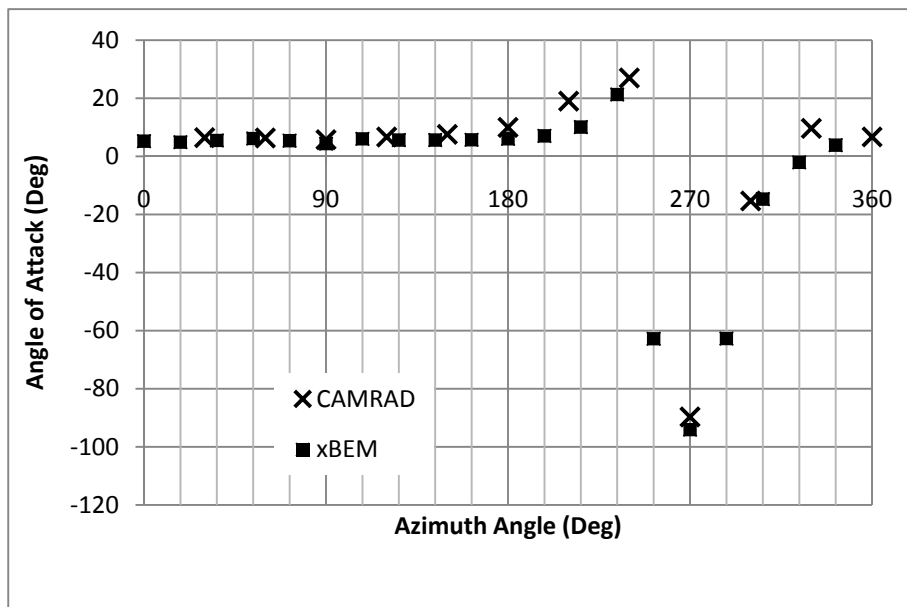


Figure 4-17 Aoa vs Azimuth angle at r/R = 0.28 (125 kts)

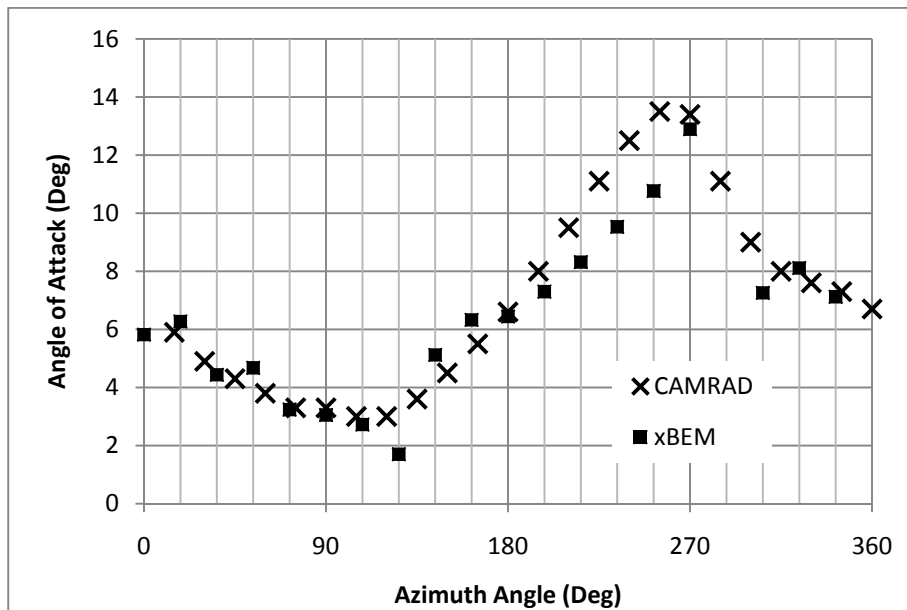


Figure 4-18 Aoa vs Azimuth angle at r/R = 0.59 (125 kts)

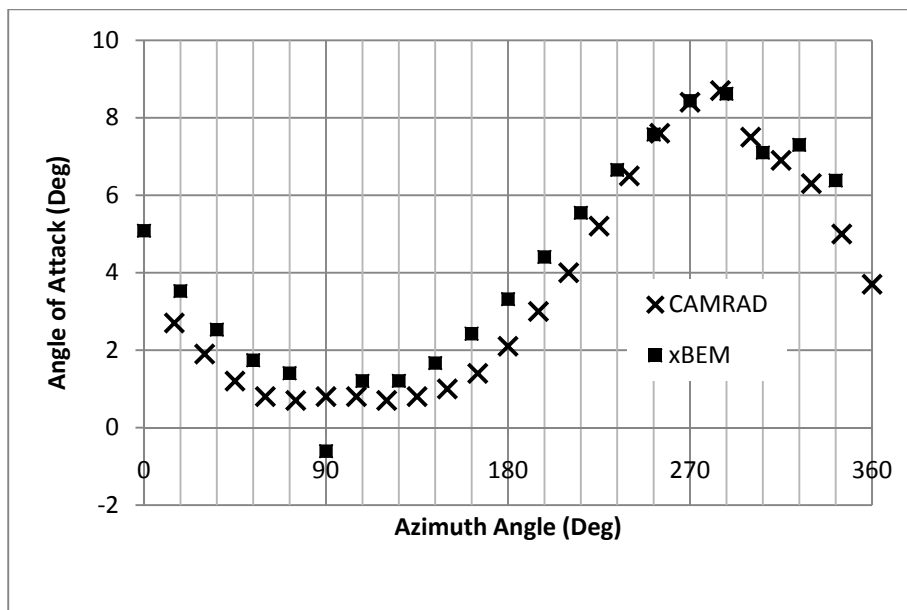


Figure 4-19 Aoa vs Azimuth angle at r/R = 0.79 (125 kts)

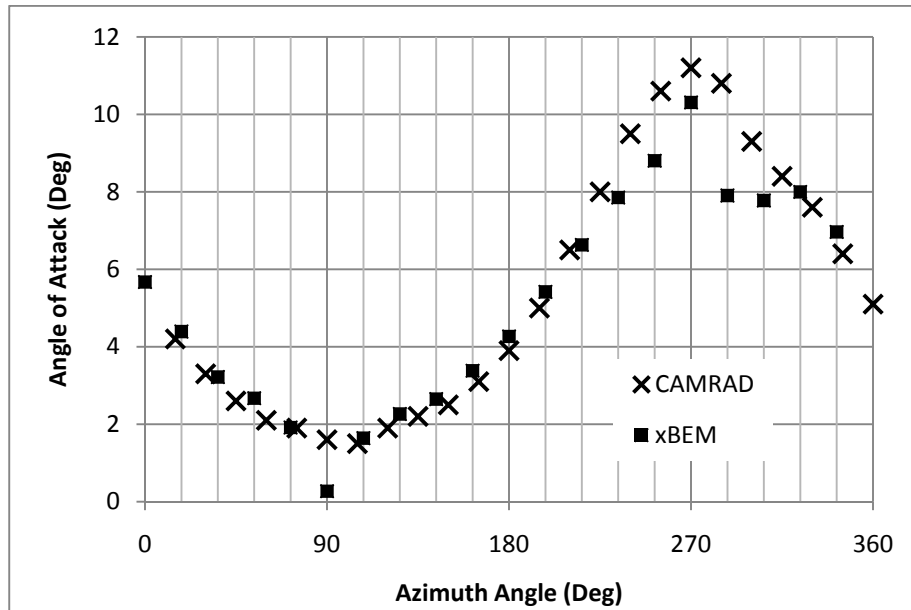


Figure 4-20 Aoa vs Azimuth angle at $r/R = 0.87$ (125 kts)

From the results given in the Figure 4-13 to Figure 4-20, both radial and azimuthal effective angle of attack distributions at different forward velocities calculated by CAMRAD and xBEM are evaluated as consistent. Even at retreating side at high forward speeds, the reversed flow is dissolved consistently. As seen from Figure 4-13 and Figure 4-17, reversed flow is encountered at locations near blade root and retreating side.

In addition, blade longitudinal, lateral flapping and coning angles calculated by the blade dynamic model of the main rotor module and the ones calculated by CAMRAD are plotted in the Figure 4-21 for comparison.

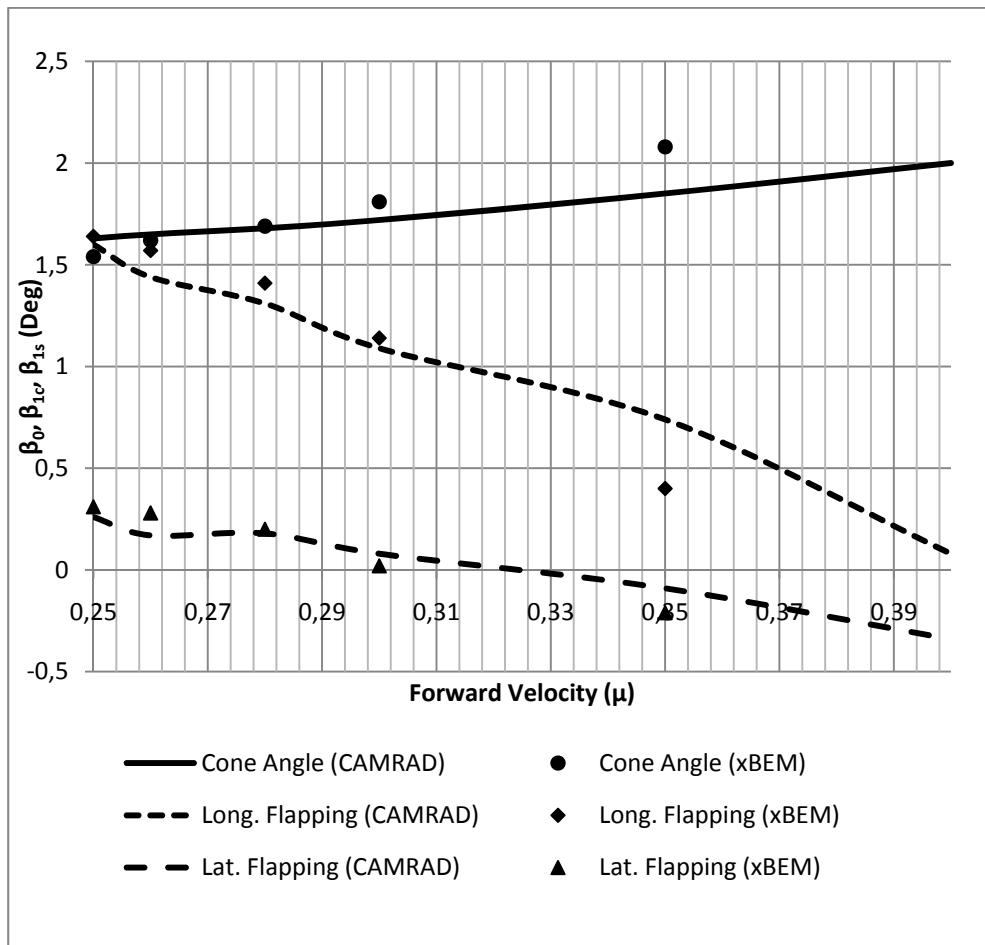


Figure 4-21 Blade Flapping Harmonics vs Advance Ratio validation with CAMRAD

In conclusion, forward flight aerodynamic analyses for Gazelle helicopter with the developed mathematical model and comprehensive analysis tool CAMRAD were performed and compared. Results showed good agreement. Total thrust and torque values generated by the main rotor were determined and compared. At high speed where freestream velocity that blade tips encounter arises up to 0.85 Mach number, the results differ dramatically from each other. This is assumed to be because of the absence of the high speed corrections in the developed mathematical model. However, for advance ratios smaller than 0.35 which corresponds to nearly 125-140 knots forward flight, the thrust and torque values calculated by both tools showed very good agreement. On the other hand, for advance ratios of 0.26 and 0.30

effective angle of attack distributions over the rotor disk are studied and compared. Even at the reversed flow conditions the results taken with the developed mathematical model and CAMRAD showed good agreement. As effective angle of attack includes the inflow, inflow angle, local blade pitch, blade flapping angle and dynamic inflow encountered because of blade flapping information, it is assumed that these parameters would show good agreement too.

4.4 UH-60 VALIDATION WITH FLIGHTLAB

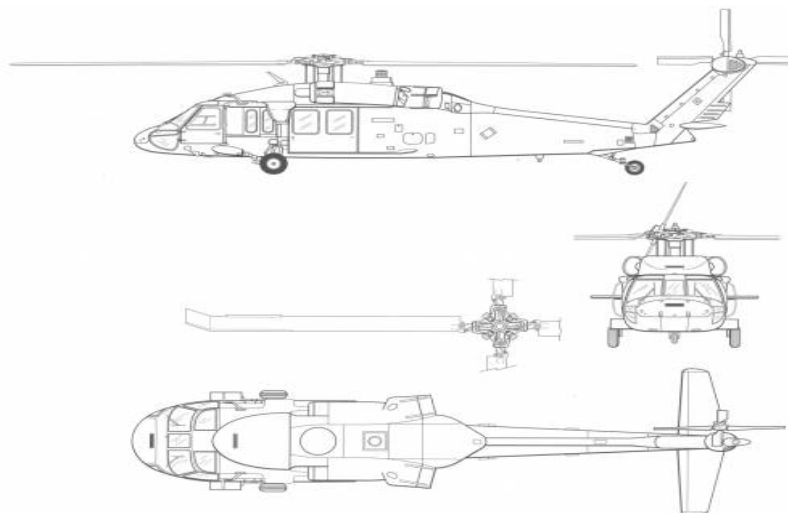


Figure 4-22 UH-60 / Blackhawk [71]

Forward flight validation of the developed aerodynamic model is done with Flightlab for UH-60 helicopter, Figure 4-22. Isolated rotor models are developed in Flightlab for UH-60 helicopter by using 45 state dynamic inflow models and Scully vortex wake inflow model. For different forward flight conditions, isolated rotor is trimmed in Flightlab for a target vertical thrust component which is approximately the weight of the UH-60 helicopter. For this study, because just the aerodynamic model is desired to be validated for forward flight conditions, the trim conditions are

supplied by Flightlab into HELCOMAS. The desired forward flight condition is defined as wind in Flightlab and the rotor is trimmed to a predefined vertical thrust value. Then the trim variables such as blade flapping angles and pilot inputs; collective and cyclic controls, are used for calculations done with HELCOMAS main rotor aerodynamic module only. The rotor configuration analyzed with both tools is given in Table 6;

Table 6 UH-60 Main Rotor Parameters [31]

Isolated UH-60 Rotor	
Number of blades	4
Rotor Radius (ft.)	27
Flap hinge offset (ft.)	1.2
Blade root cut-out (ft.)	3.5
Rotor nominal speed (rad/sec)	27
Blade root chord length (ft.)	1.73
Blade Profile	NACA 0012
Hub type	Articulated
Blade flexibility	Rigid blades

where blade twist distribution is defined as;

Table 7 UH-60 Main Rotor twist distribution [13]

Blade segments		Local Angle of attack (deg)
start(%R)	End(%R)	
13	20	0
20	25	-0.15
25	30	-0.95
30	35	-1.8
35	40	-2.75
40	45	-3.55
45	50	-4.4
50	55	-5.3
55	60	-6.15
60	65	-7.1
65	70	-7.9
70	75	-8.8
75	80	-9.65
80	85	-10.3
85	90	-10.75
90	95	-13.1
95	100	-10.9

The analysis method for HELCOMAS is selected as vortex wake theory; with Beddoes Prescribed wake geometry including 10 rotor revolutions of wake while determining the initial values for iteration from Drees linear inflow model. On the other hand, two isolated rotor models are developed in Flightlab. One is with the Peters-He dynamic inflow model with 45 states and the other is with vortex wake theory using a free wake model. Dynamic inflow model is developed with four inflow

harmonics and with a highest radial variation power of eight. Quasi-unsteady aerodynamic is used. Similarly, quasi-unsteady aerodynamics is used for vortex wake model. However this time wake is modeled with a free wake model with single peak circulation distribution and straight vortex elements. Four revolutions of wake is modeled with a tip vortex core size of 0.003 and inboard location for free wake geometry as 0.5. In the Figure 4-23 results taken with 3 models are presented. From the results, it is evaluated that vortex wake models both built in HELCOMAS and Flightlab calculates torque coefficient similar to each other.

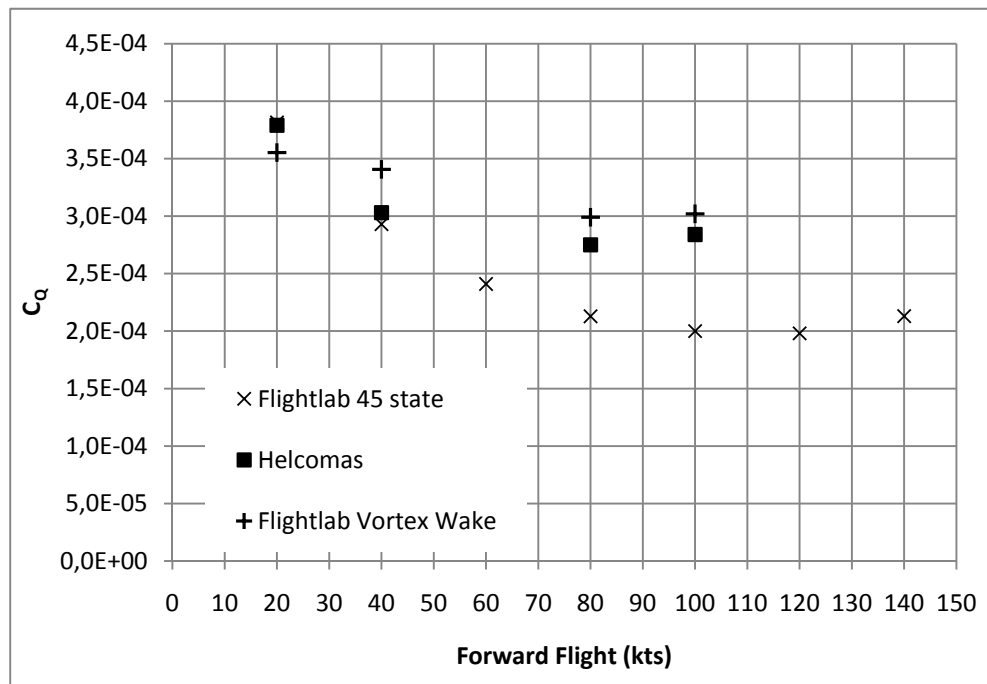


Figure 4-23 C_q vs Forward Flight validation with FLIGHTLAB

In addition to total thrust, lift coefficient distribution in both radial and azimuthal direction are compared. Analysis are done with the vortex wake method implemented into HELCOMAS tool, 45 state Dynamic Inflow model in Flightlab, and

vortex wake method in Flightlab. Analyses are done for isolated rotor configuration at forward flight velocities; 20, 40 and 80 knots. Analyses conditions are trimmed with 45 state dynamic inflow model in Flightlab and trim parameters such as tip path plane angle and pilot controls are used in the analyses done with the aerodynamic model developed. Both azimuth and radial distributions of the non-dimensional lift by the blade elements determined and compared. Non-dimensional lift azimuth variation at radial locations $r/R = 0.5, 0.75$ and 0.9 are compared in from Figure 4-24 to Figure 4-32.

20 knots forward flight

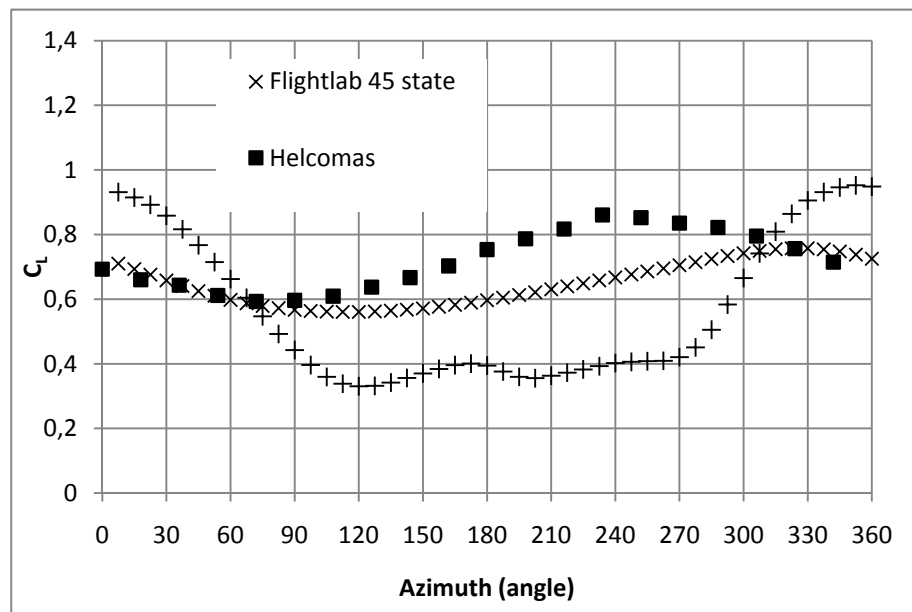


Figure 4-24 Cl vs Azimuth Angle distribution validation with FLIGHTLAB at $r/R = 0.50, 20$ kts

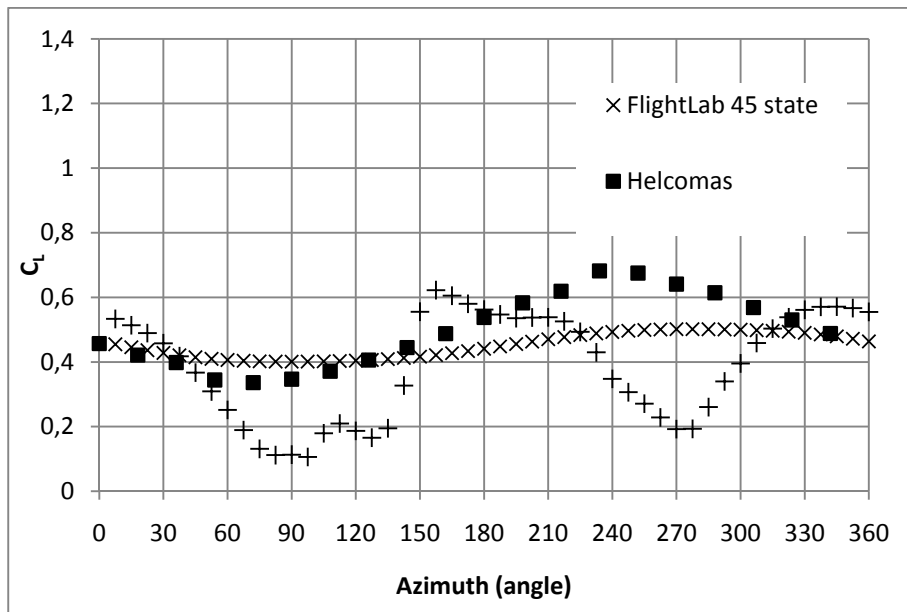


Figure 4-25 CI vs Azimuth Angle distribution validation with FLIGHTLAB at $r/R = 0.75$, 20 kts

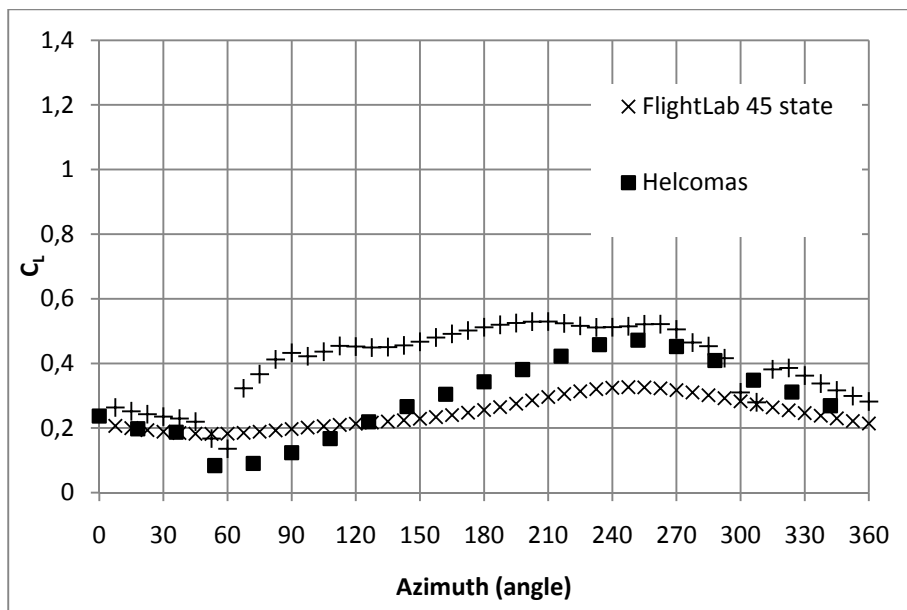


Figure 4-26 CI vs Azimuth Angle distribution validation with FLIGHTLAB at $r/R = 0.90$, 20 kts

40 knots forward flight

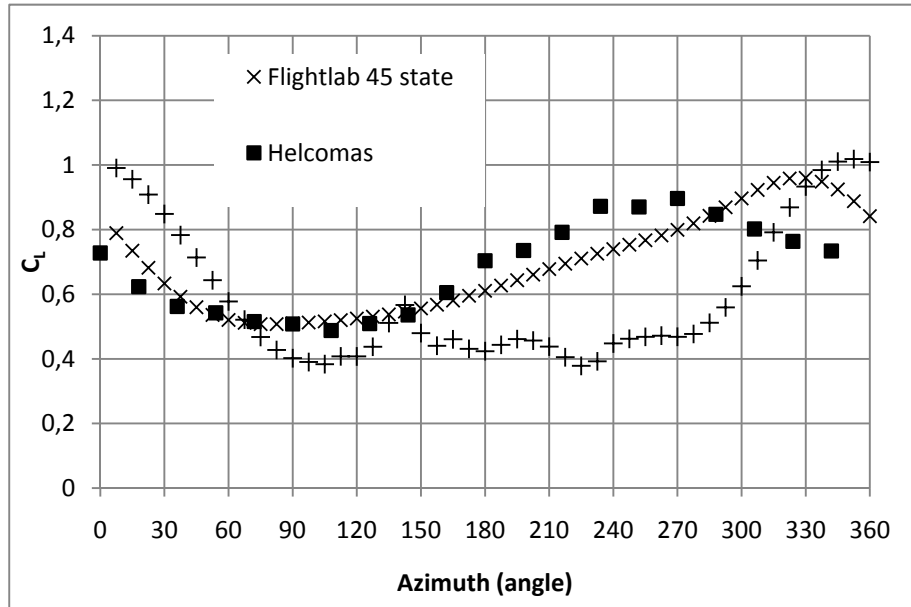


Figure 4-27 C_l vs Azimuth Angle distribution validation with FLIGHTLAB at $r/R = 0.50$, 40 kts

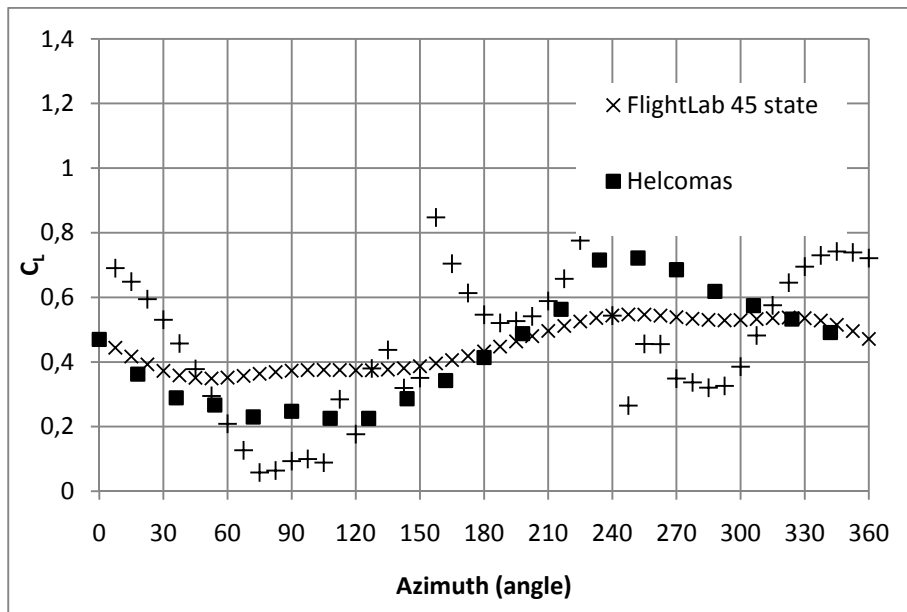


Figure 4-28 CI vs Azimuth Angle distribution validation with FLIGHTLAB at $r/R = 0.75$, 40 kts

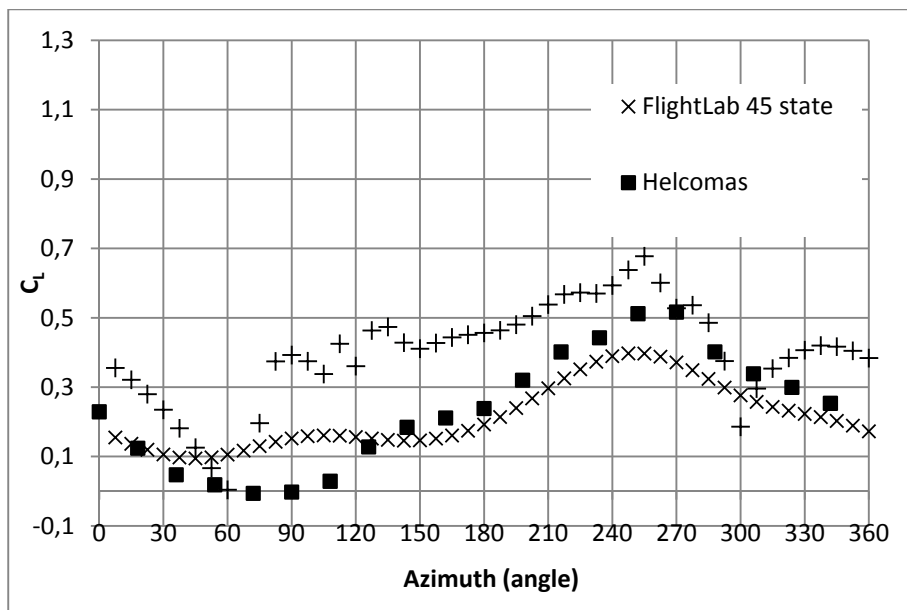


Figure 4-29 CI vs Azimuth Angle distribution validation with FLIGHTLAB at $r/R = 0.90$, 40 kts

80 knots forward flight

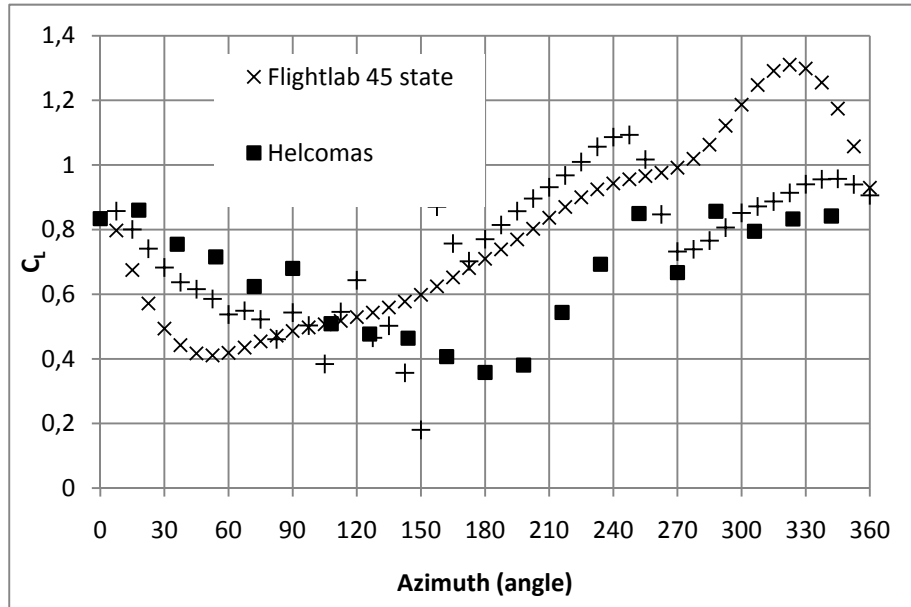


Figure 4-30 C_l vs Azimuth Angle distribution validation with FLIGHTLAB at $r/R = 0.50$, 80 kts

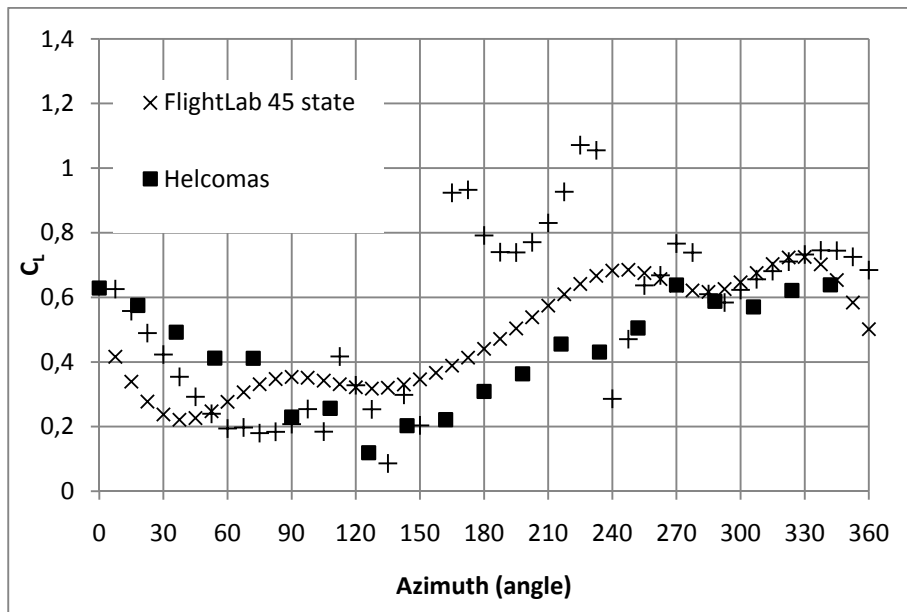


Figure 4-31 CI vs Azimuth Angle distribution validation with FLIGHTLAB at $r/R = 0.75$, 80 kts

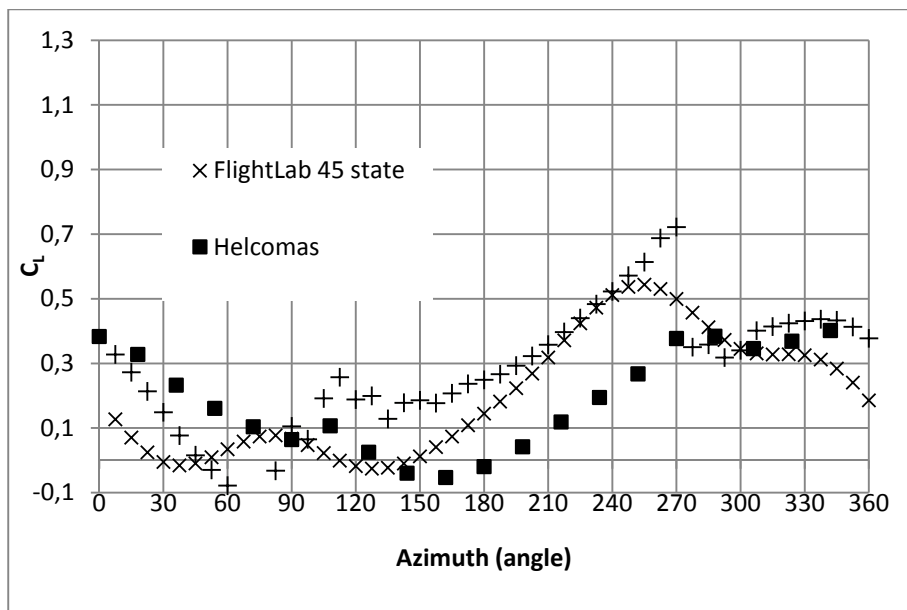


Figure 4-32 CI vs Azimuth Angle distribution validation with FLIGHTLAB at $r/R = 0.90$, 80 kts

In conclusion, forward flight aerodynamic analyses for UH-60 helicopter isolated rotor with the developed mathematical model and two Flightlab models were performed and compared. Results showed that the inflow distributions in both radial and azimuthal direction are highly dependent on the solution, trim and model parameters. Although the average force and moment coefficients generated by each model show similar values, the inflow distributions may show diverseness. The general trend and order of magnitude of the inflow distributions calculated by each model are consistent. However, model and solution parameters should be selected carefully as the inflow distribution results are highly dependent and sensitive to them. This can be seen from the figures also as even the results taken with the two isolated rotor models built in the same comprehensive analysis tool Flightlab show dramatic differences.

CHAPTER 5

TRIM MODEL

The trim problem involves determining correct pilot control settings for the desired flight condition. Trim analysis could be separated into two areas. The first one is isolated rotor trim which intends to eliminate net pitching and rolling moments transferred to the rotor shaft or intends to hold or reach to targeted tip path plane angles or shaft moments by altering swash plate control angles. Isolated rotor trim only takes rotor aerodynamics and equations of motions into account and does not deal with remaining helicopter components or the whole helicopter. On the other hand, helicopter trim analysis, intends to find the trim solution involving proper pilot controls and helicopter attitude, for the desired flight condition. Helicopter trim analysis takes the helicopter into account as a whole. Helicopter trim analysis seeks correct pilot control settings for the desired helicopter states which includes helicopter attitude, translational and rotational velocities, accelerations (if exists) etc. Therefore, for helicopter trim analysis a mathematical model representing helicopter dynamics and behavior is essential.

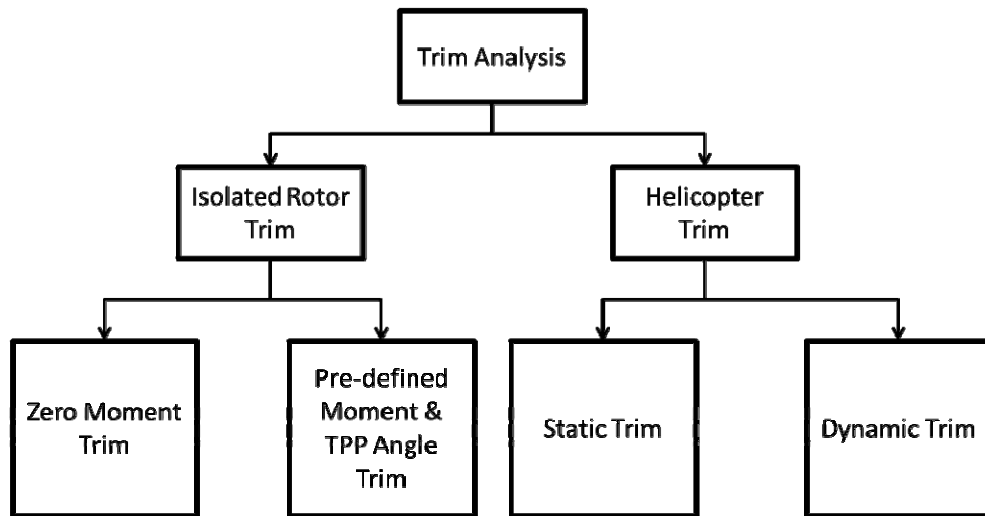


Figure 5-1 Trim analysis variations

For both comprehensive analysis and flight dynamics analysis applications, several trim solution methods exist. One of the simplest methods is to decouple longitudinal and lateral dynamics of the system and use iterative methods for loops one comprehending the other [46]. Generally, for this method, helicopter is modeled with simplified equations and with inner and outer iteration loops of the trim parameters dynamics of helicopter are decoupled. Longitudinal and lateral trim solutions are determined in order which continues until the trim solution converges. Another trim solution method is solving the inverse equations of motion problem. The state derivatives are equated to zero and trim parameters in the helicopter mathematical model equations are left alone. Then with iterative methods, trim parameters that result in zero state derivatives are determined (CAMRAD). Another trim solution method, which is developed by Peters and Izadpanah [65], uses periodic shooting method with Newton-Raphson iteration. In this method, “the correct controls and periodic solution (i.e. the correct blade initial conditions to yield periodicity) are found simultaneously” [65]. Except from the methods mentioned, yet another method exists called optimization, which is also the method used in this study.

The optimization method for trim solution used in this study ensures simultaneous computation of the trim parameters which are specified according to the flight condition to be analyzed. Simultaneous solution of the helicopter states models the longitudinal and lateral dynamics and their effects to each other at same time, resulting in coupled trim solution of the helicopter at desired flight conditions. As the mathematical model is developed in MATLAB Simulink, built in MATLAB function “fmincon” is used for the optimization problem.

“Fmincon” constrained nonlinear optimization function attempts to find a constrained minimum of a scalar function of several variables starting at an initial estimate. “Fmincon” which uses a Hessian, the second derivatives of the Lagrangian, is a gradient-based method that is designed to work on problems where the objective and constraint functions are both continuous and have continuous first derivatives. More information about the built in optimization function “fmincon” can be found in MATLAB Product Help.

As mentioned an optimization method is used for the trim model developed. The optimization function attempts to find minimum of a scalar function with several variables. Consequently, the mathematical model developed is defined as a function whose outputs are the state derivatives that are desired to be equated to zero according to the flight condition. The objective function on the other hand is defined as the sum of the squares of the state derivatives that are desired to be zero. The objective function that the optimization model tries to minimize is given as;

$$J = \sqrt{\sum_{i=1}^n Q_{ii} x_i^2}$$

(5-1)

The weighting coefficient in the objective formula is a diagonal matrix consisting of weight coefficients of the state derivatives. The weight coefficients are selected according to the importance and order of magnitude of the state derivatives. The accuracy of the optimization function depends on the weighting matrix; therefore the diagonal elements of the matrix shall be selected thoughtfully.

The trim parameters and the state derivatives of a static trim solution at any flight condition are shown in the figure below. As seen from the flow chart, optimization function computes the trim parameters where the objective function is minimum valued.

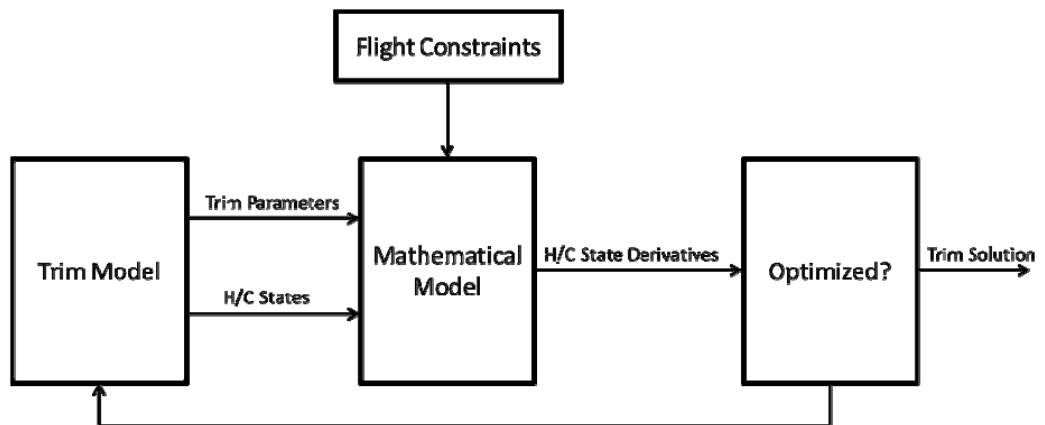


Figure 5-2 Flow chart of the developed trim model

Except from the static trim solution where translational and rotational accelerations are equated to zero, the trim model developed is also able to find dynamic trim solutions in order to model a trimmed maneuver of the helicopter. According to the maneuver to be trimmed and analyzed, not all the state derivatives have to be zero. For example, in case of a pull-up maneuver, because of the centrifugal acceleration acting on the system, the acceleration at body z-axis direction would have a value different than zero. In that case, the z axis acceleration parameter is taken out of the objective function. The optimization function then attempts to minimize the objective function excluding body z axis acceleration. The target exists as equating the remaining translational and rotational accelerations to zero whereas leaving body z axis acceleration free. As a result, dynamic trim condition of a pull-up maneuver is determined.

$$\text{Trim Parameters} \rightarrow x_p = \begin{Bmatrix} \theta_0 \\ \theta_{1c} \\ \theta_{1s} \\ \theta_{TR} \\ \phi \\ \theta \end{Bmatrix} \quad (5-2)$$

$$\text{Helicopter States} \rightarrow x_s = \begin{Bmatrix} u_b \\ v_b \\ w_b \\ \phi \\ \theta \\ \psi \\ p \\ q \\ r \end{Bmatrix} \quad (5-3)$$

$$\text{Flight Constraints} \rightarrow x_c = \begin{Bmatrix} u_i \\ v_i \\ w_i \\ p \\ q \\ r \\ x \\ y \\ z \end{Bmatrix} \quad (5-4)$$

$$\text{Helicopter State Derivatives} \rightarrow x_s = \begin{Bmatrix} \dot{u}_b \\ \dot{v}_b \\ \dot{w}_b \\ \dot{\phi} \\ \dot{\theta} \\ \dot{\psi} \\ \dot{p} \\ \dot{q} \\ \dot{r} \end{Bmatrix} \quad (5-5)$$

The trim model developed compiles for the trim solution without decoupling the longitudinal and lateral dynamics. Besides, the user defined weighting matrix including the coefficients that shifts the emphasis on state derivatives gives the option to change the accuracy and dynamic response of the helicopter in the desired direction. In addition, the selective state derivatives that are included in the cost function of the optimization model enable seek dynamic trim solutions representing helicopter maneuvers. However, on the other hand, the process of finding minimum value of an at least six dimensional function with six variables is a computationally expensive effort. When higher fidelity and accurate aerodynamic models are selected for the analysis, the computational cost increases dramatically. A solution similar to the one implemented in CAMRAD [14, 15] is developed for this problem and explained in Future Plans chapter of this study in detail.

CHAPTER 6

TRIM MODEL VALIDATION

6.1 VALIDATION WITH FLIGHTLAB

The mathematical model developed is validated with the comprehensive analysis and simulation tool FLIGHTLAB [Version: 3.2]. A helicopter with maximum takeoff weight (MTOW) 300 kg is modeled with both tools. The helicopter modeled is very close to the MOSQUITO XE helicopter, Figure 6-1, with simplifications and approximations. Velocity sweep analyses at sea level from hover to 80 knots forward flight are conducted and results such as pilot controls, helicopter attitudes at trimmed conditions are compared in this section.

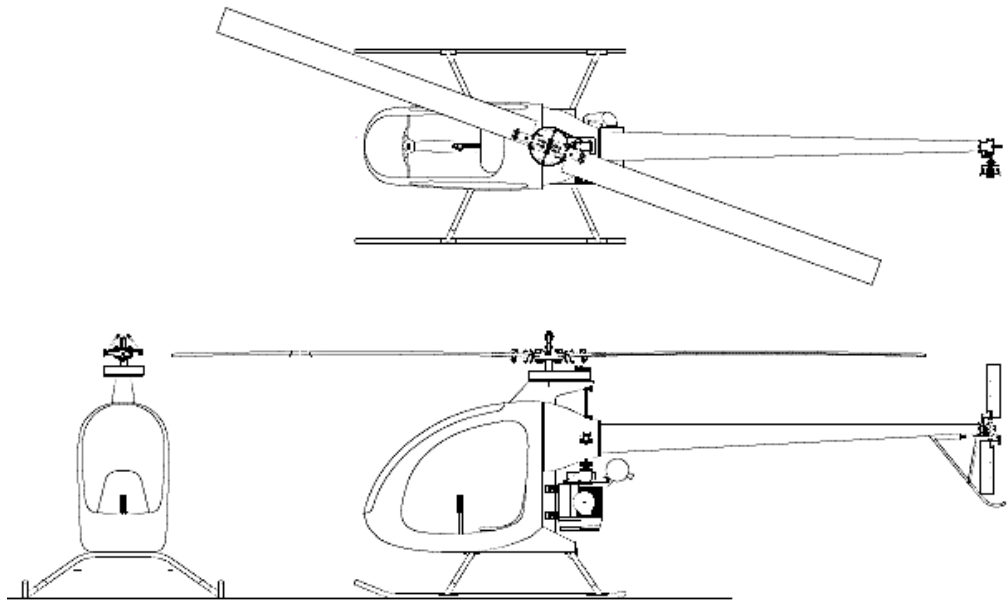


Figure 6-1 Mosquito XE [74]

The helicopter configuration that was modeled with both tools and used in analyses is given in Table 8. The fuselage parameters are scaled from UH-60 helicopter with a factor of weight ratio between the two helicopters.

Table 8 Mosquito Helicopter parameters [74]

Main Rotor Parameters	
Number of Blades	2
Rotor Diameter (m)	6
Blade Root Cut-Out (%)	20
Tip speed (m/s)	167.86
Rotor RPM	534.5
Flapping Hinge Position (%)	3.517
Precone Angle (deg)	0
Blade Twist (deg)	0
Shaft Tilt (deg)	0
Blade Mass (uniform) (kg)	7.5
Tail Rotor Parameters	
Number of Blades	2
Rotor Diameter (m)	1
Rotor RPM	2450
Lift Curve Slope	5.73
Profile C_{d0}	0.01
Fuselage Parameters	
Total Vehicle Mass (kg)	280
I_{xx} (kg - m ²)	250
I_{yy} (kg - m ²)	400
I_{zz} (kg - m ²)	200
I_{xy} (kg - m ²)	0
I_{xz} (kg - m ²)	0
I_{yz} (kg - m ²)	0

FlightLab Model

Main rotor is modeled with articulated hub type. Blade element method is used for quasi-steady air load calculations for counter-rotating main rotor with a tip loss factor of 0.97. NACA 23012 aerodynamic coefficient tables which are dependent on the angle of attack and local Mach number are used for blade element method inputs; while inflow distribution over the rotor disk is modeled with Peters-He 3 state dynamic inflow model. Blades are modeled as rigid blades and only flapping dynamics are enabled.

Tail rotor which is one of the main force and moment contributors to the helicopter is modeled as disk rotor with collective control only.

Fuselage is modeled as rigid airframe for which aerodynamic coefficients are provided as tables in wind reference frame depending on the angle of attack and sideslip angles.

Helcomas Model

Same helicopter configuration as the one explained in the previous section is modeled with the developed mathematical model. For main and tail rotor aerodynamic models, for hover flight conditions momentum theory modified with Prandtl's tip loss function is used whereas for forward flight conditions Drees's Inflow Model is used in order to get the same fidelity with the Flightlab model. Blade dynamics are modeled with Chen's tip path plane dynamic equations which are modified in this study, and rigid main rotor blades are assumed to be uniform.

Trim results

After similar fidelity level models are constructed with both tools, trim analyses are done at sea level. Hover analyses and velocity sweep analyses are done at leveled forward flight cases up to 80 knots. Pilot controls such as main rotor collective, longitudinal and lateral cyclices and helicopter attitudes (Euler angles) such as pitch and roll angles for trimmed flight cases are compared and validated.

The change of collective angle, longitudinal cyclic, lateral cyclic, pitch and roll angles of the helicopter at trimmed flight conditions with forward flight up to 80 knots (40 m/s) are analyzed and compared and the results are given in Figure 6-2 to Figure 6-5.

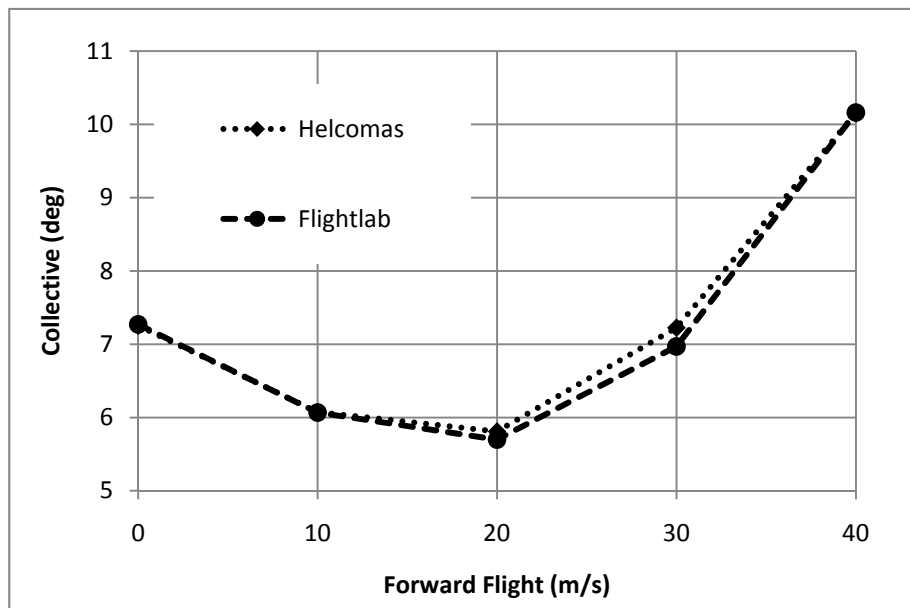


Figure 6-2 Collective vs Forward Flight trim validation with FLIGHTLAB

Hover and maximum forward flight conditions require the high power to perform. Therefore, the trimmed collective angle starts with a relatively high value and decreases as the forward velocity approaches to the cruise speed and then again increases rapidly as the forward flight continues to increase to maximum forward flight speed.

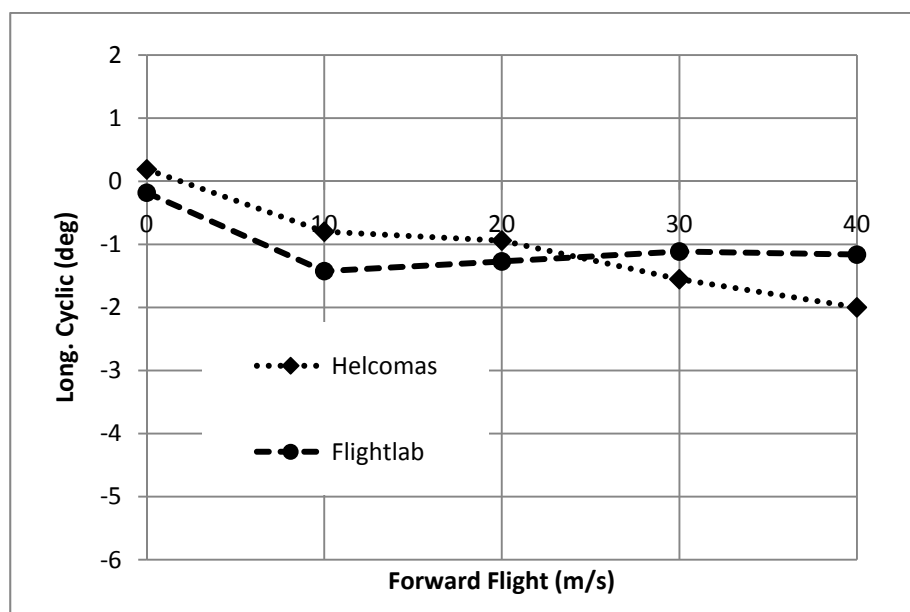


Figure 6-3 Longitudinal Cyclic vs Forward Flight trim validation with FLIGHTLAB

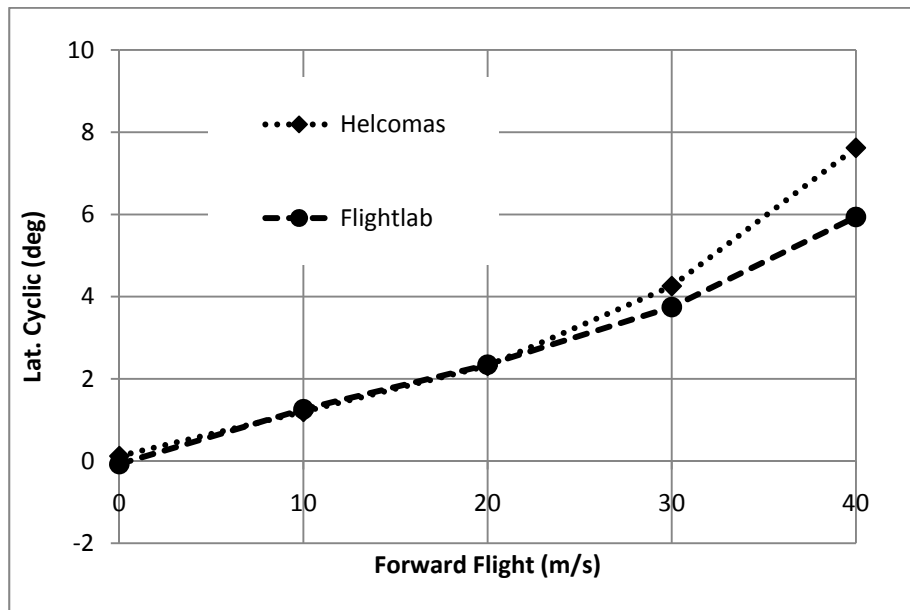


Figure 6-4 Lateral Cyclic vs Forward Flight trim validation with FLIGHTLAB

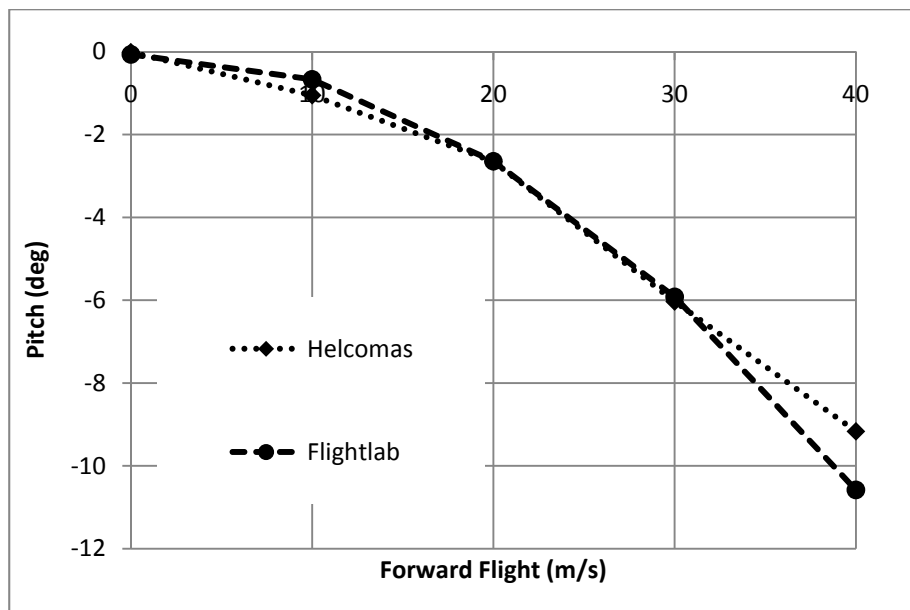


Figure 6-5 Helicopter Pitch Angle vs Forward Flight trim validation with FLIGHTLAB

Pitch angle of the helicopter reaches up to 10 degrees at maximum forward flight speed in order to supply the required forward thrust to maintain the high total drag of the helicopter at the related dynamic pressure.

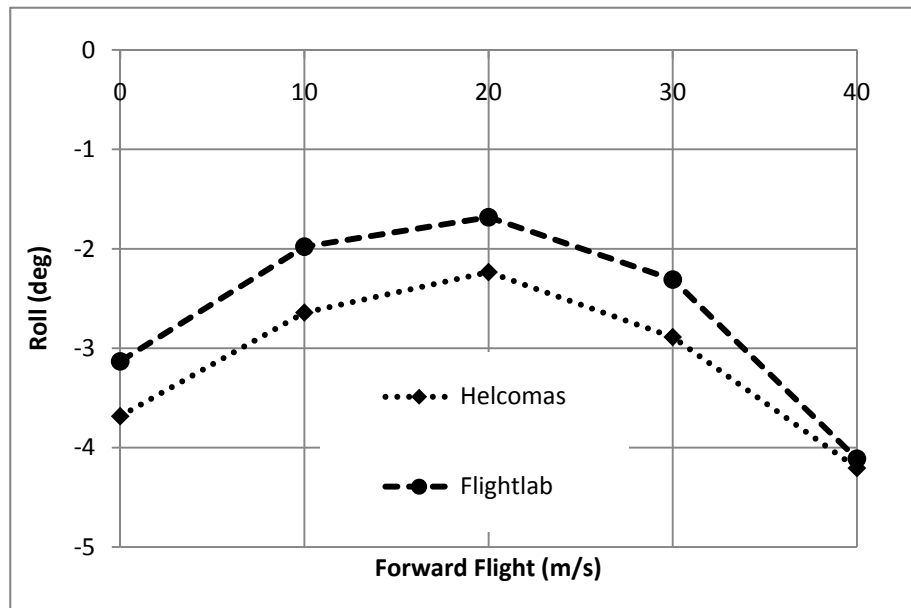


Figure 6-6 Helicopter Roll Angle vs Forward Flight trim validation with FLIGHTLAB

Generally the results taken with both tools are consistent with each other. However there are small differences which are evaluated as arising from differences in modeling techniques of each tool.

CHAPTER 7

SIMULATION RESULTS

Bo105 helicopter is modeled with the mathematical model developed and nonlinear time response simulations are done. In order to validate the trim model, developed, and study the dynamic response of a helicopter determined with the mathematical model, during a simulation, mathematical model of the Bo105 helicopter, Figure 7-1, is built. Firstly Bo105 helicopter is trimmed in hover flight condition and the trim solution determined is used as initial values for simulation. Then simulation is done for 5 seconds and helicopter position in earth reference frame, helicopter states and states derivatives such as velocity components in earth reference frame and p, q, r rates are investigated. Dynamic simulations of the Bo105 helicopter showed that, the trim solution calculated by the trim model developed is really the trim condition of the helicopter at hover flight as the helicopter continues its steady hovering flight without changing its attitude and flight condition.

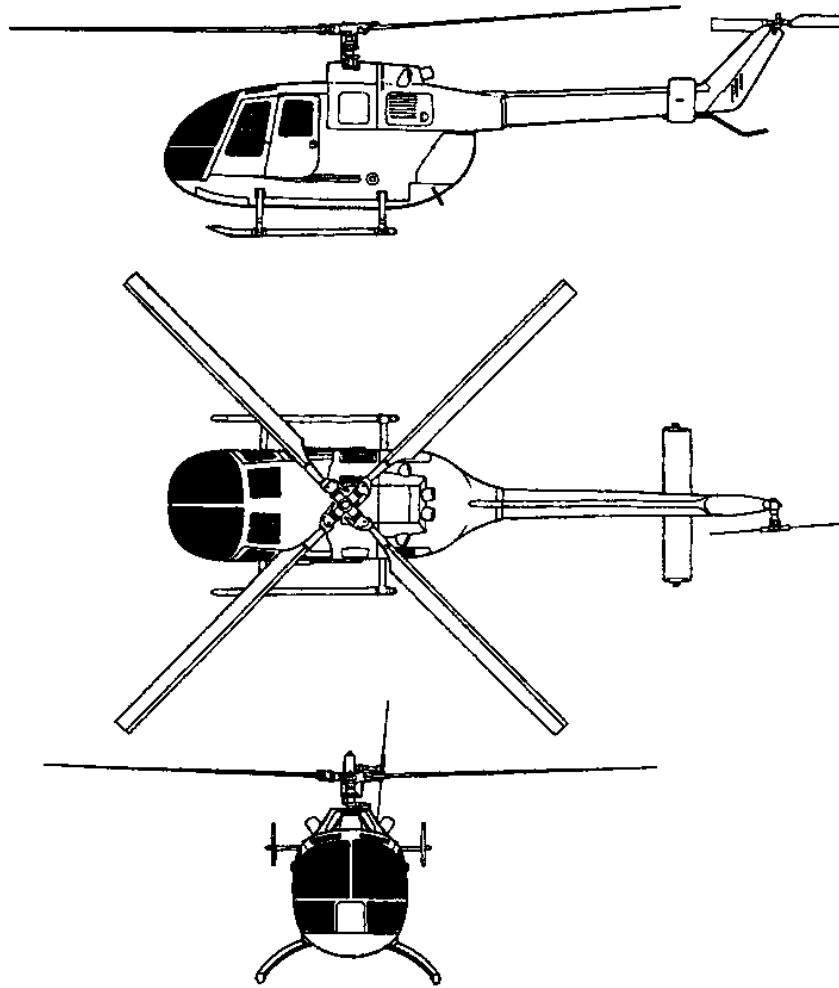


Figure 7-1 Bo 105 Masserschmidt [70]

The parameters of the Bo105 helicopter configuration used in the simulations are given in the Table 9 [31];

Table 9 BO105 Helicopter Parameters [31]

MAIN ROTOR	
Number of blades	4
Rotor Radius (ft.)	16.12
Blade chord Length (ft.)	0.89
Rotational speed (rad/sec)	44.4
Tip speed (ft./sec)	715.73
Shaft tilt (deg)	-3
Blade profile	NACA 23012
Root cut-out (ft.)	3.61
Precone angle (deg)	2.5
Blade twist (linear),(deg)	-6.2
Solidity	0.07
Lock umber	5.54
FUSELAGE	
Gross weight (lbs.)	4850.17
Pitch Inertia (lbs-ft ²)	3667.92
Roll Inertia (lbs-ft ²)	1056.17
Yaw Inertia (lbs-ft ²)	3023
CG below hub (ft.)	3.15
TAIL ROTOR	
Number of blades	2
Rotor Radius (ft.)	3.18
Blade chord Length (ft.)	0.59
Rotational speed (rad/sec)	233
Tip speed (ft./sec)	726.21
Shaft tilt (deg)	-4.2

Helicopter is trimmed at hover flight condition at 100 ft. above the sea level. The nonlinear time response simulation is done for five seconds by using the trim solution as starting point. It is evaluated from the results that, helicopter maintains its initial condition throughout the simulation. Therefore the trim model validates itself. The trim solution found by the trim model, is validated by the simulation. In Figure 7-2, Figure 7-3 and Figure 7-4, the simulation results are presented. For five seconds, change in helicopter states and state derivatives are always in the tolerable region.

In Figure 7-2 helicopter roll, pitch and yaw responses are presented. It is evaluated that, the pitch and yaw angles remain zero throughout the five second simulation. On the other hand, roll angle of the helicopter whose initial condition is determined from the trim model, is nearly constant throughout the simulation. The one of thousandth of a radian change in the roll angle is associated with the trim solution tolerances.

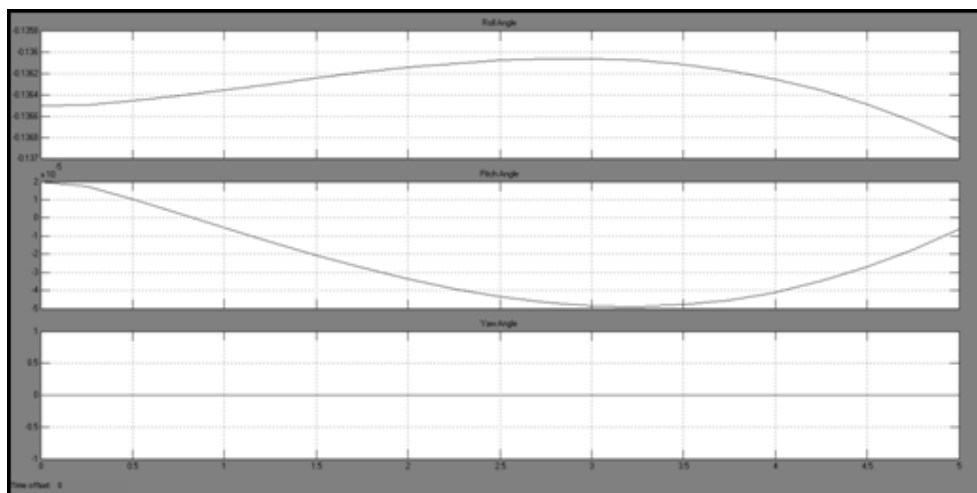


Figure 7-2 Helicopter Roll, Pitch and Yaw Angle vs Simulation Time

Apart from the helicopter attitude, helicopter position in earth reference frame is also studied. From the figure below, it can be evaluated that the helicopter remains nearly constant at its initial position. As mentioned before, the trim solution is determined at 100 ft. altitude, which is reflected to the z position of the helicopter.

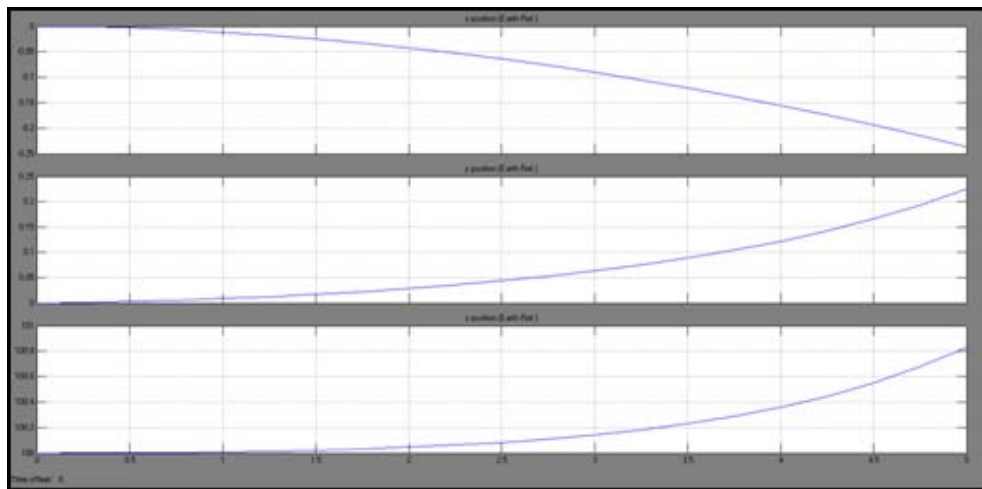


Figure 7-3 Helicopter Earth x,y and z position vs simulation time

In addition, except from the change in the attitude of the helicopter, it is also important to study the states and state derivatives of the helicopter as they include the information of the translational or rotational accelerations. In the figure below; it is deduced that, helicopter p,q and r rates remain constant during the simulation as trim solution suggests.

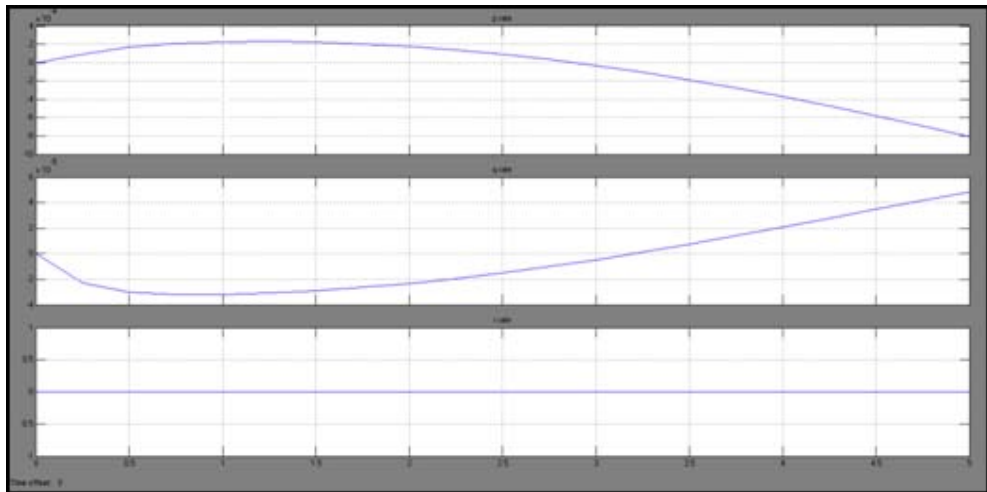


Figure 7-4 Helicopter p,q and r rates vs simulation time

In order to study helicopter dynamic response to any pilot input, simulations are done starting from the trim condition at hover flight. Helicopter nonlinear time response is simulated for five seconds to a pilot collective input. A 0.1 radian pilot collective control is inputted after two seconds simulation is started, Figure 7-5. Helicopter position change at earth reference frame and helicopter translational velocity change for five seconds are simulated and given in Figure 7-6 and Figure 7-7. A collective input, as expected, results in a direct response in helicopter rotor thrust and climb velocity. It is evaluated that helicopter trimmed at 100 ft altitude suddenly starts to climb vertically with acceleration at the time the collective input is applied.

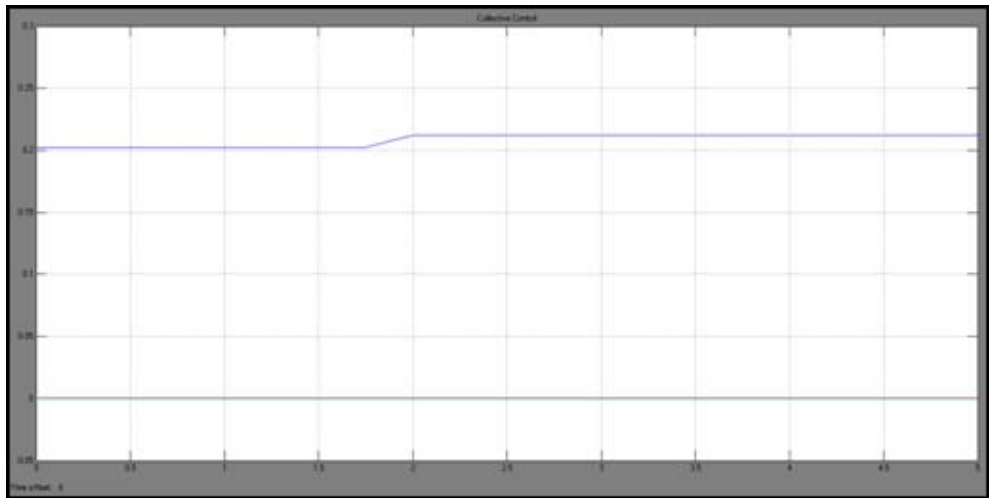


Figure 7-5 Collective control vs simulation time

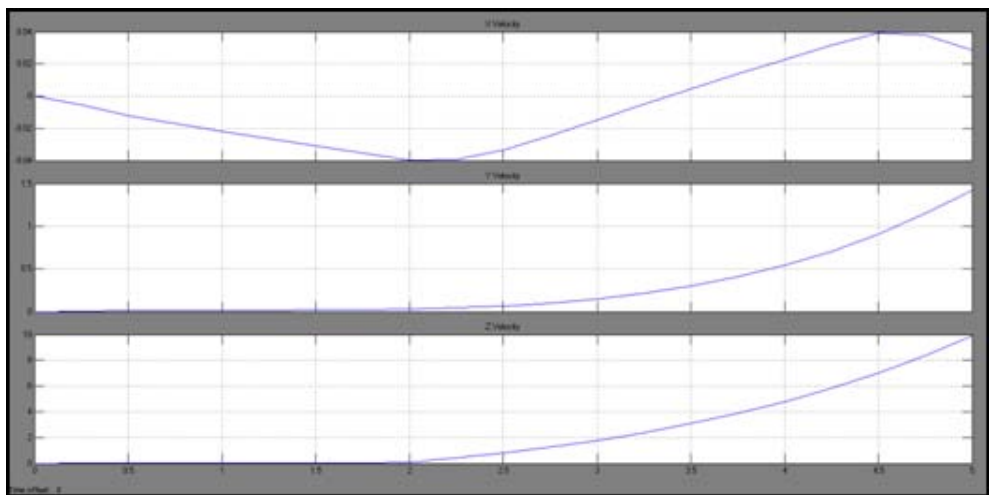


Figure 7-6 Helicopter x,y and z velocities vs simulation time (in earth reference frame)

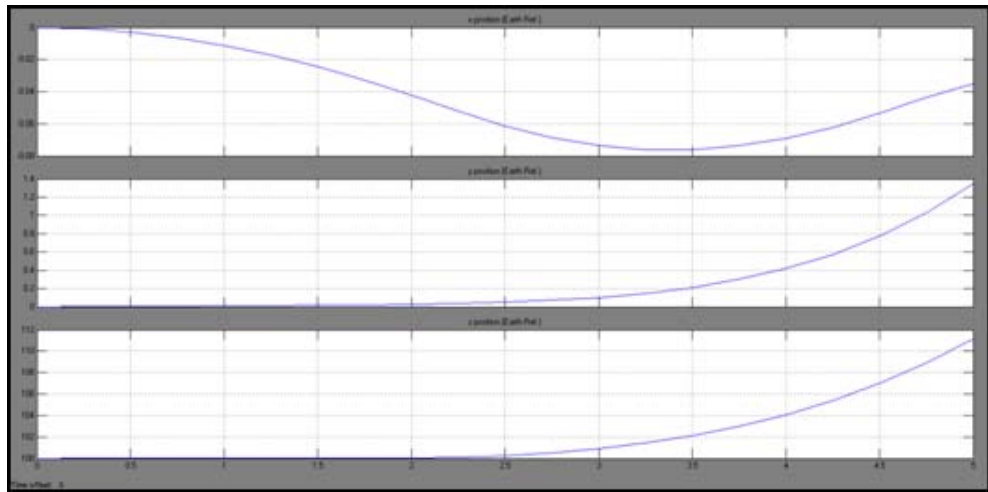


Figure 7-7 Helicopter Earth x,y and z positions vs simulation time

In order to study the helicopters dynamic response to pilot controls, a real time piloted simulation has to be done or a controller has to be built. As all the controls inputs are highly coupled in a nonlinear mathematical model, a control input from just one channel would not result enough information to decouple the helicopter's response and investigate the response which is a result of the input only. As a controller design or a real time piloted simulation with the developed mathematical model are planned as future works, the study on the nonlinear time response is paused here.

CHAPTER 8

SUMMARY AND CONCLUSIONS

8.1 Summary

A mathematical model developed in this study defines a helicopter and all helicopter components that are force and moment contributors to the system with empirical and analytical models, in order to describe rigid body dynamics of the helicopter. Helicopter components such as fuselage, horizontal tail, vertical tail, tail rotor and main rotor are mathematically modeled in order to formulate the whole helicopter system as first order, coupled and non-linear differential equations

The mathematical model is developed throughout this study in a modular structure. A tree like structure is used for the mathematical model where each module defines a helicopter component that has force and moment contributions to the total force and moments acting on the helicopter center of gravity. The basic flowchart of the mathematical model is given in Figure 8-1.

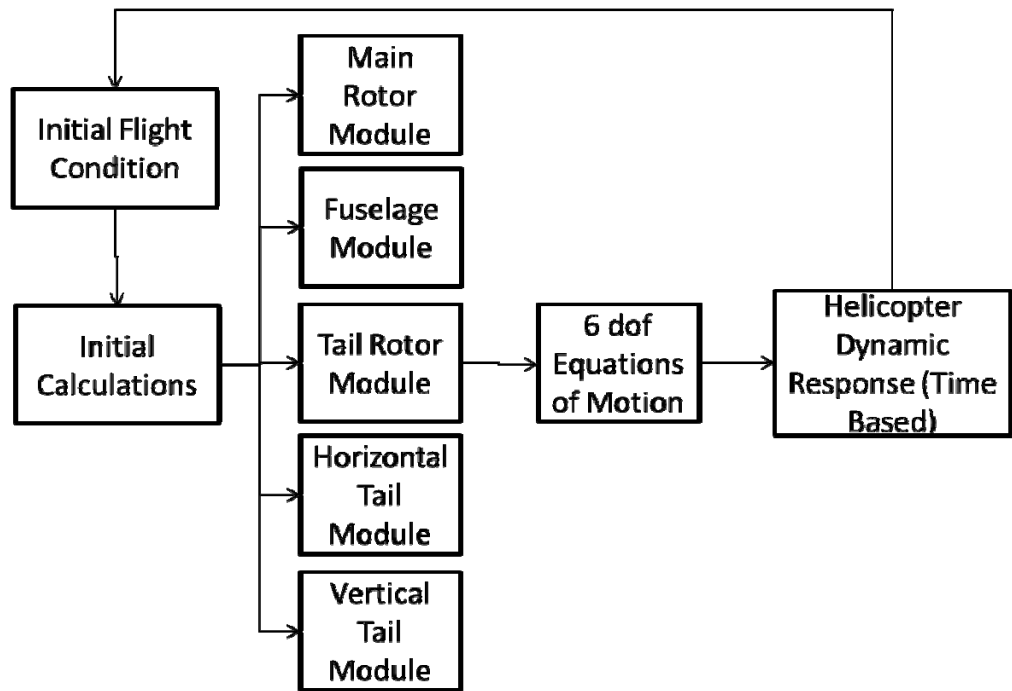


Figure 8-1 Basic flowchart of the mathematical model developed

In addition a trim model is developed that controls the mathematical model from outside and an optimization model iterates the mathematical model until the trim conditions at desired flight condition is reached. The basic flowchart of the trim model is given at Figure 8-2;

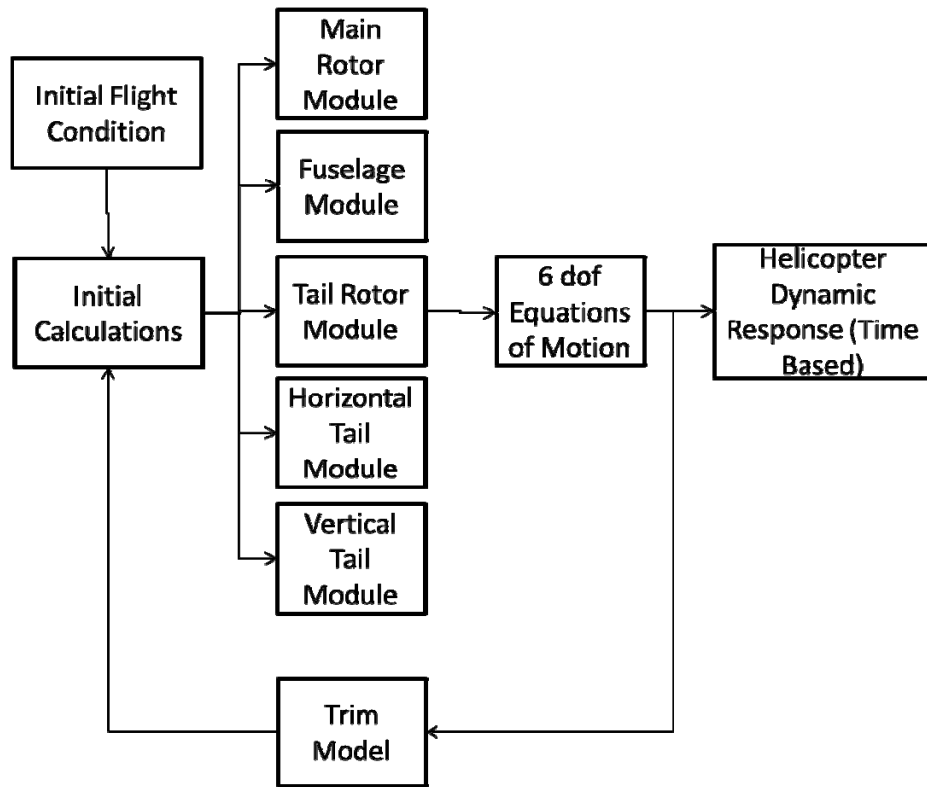


Figure 8-2 Basic trim model flowchart including the mathematical model

Initial calculations for the constants related with air properties and flight conditions are calculated in the environmental module. According to the flight condition, such as altitude and temperature, air properties that are directly or indirectly related with the aerodynamic loads generated are determined. Air density and speed of sound which are used in aerodynamic force and moments calculations and air viscosity which is used in vortex wake method while determining the vortex core radius are calculated within the environmental module.

Main Rotor Module

As being the most dominant force and moment contributor to the system, main rotor aerodynamics is defined with several models with different fidelity and accuracies. Each aerodynamic model is at different level of the tradeoff between fidelity, accuracy and computational cost. Main rotor aerodynamic model is divided into sub-models such as tip path plane dynamics model, inflow & load model and the integrator model. Blade flapping angle, changing with azimuth angle, is calculated in tip path plane dynamics model. Force & moment equilibrium about flapping hinge at each azimuth angle, specified, is formulated and the blade flap angle which ensures the force and moment equilibrium is determined. Blade aerodynamic loading, gravitational, centrifugal and Coriolis accelerations, inertial forces generated because of the platform acceleration and rotation and spring moments (if exist) are taken into account individually at each azimuth angle while the force and moment equations are derived. The blade aerodynamic force and moments used in the flapping model is determined by the aerodynamic load model of the main rotor. Rotor induced velocity distribution; relative freestream velocities and dynamic inflow distribution which is formed because of the blade flap angle time derivative are taken into account in the aerodynamic load model. The flap angle derivation depends on the aerodynamic loading where on the other hand aerodynamic loading of the blade depends on the flap angle. Therefore an iterative procedure is developed between tip path plane dynamics model and aerodynamic loading model. Related information is exchanged between blade dynamic model and aerodynamic load model until the flapping angle at each azimuth angle converges.

The inflow prediction method is one of the most important steps in aerodynamic modeling. In the developed mathematical model, several inflow prediction methods with different fidelity and accuracies are implemented. For hover flight conditions, momentum theory combined with Prandtl's Tip Loss function and vortex wake method combined with blade element method are implemented. Prandtl's tip loss function which is the lower fidelity inflow prediction method can be used for analyses where the accuracy is at second importance such as flight dynamics applications for which time based real time simulations are performed. For

these analyses, the computational cost of the calculations receives higher importance than accuracy. On the other hand, when detailed aerodynamic analysis is required, vortex wake theory could be used instead. Counterweight to high computational cost, high fidelity and accuracy is the biggest advantage of this method. The high fidelity and accuracy of the vortex wake method is a result of taking the rotor wake effect into account in the calculations. For hover flight conditions, Landgrebe's prescribed wake geometry model is implemented. For forward flight analyses, Drees linear Inflow model, Mangler & Squire's Nonuniform Inflow model and the Vortex Wake Method are implemented. Drees linear inflow model which is lowest in fidelity and accuracy and Mangler & Squire nonuniform inflow model are mostly used for analyses where again the accuracy is of second importance. On the other hand, vortex wake model which has dramatically higher computational cost when compared with the Drees and Mangler & Squire inflow models is more accurate and has higher fidelity. Wake geometry is predicted with Undistorted Prescribed Wake model or Beddoes Distorted Prescribed Wake model, where the option of selection is left to the user.

The converged flapping angle and aerodynamic loads are then used by the integrator model where aerodynamic force and moments are integrated along the blade at each azimuth step. Gravitational and centrifugal forces generated by the blade are taken into account and total force and moments generated and transferred to the hub are calculated at each azimuth angle. For main rotor total thrust, torque and power coefficients, the net force and moments transferred to the hub by the blade are non-dimensionalized and azimuthally averaged.

Tail Rotor Module

Similar to main rotor module except from the blade dynamic model, tail rotor module is also consists of sub-models such as tail rotor aerodynamic model and integrator model. Tail rotor blades and hub are assumed to be rigid which prevents tail rotor blades from deforming or deflecting about any hinge. The absence of the flapping hinge eliminates net centrifugal forces transferred to the hub, dynamic

inflow that each blade element encounters because of the flap angle time derivative and the tilt of the tip path plane. However, the prediction of induced velocity distribution over the rotor disk is still important. Therefore, tail rotor module can be evaluated as a simplified version of the main rotor mathematical model.

Induced velocity distribution prediction of the tail rotor is divided into two parts. The total freestream velocity including platform's translational velocities and relative velocities because of platform's rotational velocities, are calculated at tail rotor hub in tail rotor reference frame system. If the total tangential air velocity calculated at tail rotor hub, is zero, which corresponds to hover or axial flight conditions, then Prandtl's tip loss function combined with momentum theory is used for inflow prediction. On the other hand, if the total tangential air velocity that tail rotor hub encounters is not equal to zero, which corresponds to a forward flight condition, then Drees Linear Inflow model is used in order to determine the non-symmetric inflow distribution over the rotor disk. The inflow distribution over the rotor disk is then used to determine the aerodynamic force and moments generated by each blade element.

The integrator model inside the tail rotor module integrates the aerodynamic force and moments of each blade element along the rotor blade in order to determine total force and moments transferred to the tail rotor hub by each blade at each azimuth step. Azimuthal distribution of total force and moments of each blade is averaged and the net force and moments generated by the tail rotor and transferred to the tail rotor hub is derived.

Fuselage Module

Fuselage is modeled as a solid body with center of gravity coincident with center of gravity of the whole system. Fuselage's inertial forces are calculated directly at the mass center. On the other hand, aerodynamic forces are calculated at aerodynamic center which is by default taken to be coincident with center of gravity. However, if desired aerodynamic offset may be included in the mathematical model. Aerodynamic force and moments are determined by simple aerodynamic relations

where three force and three moment coefficients are determined from look-up table method. A table containing aerodynamic force and moment coefficients which depend on angle of attack and sideslip angles is introduced into the mathematical model. Local total velocity components are calculated by taking helicopter translational motion and main rotor downwash effect into account. Aerodynamic coefficients and dynamic pressure are used to determine total aerodynamic force and moments generated by the fuselage.

Horizontal tail module

Aerodynamic force and moments that are generated by the horizontal tail are firstly determined in horizontal tail aerodynamic center in horizontal tail reference frame which is normally coincident with the body reference frame system. Then they are transferred to the helicopter center of gravity in order to determine the force and moment contribution to the whole system. The aerodynamic force and moments generated by the horizontal tail are directly calculated from simple aerodynamic relations. The aerodynamic force and moment coefficients are determined by look-up table method where horizontal tail profile lift, drag and moment coefficients are inputted to the mathematical model in a table depending on angle of attack and local Mach number. The components of total velocity are calculated from helicopter translational motion, rotational motion which generates relative freestream velocity on horizontal tail and main rotor downwash effect. Angle of attack that horizontal tail encounters are then determined from trigonometric relations. The total velocity components that horizontal tail encounters are also used to determine local Mach number.

Vertical tail module

Vertical tail force and moment contributions to the system are calculated with exactly the same method used for horizontal tail except aerodynamic coefficient tables are inputted according to vertical tail profile.

Validation

Validation of the developed mathematical model is done with both flight test data and comprehensive analysis tools such as Flightlab and Camrad. Trim solution is validated with Flightlab where a helicopter model at same fidelity and accuracy are built in both Flightlab and the mathematical model developed. Then for various flight conditions, the trim solutions determined by both tools are compared. On the other hand, the main rotor aerodynamic module, which is considered the most important and dominant component of a helicopter mathematical model, is validated with both flight test data of various helicopters and comprehensive analysis tools such as Flightlab and CAMRAD.

One of the main rotor mathematical model validations is done with Westland Wessex helicopter using flight test data at hover flight conditions. Thrust coefficient versus torque coefficient at various collective angles are analyzed and compared with the flight test data [37]. The results seem consistent with flight test data. Then the effect of radial blade element number on accuracy is investigated using the same configuration and test data. Analyses are done with various blade element numbers and it is found that, analyses with 20 blade elements result in optimum solutions in both computation cost and accuracy aspects.

Another main rotor mathematical model validation is done with OH-58 helicopter. Power coefficient change with thrust coefficient for hover flight conditions are investigated at various collective inputs. Results determined with the mathematical model developed are compared with the flight data of OH-58 [66]. It is found that analysis results are consistent with flight test data. Then blade radial

sectional thrust distribution determined by the mathematical model developed is compared again with the flight test data at hover flight. In addition to hover flight analyses, power coefficient change with thrust coefficient at forward flight conditions are investigated. At various forward flight speeds and collective inputs, power and thrust coefficient values are compared with flight data. Both radial thrust distribution at hover flight condition and power and thrust coefficient values calculated at various advance ratios and collective inputs determined by the mathematical model developed are evaluated as consistent with flight test data.

In addition to validations with flight test data, the mathematical model is validated with helicopter comprehensive analysis and simulation tools also. SA 349/Gazalle helicopter is both modeled with CAMRAD/JA and the mathematical model developed in this study. Analyses for forward flight conditions at higher advance ratios than 0.25 are conducted and results are compared. Thrust and torque values at various advance ratios are determined by both tools and compared. The results showed good agreement with each other except at high forward speed. Results until 0.3 advance ratios show good agreement whereas the results at higher advance ratios show differences. In addition, effective angle of attack distributions over the rotor disk at various forward flight conditions are compared. Effective angle of attack distribution over both radial and azimuthal direction determined by both tools showed good agreement with each other.

Another validation study was done with FLIGHTLAB using UH-60 helicopter. Main rotor of UH-60 was modeled with both Flightlab and the mathematical model developed. Analyses were done on various forward flight conditions and results were compared. Both vortex theory and dynamic inflow models are used in Flightlab models in order to study the effect of different inflow models on accuracy and inflow distribution. Torque coefficient change with changing forward velocity determined by both tools are compared. As being at same fidelities, results of Flightlab model with vortex theory and the mathematical model developed showed good agreement. In addition, lift coefficient distributions on both radial and azimuthal directions at various forward velocities are compared. Results showed consistency while differences appear between different inflow models.

Trim model validation on the other hand is done with only Flightlab model as both tools require similar helicopter and rotor parameters in order to determine the trim solution. Besides, the selective and modular structures of both tools enable to build helicopter models at similar fidelity and accuracy. Same helicopter model is built with both Flightlab and the developed mathematical model. The helicopter modeled is basically Mosquito XE helicopter however with simplified parameters. Trim solution at different forward velocities and hover flight conditions are determined and compared. Pilot collective, longitudinal, lateral and pedal control inputs as well as helicopter attitudes are determined at trim conditions and compared. Results are evaluated as highly consistent.

In addition to validation studies, a time based simulation is also done in order to investigate helicopter dynamic response to various pilot control inputs. BO 105 helicopter is modeled with the developed mathematical model and trimmed at hover flight condition. Time based simulation is done for five seconds and it is found that helicopter remains at its steady flight condition. As being at trimmed flight conditions, the trim model validated itself. Besides, a pilot collective step input was given to the helicopter while at hover flight condition and dynamic response of the helicopter to the input was investigated. Results evaluated as reasonable.

8.2 Conclusion

In conclusion, a mathematical helicopter model is developed throughout this study which can be used in aerodynamic load analysis; trim solution analysis and flight dynamic analysis activities. The main rotor aerodynamic and dynamic models are validated with both flight test data and comprehensive helicopter analysis tools. It is evaluated that, the developed mathematical model predicts the main rotor aerodynamic characteristics, such as aerodynamic load distributions, wake geometries, wake induced velocity distributions over the rotor disk, and helicopter dynamic responses such as trimmed flight conditions at both hover and forward flight successfully when compared with flight test data and comprehensive analysis tools.

The developed mathematical model outputs the aerodynamic load distribution over the rotor disc if desired, which is defined with an example at Appendix C. The ability of determining the aerodynamic load distribution over the rotor disc brings the advantage over CAMRAD/JA and FLIGHTLAB where aerodynamic load distribution over the rotor disc is defined with non-dimensional force coefficients. Without any additional operation on the outputs, such as making the force coefficient dimensional, aerodynamic force and moment distributions over the rotor disc may be directly investigated from the outputs of the developed mathematical model. Besides, total root aerodynamic force and moments generated by each blade at each azimuth angle are also defined as an output of the mathematical model. This again brings an advantage; over CAMRAD/JA and FLIGHTLAB where additional routines are required to integrate the radial force and moment distributions along the blade in order to determine total aerodynamic force and moments generated by each blade at blade root. Aerodynamic load distribution or blade total force and moments generated at blade root output abilities of the developed mathematical model [Appendix C] shows its importance mostly at preliminary blade design stages. Maximum and minimum loads that blades encounter at several flight conditions and maneuvers are at highest interest at preliminary blade geometrical or structural design stages. Instead of using computational fluid dynamics methods which would take days to solve for even one flight condition, several analyses may be conducted with the developed mathematical model within minutes.

The inflow models implemented into the mathematical model are compared with each other [Appendix C] and from the results it is evaluated that except from the near tip locations along the blade the aerodynamic loads determined by each inflow model show good agreement with each other. Besides rotor total thrust and torque values calculated with each inflow model results in similar values. As the tip losses, peaks of induced velocity near tips and stall region at the retreating side are the critical aspects that affect the rotor performance the inflow model desired to be used shall be selected thoughtfully. On the other hand, as the rotor force and moments determined by lower fidelity models are approximately same with the higher fidelity models, for flight dynamics activities such as handling quality investigations or maneuver simulations, they are evaluated to be appropriate to use.

Throughout the study, it is evaluated that good inputs to the mathematical model results in good outputs while bad inputs results in worse outputs. Modeling a helicopter or a helicopter rotor requires several model selections such as inflow models, wake models or blade dynamic models. Each model requires its own specific input parameters which are also specific to each helicopter. Besides some implemented inflow or wake models requires parameters that has to be determined by flight test or with engineering sense. Therefore, the modeling input parameters shall be selected thoughtfully and carefully.

Throughout the study, it is evaluated that modeling of a helicopter or a helicopter rotor only requires tradeoff decisions to be made between accuracy, fidelity, complexity and computational cost. It is evaluated that as the accuracy and fidelity of the model increases, the computational effort and complexity increases. Therefore, according to the aim of the usage of the mathematical model, the tradeoff decisions shall be made thoughtfully. For example lower fidelity models shall be used for flight dynamic activities such as simulations or trim solution whereas higher fidelity and computationally expensive models shall be used for detail analyses such as blade critical load investigations or aerodynamic load distribution analyses over the rotor disc.

For helicopter simulations, lower fidelity aerodynamic models are appropriate to use as the computational cost for them are much lower. However, if a flight simulation with higher fidelity aerodynamic model such as vortex theory is desired to be done, then the mathematical model shall be improved in a way that the computational cost decreases. This is planned as a future work and mentioned in detail in future plans chapter. Besides, simulation validation which is also planned as future work, with flight test data and comprehensive simulation tools shall be done.

The developed mathematical model assumes the blades as rigid therefore no structural model has implemented into it. With the rigid blade assumption, structural load coming from blade elastic deformation drops. The rigid blade assumption results in deviation from real case. However, the modular structure of the model enables development and improvement on any desired module. Therefore implementation of an elastic blade model is possible. Besides, the modular structure enables user to use any module individually. For example the main rotor

aerodynamic module developed throughout the study has been used in a study which mainly concentrates on elastic blades [68]. The structural model is coupled with the aerodynamic model developed and a rotor with elastic blades is defined mathematically.

CHAPTER 9

FUTURE WORKS

In order to further develop or improve the mathematical model, some future works are planned. One of the future works planned during this study is to decrease the computational cost of the trim solution calculation. A way, similar to the one used in CAMRAD [14, 15], which is to exclude the wake geometry and influence coefficient matrix calculation from the trim model, is planned. As being the most computationally expensive part of the aerodynamic model for main rotor, prediction of the wake geometry and influence matrix at each trim iteration step, increases the total computation time dramatically. Besides, the change in the wake geometry and influence matrix with the change in the aerodynamic loads at each iteration step may be neglected for flight dynamics activities [14, 15]. Therefore, with an initial approximate aerodynamic model of the main rotor, an approximate wake geometry and influence coefficient matrix may be derived and used for all iterations of the trim model. This procedure approximately decreases the trim solution derivation of helicopter nearly 50-60 times.

Another future work planned is to linearize the nonlinear mathematical model developed so that whole system works with much less computational effort. This would enable to design a controller which would make the simulations more meaningful. A PID or PID combined with LQR controller is planned to be designed as future work. As a result, with linearized model and with the help of the controller, real time simulations using the mathematical model developed would be possible.

Implementation of the hub types except from the articulated are planned as future works for this study. With addition of an elastic blade model which would model the blades elastically and takes the blade elastic deformations under any loading into account, hingeless and bearingless hub types would be available to be

implemented. For teetering hub type, some modifications on the articulated hub type is possible that would lead a model of a teetering hub and is left as future work of this study.

Another future study that is planned is to model the aerodynamic damping that blades encounter at any flight condition. The aerodynamic damping is planned to be implemented as a spring & damper system at the blade roots.

REFERENCES

1. Cvetkovic, D., Kostic, I., Mitrovic, C., Bengin, A., and Radakovic, D., "*Numerical Model of Single Main Rotor Helicopter Dynamics*", Proceedings of the 23rd International Congress of Aeronautical Sciences, Toronto, Canada, September 2002.
2. Johnson, W., "*Helicopter Theory*", Dover Publications, New York, 1994.
3. Talbot, P. D., Tinling, B. E., Decker, W. A., and Chen, R. T. N., "*A Mathematical Model of a Single Main Rotor Helicopter for Piloted Simulation*", NASA Technical Memorandum 84281, September 1982.
4. Salazar T., "*Mathematical Model and Simulation for a Helicopter with Tail Rotor*", Proceedings of the 9th WSEAS International Conference on Computational Intelligence, Man-Machine Systems and Cybernetics, Merida, Venezuela, December 2010, pp.27-32.
5. Takahashi, M. D., "*A Flight Dynamic Helicopter Mathematical Model with a Single Flap-Lag-Torsion Main Rotor*", NASA Technical Memorandum 102267, February 1990.
6. Heffley, R. K., and Mnich, M. A., "*Minimum Complexity Helicopter Simulation Math Model*", NASA Contractor Report 177476, April 1988.
7. Hilbert K. B., "*A Mathematical Model of the UH-60 Helicopter*", NASA Technical Memorandum, 85890, April 1984.
8. Yılmaz D., "*Evaluation and Comparison of Helicopter Simulation Models with Different Fidelities*", Master's thesis, Middle East Technical University, Ankara, July 2008.
9. Munzinger C., "*Development of a Real-Time Flight Simulator for an Experimental Model Helicopter*", Diploma thesis, Georgia Institute of Technology, Atlanta, December 1998.

10. Vigan'o L., Magnani, G., "*Acausal Modelling of Helicopter Dynamics for Automatic Flight Control Applications*", Proceedings of the 5th International Modelica Conference, Vienna, Austria, September 2006, pp.377-384.

11. Hald, U. B., Hesselbæk M. V., Holmgaard, J. T., Jensen, C. S., Jakobsen, S. L., Siegumfeldt, M., "*Autonomous Helicopter-Modelling and Control*", Report, Aalborg University, 2005.

12. Kim, S. K., Tilbury, D. M., "*Mathematical Modeling and Experimental Identification of a Model Helicopter*", AIAA Paper 98-4357, 1998.

13. Advanced Rotorcraft Technology Inc., "*FLIGHTLAB Theory Manual*", Mountain View, California, USA, July 2008.

14. Johnson W., "*A Comprehensive Analytical Model of Rotorcraft Aerodynamics and Dynamics, CAMRAD/JA*", Theory Manual Volume I, 1988.

15. Johnson W., "*A Comprehensive Analytical Model of Rotorcraft Aerodynamics and Dynamics, CAMRAD/JA*", Theory Manual Volume II, 1988.

16. Wheatley, John B., "*An Aerodynamic Analysis of the Autogyro Rotor with a Comparison between Calculated and Experimental Results*", Report, National Advisory Committee Aeronautics, No. 487, 1934.

17. Glauert, H., "*A General Theory of the Autogyro*", Aeronautical Research Council Report and Memorandum, No.1111, November 1926.

18. Drees, J. M. Jr., "*A Theory of Airflow through Rotors and its Application to Some Helicopter Problems*", Helicopter Association Great Britain, Vol. 3, No.2, July-September 1949.

19. Leishman, J. G., "*Principles of Helicopter Aerodynamics*", Cambridge University Press, New York, 2006.

20. Spera, D., A., "*Wind Turbine Technology – Fundamental Concepts of Wind Turbine Engineering*", ASME Press, New York, 1994.

21. Milgram, J., Chopra, I., Straub, F., "A Comprehensive Rotorcraft Aeroelastic Analysis with Trailing Edge Flap Model: Validation with Experimental Data", Proceedings of American Helicopter Society 52nd Annual Forum, Washington, D.C., June 1996.

22. Gennaretti, M., Colella M. M., and Bernardini, G., "Analysis of Helicopter Vibratory Hub Loads Alleviation by Cyclic Trailing-Edge Blade Flap Actuation", The Aeronautical Journal, Vol: 113, No:1146, August 2009.

23. Bir, G. S., Chopra, I., Ganguli, R., Ganguli, R., Smith, E. C., Vellaichamy, S., Wang, J., Kim, K. C., Chan, W. Y., Nixon, M. W., Kimata, N. W., Smith, J. A., Torok, M., and Nguyen, K. Q., "University of Maryland Advanced Rotorcraft Code (UMARC)," Theory Manual, Center for Rotorcraft Education and Research, University of Maryland, College Park, MD, July 1994.

24. Johnson, W., "NDARC — NASA Design and Analysis of Rotorcraft Theoretical Basis and Architecture", American Helicopter Society Aeromechanics Specialists' Conference, San Francisco, CA, January 2010.

25. Masarati, P., "MBDyn Theory and Developer's Manual Version 1.X-Devel", Manual, Dipartimento di Ingegneria Aerospaziale, May 2010.

26. Bramwell, A., R., S., Done, G., T., S., Balmford, D., *Bramwell's Helicopter Dynamics*", American Institute of Aeronautics, 2nd edition, 2001.

27. Chen, R. T. N., "A Survey of Nonuniform Inflow Models for Rotorcraft Flight Dynamics and Control Applications", NASA Technical Memorandum 102219, November 1989.

28. Yücekayalı, A., Ortakaya, Y., "Girdap Teorisi ve Pal Elemanları Metodu ile Helikopter Rotorunun Aerodinamik Modellenmesi", Proceedings of III. Ulusal Havacılık ve Uzay Konferansı, Eskişehir, September 2010.

29. Huh, K., "Helicopter Rotor Blade Loading Calculations Using an Axisymmetric Vortex Sheet and the Free Wake Method", Master's Thesis, Massachusetts Institute of Technology, January 1988.

30. Liu, H., "Interfacing Comprehensive Rotorcraft Analysis with Advanced Aeromechanics and Vortex Wake Models", Ph.D. Dissertation, Georgia Institute of Technology, Atlanta, April 2008.

31. Theodore, C. R., "*Helicopter Flight Dynamics Simulation with Refined Aerodynamic Modeling*", Ph.D. Dissertation, University of Maryland, College Park, 2000.

32. Reddy, K. R. and Stewart, C. J., "*Simulation, a valuable tool in the estimation of helicopter flight dynamic characteristics*", Proceedings of the 18th World IMACS/MODSIM Congress, Cairns, Australia, July 2009.

33. Glässel, H., Kahl, J., Dieterich, O., and Rudolph, S., "*Neural Networks for BVI System Identification*", Proceedings of the 29th European Rotorcraft Forum, Friedrichshafen, September 2003.

34. Ramasamy, M., Gold, N. P., and Bhagwat, M. J., "*Rotor Hover Performance and Flowfield Measurements with Untwisted and Highly-twisted Blades*", Proceedings of the 36th European Rotorcraft Forum, Paris, France, September 2010.

35. Castles, W., De Leeuw, J. H., "*The Normal Component of the Induced Velocity in the Vicinity of a Lifting Rotor and Some Examples of Its Application*", NACA Technical Note 2912, March 1953.

36. Anderson, J., D., Jr., "*Fundamentals of Aerodynamics*", McGraw-Hill Series in Aeronautical and Aerospace Engineering, 2001.

37. Young, C., "*The Prediction of Helicopter Rotor Hover Performance using a Prescribed Wake Analysis*", Aeronautical Research Council Paper, C.P. No.1341, 1976.

38. Ramasamy, M., Johnson, B., Leishman, J. G., "*Toward Understanding the Aerodynamic Efficiency of a Hovering Micro-Rotor*", Proceedings of American Helicopter Society International Specialists Meeting on Unmanned Rotorcraft, Phoenix, AZ, January 2007.

39. Mahalingam R., Komerath N., "Measurements of the Near Wake of a Rotor in Forward Flight", AIAA 98-0692.

40. Wong, O., Mahalingam, R., Tongchitpakdee, C., and Komerath, N. M., "*The Near Wake of a 2 Bladed Rotor in Forward Flight*", Proceedings of American

Helicopter Society Aeromechanics Specialists Meeting, Atlanta, Georgia, November 2000.

41. Chen, R. T. N., "A Simplified Rotor System Mathematical Model for Piloted Flight Dynamics Simulation", NASA Technical Memorandum 78575, May, 1979.
42. Prouty, R., W., "Helicopter Aerodynamics", Eagle Eye Solutions, Lebanon, OH, 2009.
43. Prouty, R., W., "Helicopter Performance, Stability and Control", Krieger Publications, 1995.
44. Chen, R. T. N., "Effects of Primary Rotor Parameters on Flapping Dynamics", NASA Technical Paper 1431, January 1980.
45. Talbot, P. D., Corliss, L. D., "A Mathematical Force and Moment Model of a UH-1H Helicopter for Flight Dynamics Simulations", NASA Technical Memorandum 73254, June 1977.
46. Padfield, G. D., "Helicopter Flight Dynamics: The Theory and Application of Flying Qualities and Simulation Modeling," AIAA Education Series, 1996.
47. Peters, D. A., Boyd, D. D., He, C. J., "Finite-State Induced-Flow Model for Rotors in Hover and Forward Flight", Proceedings of the 43rd Annual Forum of the American Helicopter Society, St.Louis, Mo., May 1987.
48. Peters D.A., He C.J., "Correlation of Measured Induced Velocities with a Finite State Wake Model", 45th Annual National Forum of the American Helicopter Society, Boston, Mass., May 1989.
49. Peters D.A., He C.J., "Finite State Induced Flow Models Part II: Three-Dimensional Rotor Disk", Journal of Aircraft, Vol. 32, No. 2, March-April 1995.
50. Yavrucuk I., Tarimci O., Katircioglu M., Kubali E., Yilmaz D., "A New Helicopter Simulation and Analysis Tool: Helidyn+", www.aerotim.com.tr, 2011.

51. Krothapalli, K. R., Peters, D.A., “*Study of a Rotor Flap-Inflow Model Including Wake Distortion Terms*”, *Proceedings of RTO SCI Symposium on “System Identification for Integrated Aircraft Development and Flight Testing*”, Madrid, Spain, May 1998.

52. Trchalik, J., “*Aeroelastic Modelling of Gyroplane Rotors*”, Ph.D. Dissertation, University of Glasgow, Glasgow, July 2009

53. Landgrebe A .J., “*An Analytical method for predicting rotor wake geometry*”, *American Helicopter Society Journal*, Vol:14, No:4, 1969, pp. 20-32.

54. Egolf, T. A., Landgrebe, A. J., “*A Prescribed Wake Rotor Inflow and Flow Field Prediction Analysis – User’s Manual and Technical Approach*”, NASA Contractor Report 165894, June 1982.

55. Young, L. A., “*Vortex Core Size in the Rotor Near-Wake*”, NASA Technical Memorandum 2003-212275, June 2003.

56. Prouty, R. W., “*Part I: A Second Approximation to the Induced Drag of a Helicopter Rotor in Forward Flight, Part II: The instantaneous Induced Velocity at the Blade of a Finite-Bladed Rotor in Forward Flight*”, Diploma Thesis, California Institute of Technology, Pasadena, California, 1958.

57. Beddoes, T. S., “*A Wake Model for High Resolution Airloads*,” *Proceedings of 2nd International Conference on Basic Rotorcraft Research*, Research Triangle Park, North Carolina, 1985.

58. Lee, J., Yee, K., Oh, S., Kim, D. H., “*Development of an Unsteady Aerodynamic Analysis Module for Rotor Comprehensive Analysis Code*”, *International Journal of Aeronautical & Space Sciences*, Vol. 10, No.2, November 2009, pp. 23-33.

59. Szymendera, C. J., “*Computational Free Wake Analysis of a Helicopter Rotor*”, Master’s Thesis, Pennsylvania State University, Pennsylvania, May 2002.

60. Beedy, J., “*Summary of Beddoes/WHL Aerodynamic Model*”, *Aerospace Engineering Report 0207*, University of Glasgow, United Kingdom, March 2004.

61. Sankar, N. L., "*Computational Studies of Horizontal Axis Wind Turbines*", Quarterly Progress Report submitted to National Renewable Energy Laboratory, Atlanta, June 2001.
62. Klesa, J., "*Increasing of Aircraft Propeller Efficiency by Using Variable Twist Propeller Blades*", Proceedings of the Students' Conference of Czech Technical University, Dubna, 2008.
63. Todorov, M., "Aeroelastic Modelling of Hingeless Helicopter Blade in Forward Flight", International Virtual Journal for Science, Technics and Innovations for the Industry, Vol: 5, Issue: 1, 2011, pp. 26-31.
64. Shen, W.Z., Hansen, M.O.L., Sorensen, J.N., "Determination of the angle of attack on rotor blades." Wind Energy, Vol:12, Issue:1, January 2009, pp. 91-98.
65. Peters, D.A. and Izadpanah, A.P., "Helicopter trim by periodic shooting with Newton-Raphson iteration". Proceedings of the 37th Annual Forum of the American Helicopter Society, AHS International, New Orleans
66. Hoffrichter, J., S., "*OH-58 Composite Main Rotor Blade Preliminary Design Investigation*", BOEING VERTOL CO., PHILADELPHIA, 1978.
67. Heffernan, R., M., Gaubert, M., "*Structural and Aerodynamic Loads and Performance Measurements of an SA349/2 Helicopter with an Advanced Geometry Rotor*", NASA Technical Memorandum 88370, 1986
68. Tamer, A., Şen, S., Yücekayalı, A., Ortakaya, Y., "*Helikopter Rotoru Aerodinamik ve Yük Analizleri İçin Pal Aeroelastik Çırpma Modelinin Geliştirilmesi*", Proceedings of III. Ulusal Havacılık ve Uzay Konferansı, Eskisehir, September 2010.
69. Donald, D., "*The Complete Encyclopedia of World Aircraft*", 1997
70. Munson, K., "*Helicopters and Other Rotorcraft Since 1907*", 1968

71. Evolution Graphics, "*Sikorsky UH-60 Blackhawk*", www.theblueprints.com/blueprints/modernplanes/helicopters-n-z/22996/view/uh-60_blackhawk, 17/08/2011
72. Jackson, R., "*Helicopters: Military, Civilian, and Rescue Rotorcraft*", Thunder Bay Press, October 2005
73. Evolution Graphics, "*Aerospatiale Gazalle*", www.theblueprints.com/blueprints/helicopters/aerospatiale/23626/view/aerospatiale_gazelle/, 17/08/2011
74. Mosquito Aviation LTD., "*Mosquito XE*", www.innovator.mosquito.net.nz, 17/08/2011

APPENDIX A

TRANSFORMATIONS BETWEEN DIFFERENT REFERENCE FRAMES

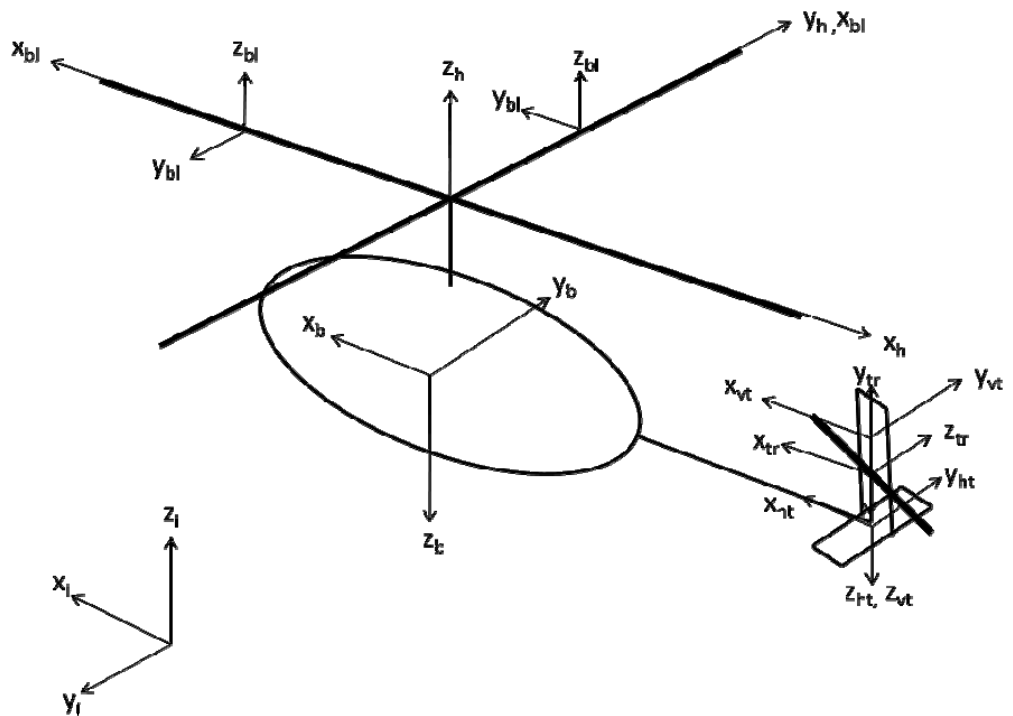


Figure A-1 Coordinate systems used in the developed mathematical model

Subscripts

X_i = coordinate system in inertial reference frame

X_b = coordinate system in helicopter body reference frame

X_h = coordinate system in main rotor hub reference frame

X_{bl} = coordinate system in main rotor blade reference frame

X_{tr} = coordinate system in tail rotor hub reference frame

X_{ht} = coordinate system in horizontal tail reference frame

X_{vt} = coordinate system in vertical tail reference frame

Inertial to Body Reference Frame Transformation Matrix

In order to transform parameters from inertial reference frame to body reference frame 3 rotations on 3 axes are done. For convenience the rotations are φ (roll angle) about body x axis, θ (pitch angle) about body y axis and ψ (yaw angle) about body z axis, Figure A-2. For each angle rotation, a transformation matrix is derived then these transformation matrices are multiplied in order to derive the full transformation matrix from inertial reference frame components to body reference frame components.

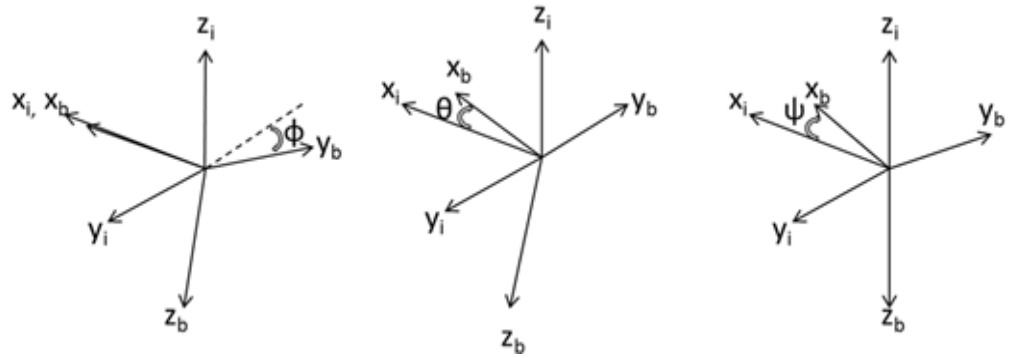


Figure A-2 Transformation between inertial and body reference frame systems

x transformation

$$L_{\phi} = \begin{vmatrix} 1 & 0 & 0 \\ 0 & -\cos\phi & -\sin\phi \\ 0 & \sin\phi & -\cos\phi \end{vmatrix}$$

(A-1)

y transformation

$$L_{\theta} = \begin{vmatrix} \cos\theta & 0 & \sin\theta \\ 0 & -1 & 0 \\ \sin\theta & 0 & -\cos\theta \end{vmatrix}$$

(A-2)

z transformation

$$L_\varphi = \begin{bmatrix} \cos\varphi & -\sin\varphi & 0 \\ -\sin\varphi & -\cos\varphi & 0 \\ 0 & 0 & -1 \end{bmatrix}$$

(A-3)

Full transformation matrix;

$$L_{BI} = L_\varphi L_\theta L_\phi = \begin{bmatrix} 1 & 0 & 0 \\ 0 & -\cos\phi & -\sin\phi \\ 0 & \sin\phi & -\cos\phi \end{bmatrix} \begin{bmatrix} \cos\theta & 0 & \sin\theta \\ 0 & -1 & 0 \\ \sin\theta & 0 & -\cos\theta \end{bmatrix} \begin{bmatrix} \cos\varphi & -\sin\varphi & 0 \\ -\sin\varphi & -\cos\varphi & 0 \\ 0 & 0 & -1 \end{bmatrix}$$

(A-4)

$$L_{BI} \rightarrow \begin{bmatrix} x_B \\ y_B \\ z_B \end{bmatrix} = \begin{bmatrix} \cos\theta\cos\varphi & -\cos\theta\sin\varphi & -\sin\theta \\ -\sin\phi\sin\theta\cos\varphi - \cos\phi\sin\varphi & \sin\phi\sin\theta\sin\varphi - \cos\phi\cos\varphi & -\sin\phi\cos\theta \\ -\cos\phi\sin\theta\cos\varphi + \sin\phi\sin\varphi & \cos\phi\sin\theta\sin\varphi + \sin\phi\cos\varphi & -\cos\phi\cos\theta \end{bmatrix} \begin{bmatrix} x_I \\ y_I \\ z_I \end{bmatrix}$$

(A-5)

Wind Axis to Body Reference Frame Transformation Matrix

Full transformation matrix [26];

$$L_{BW} \rightarrow \begin{bmatrix} x_B \\ y_B \\ z_B \end{bmatrix} = \begin{bmatrix} \cos\alpha\cos\beta & -\cos\alpha\sin\beta & -\sin\alpha \\ \sin\beta & \cos\beta & 0 \\ \sin\alpha\cos\beta & -\sin\alpha\sin\beta & \cos\alpha \end{bmatrix} \begin{bmatrix} x_W \\ y_W \\ z_W \end{bmatrix}$$

(A-6)

Hub to Body Reference Frame Transformation Matrix

$$L_{BH} \rightarrow \begin{bmatrix} x_B \\ y_B \\ z_B \end{bmatrix} = \begin{bmatrix} -\cos\alpha_{shaft} & 0 & -\sin\alpha_{shaft} \\ 0 & 1 & 0 \\ \sin\alpha_{shaft} & 0 & -\cos\alpha_{shaft} \end{bmatrix} \begin{bmatrix} x_H \\ y_H \\ z_H \end{bmatrix}$$

(A-7)

Blade to Hub Reference Frame Transformation Matrix

$$L_{HBL} \rightarrow \begin{bmatrix} x_H \\ y_H \\ z_H \end{bmatrix} = \begin{bmatrix} \cos\varphi & -\sin\varphi & 0 \\ \sin\varphi & \cos\varphi & 0 \\ 0 & 0 & 1 \end{bmatrix} \begin{bmatrix} x_{BL} \\ y_{BL} \\ z_{BL} \end{bmatrix}$$

(A-8)

Blade reference to blade Frame Transformation Matrix

$$L_{BL \leftarrow B_{ref}} \rightarrow \begin{bmatrix} x_{BL} \\ y_{BL} \\ z_{BL} \end{bmatrix} = \begin{bmatrix} \cos\beta & 0 & -\sin\beta \\ -\sin\alpha\sin\beta & \cos\alpha & -\sin\alpha\cos\beta \\ \sin\alpha\sin\beta & \sin\alpha & \cos\alpha\cos\beta \end{bmatrix} \begin{bmatrix} x_{B_{ref}} \\ y_{B_{ref}} \\ z_{B_{ref}} \end{bmatrix}$$

(A-9)

Tail rotor to body reference frame Transformation Matrix

$$L_{BTR} \rightarrow \begin{bmatrix} x_B \\ y_B \\ z_B \end{bmatrix} = \begin{bmatrix} 1 & 0 & 0 \\ 0 & 0 & 1 \\ 0 & -1 & 0 \end{bmatrix} \begin{bmatrix} x_{TR} \\ y_{TR} \\ z_{TR} \end{bmatrix}$$

(A-10)

APPENDIX B

ALTERNATIVE METHOD FOR BLADE FLAPPING MODEL

This section describes two alternative ways to determine main rotor blade flapping angle at any flight condition. First method may be seemed as the simplest blade flapping angle model as it only takes gravitational, centrifugal and aerodynamic forces into account. The second method is the flapping equations derived by Wayne J. [2].

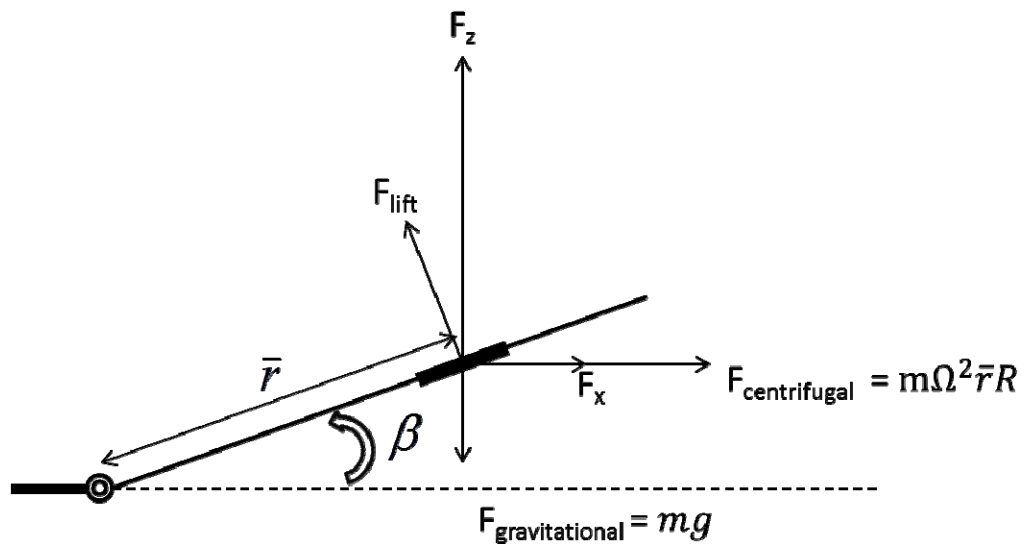


Figure B-1 Blade element force equilibrium

The first method is described by the equation (B-1), where the first term is inertial acceleration, second is the centrifugal force and the third is the resultant z force of each individual blade element for which resultant is determined by superposing gravitational and aerodynamic forces together. The flapping equilibrium equation is described at each azimuth angle and solved for each azimuth angle.

$$\int_0^R mr\ddot{\beta}rdr + \int_0^R m\Omega^2r(r\beta)dr - \int_0^R F_zrdr = 0 \quad (\text{B-1})$$

The second method for blade flap angles is derived by Wayne J. [2] with uniform inflow and linear twist assumptions. The integration over blade span and azimuth angle are included in the flapping equations therefore there is no need to solve the equations at each azimuth angle but once.

$$\beta_{1c} + \theta_{1s} = \frac{(8/3)\mu[\theta_{.75} - (3/4)\lambda_{TPP}]}{1 + (3/2)\mu^2} \quad (\text{B-2})$$

$$\beta_0 = \gamma \left[\frac{\theta_{.75}}{8} (1 + \mu^2) - \frac{\mu^2}{60} \theta_{tw} - \frac{\lambda_{TPP}}{6} + \frac{\mu}{6} (\beta_{1c} + \theta_{1s}) \right] \quad (\text{B-3})$$

$$\beta_{1s} - \theta_{1c} = \frac{-(4/3)\mu\beta_0}{1 + (1/2)\mu^2} \quad (\text{B-4})$$

APPENDIX C

MAIN ROTOR AERODYNAMIC ANALYSIS FOR WESSEX

In this section, inflow distributions over the rotor disk are determined by each inflow model implemented into the mathematical model are compared. Then aerodynamic lift distribution over the rotor disc at various forward flight speeds and control angles are determined and given. Inflow comparison analyses are conducted at 30 m/s forward flight speed with Westland Wessex helicopter rotor and inflow distributions over the rotor disk are compared. On the other hand aerodynamic lift distribution analyses are conducted at hover and various forward flight speeds. Although Westland Wessex helicopter main rotor parameters are given at Wessex Validation chapter and it is repeated at Table 10 for convenience.

Table 10 Westland Wessex helicopter main rotor parameters

Main Rotor Parameters	
Number of Blades	4
Rotor radius (m)	8.53
Blade Root Cut-Out (%)	16
Chord Length (m)	0.417
Tip speed (m/s)	205
Rotor RPM	229.6
Flapping Hinge Position (%)	3.5
Precone Angle (deg)	0
Blade Twist (deg)	-8
Shaft Tilt (deg)	0
Blade Profile	NACA 0012

Load distributions over the rotor disk are determined by Drees linear, Mangler & Squires non-linear inflow models and vortex wake theory at 30 m/s forward flight and compared at Figure and Figure .

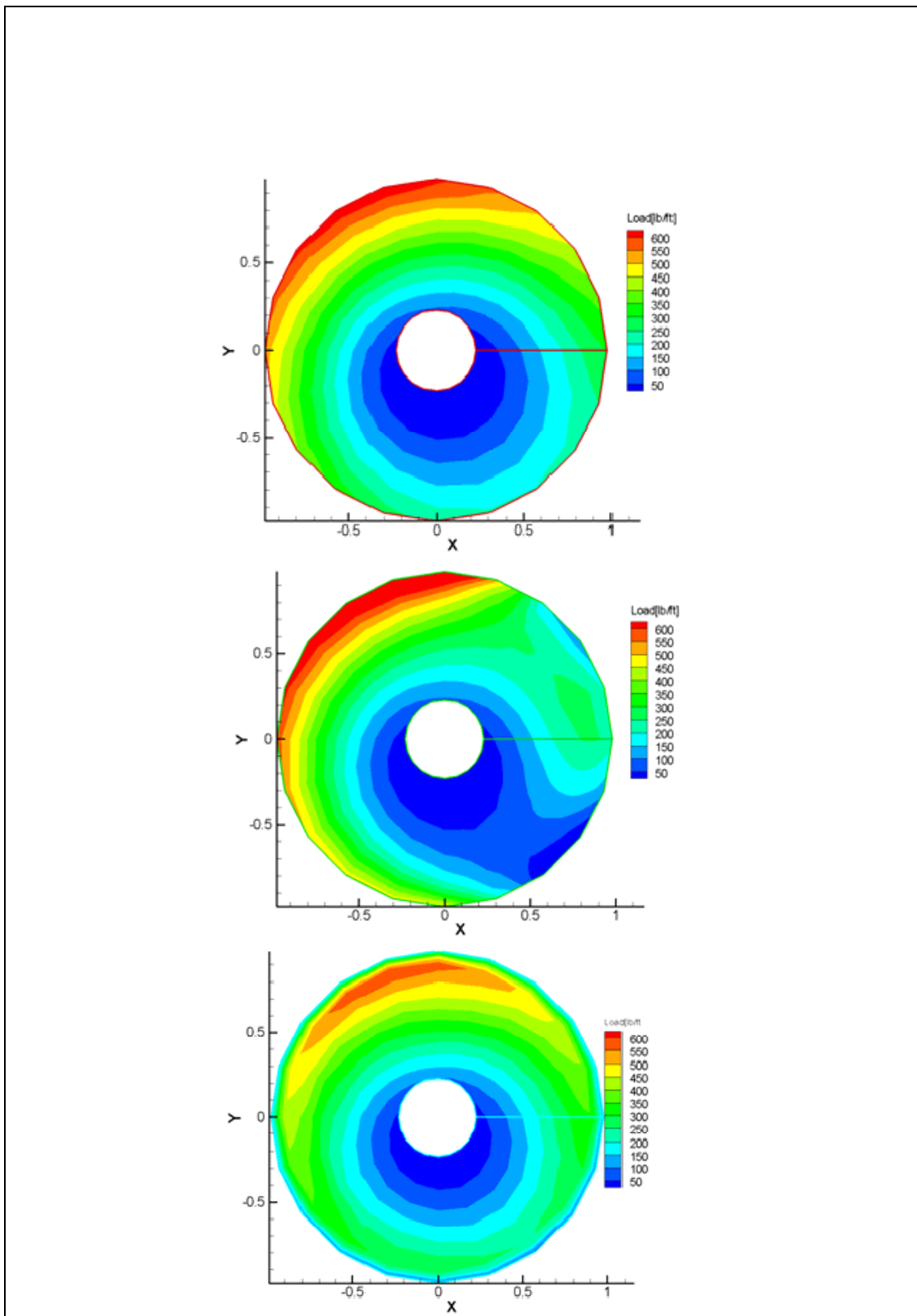


Figure C-1 Load distribution over the rotor disk [28] (Drees, Mangler & Squire and Vortex Wake)

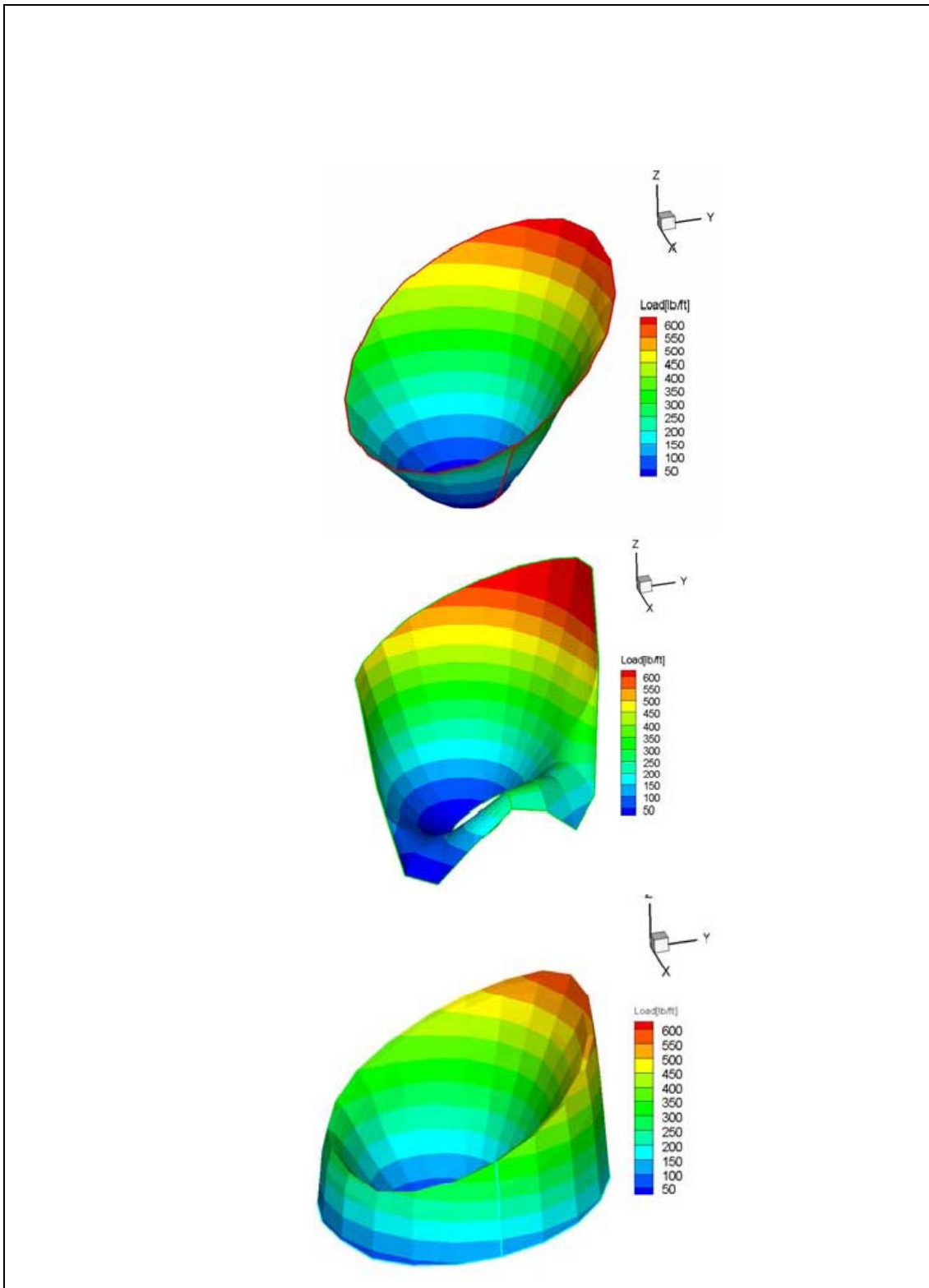


Figure C-2 Load distribution over the rotor disk [28] (Drees, Mangler & Squire and Vortex Wake)

From the load distribution results, it is evaluated that the tip losses could only be modeled with vortex wake theory. Besides, the order of magnitude, maximum and minimum load distribution values that are determined with all three methods are similar. As the aerodynamic thrust distribution over to rotor disk is directly related to the inflow distribution, the evaluated aspects are also valid for the inflow distribution over the rotor disc.

Aerodynamic thrust distribution over the rotor disc at various forward flight speeds and control angles for Wessex helicopter are determined by vortex theory and given in Figure to Figure . Positive x axis is the freestream direction for the given analyses.

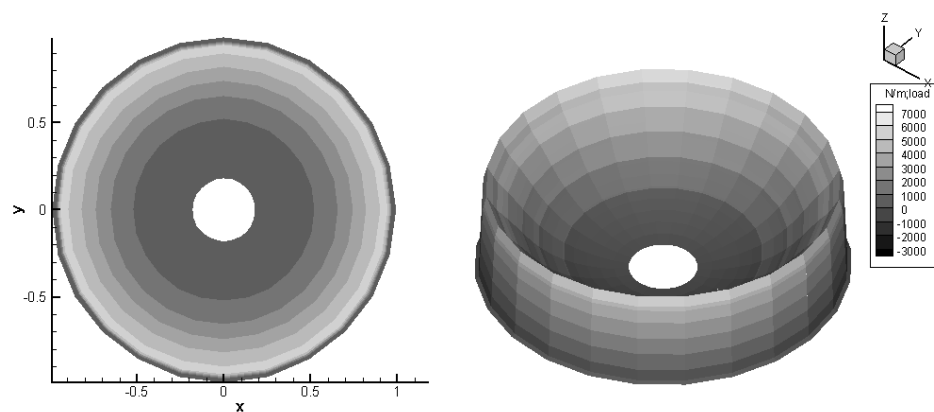


Figure C-3 Hover flight and 9 degrees of collective load distribution

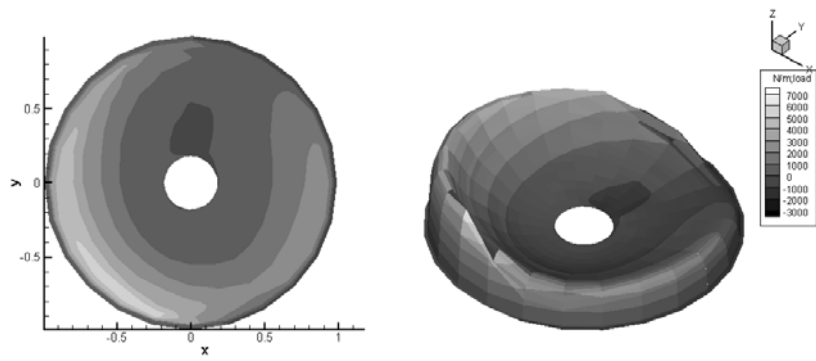


Figure C-4 μ : 0.15, Coll.: 6° , Long. cyclic: -5° load distribution

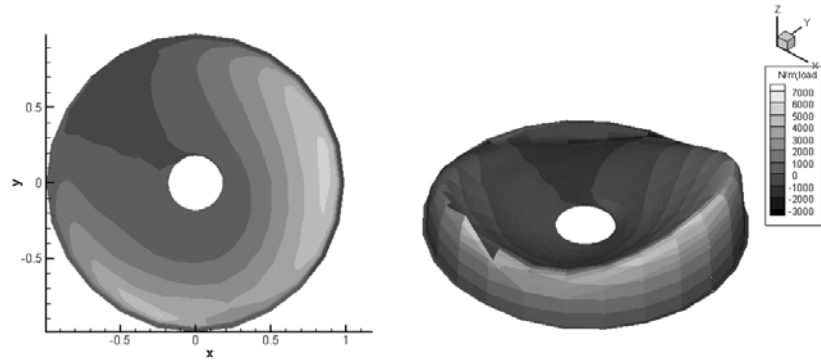


Figure C-5 μ : 0.15, Coll.: 6° , Long. cyclic: -5° , Lat. cyclic: -5° load distribution

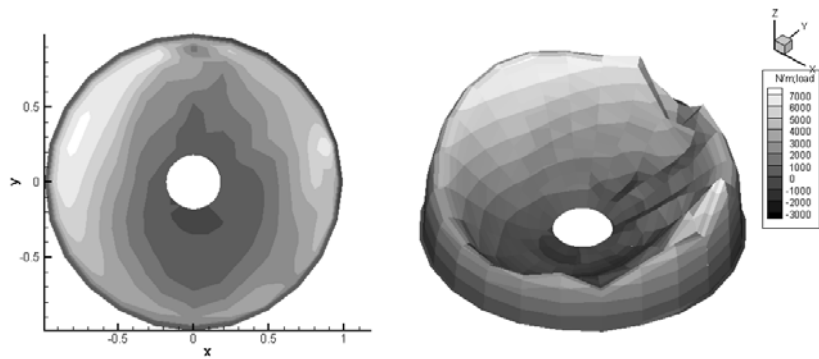


Figure C-6 μ : 0.40, Coll.: 9° , Long. cyclic: -8° load distribution

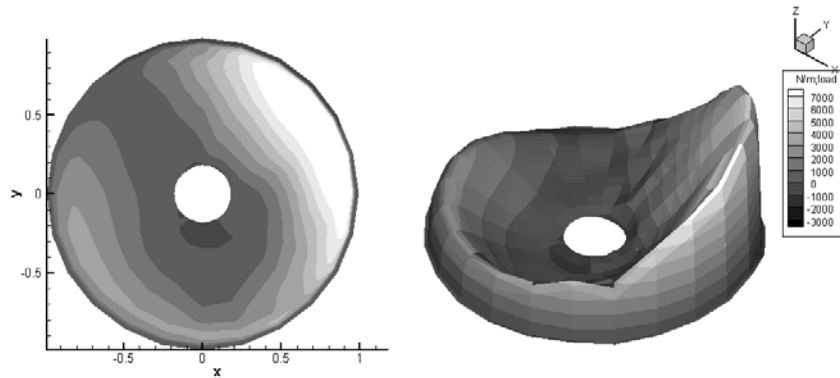


Figure C-7 μ : 0.40, Coll.: 9°, Long. cyclic: -7°, Lat. cyclic:-7.5° load distribution

In addition, azimuthal change of total z axis force generated by an individual blade at blade root is determined for Wessex helicopter at 0.15 advance ratio, 7 degrees collective and -5 degrees longitudinal cyclic. The flight condition and the result given in Figure are just a fictitious example to show the detailed analysis ability of the mathematical model developed.

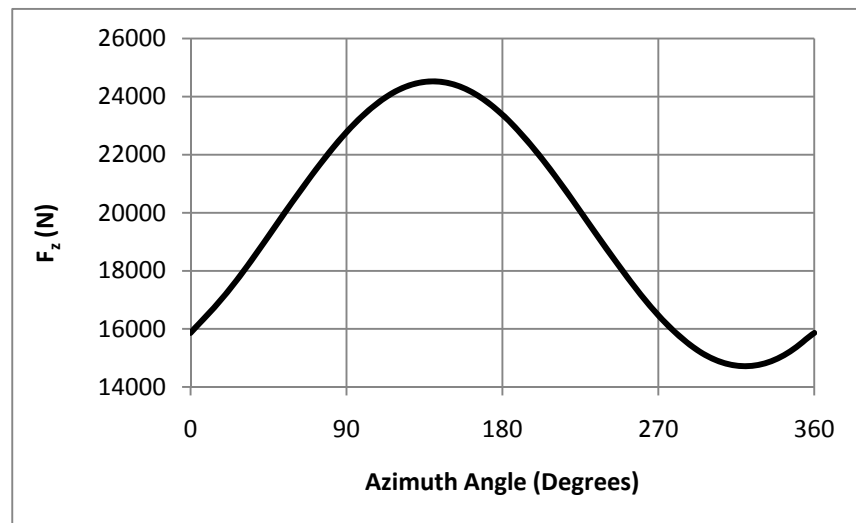


Figure C-8 Blade root total shear force azimuthal distribution